Making SUSY Natural Again

Investigating the Naturalness Reach of the International Linear Collider

by

Eli Bæverfjord Rye

Thesis

for the degree of

Master of Science

Faculty of Mathematics and Natural Sciences
University of Oslo

December 2016

Abstract

When designing and selecting future collider projects, it is important to understand the physics potential of the different alternatives. Here, we investigate the naturalness reach of the International Linear Collider (ILC) in simple constrained supersymmetric models, and compare it to the reach of the High-Luminosity Large Hadron Collider (HL-LHC), based on the results in [1]. The reach is quantified both in terms of the range of naturalness covered, given by the Barbieri–Giudice measure, and in terms of the information gained about naturalness, quantified by the Kullback–Leibler divergence.

Two particular scenarios (parameter choices) for the Constrained Supersymmetric Standard Model (CMSSM) are studied, and one for the second Non-Universal Higgs Mass (NUHM2) model. We find that the HL-LHC in general has a higher naturalness reach than the ILC in the two CMSSM scenarios. However, for the NUHM2 scenario, it is the other way around. In this scenario, we find that the information gain from the 1 TeV ILC searches are over ten times as large as the information gain from the HL-LHC searches. Post HL-LHC naturalness scores below $c \sim 20$, or a tuning to no worse than 5%, are allowed. Thus, the particular variant of the NUHM2 model studied in this work motivates building the ILC.

Make SUSY Natural Again

Takk

Først og framst, takk til Are Raklev for å ha introdusert meg for supersymmetri, og for god rettleiing gjennom denne mastergraden. Det har vore både spanande, intenst og artig. Takk for at du har vore så tolmodig og tilgjengeleg.

Takk til alle på teorigruppa, for at de har gjort dei siste to og eit halvt åra på Blindern fine og sosiale. Eg trur ikkje eg nokon sinne kjem til å oppleve så mange rare og artige samtalar rundt eit lunsjbord igjen. Ein spesiell takk til Anders Kvellestad, for alt du har bidrege med, og for at du har vore guruen vår. Nemnast må også Ola Liabøtrø og Marius Ladegård Meyer, som har bidrege med sårt trengt hjelp i C++.

Takk til alle forelesarar og gruppelærarar eg møtt på min veg, for at de har heldt ut alle spørsmål og til tider rare utbrot. Ein spesiell takk til Tom Lindstrøm, som tidleg forsikra meg om at det er bruk for alle, og til Anders Malthe-Sørenssen, for at eg har fått vere med på å spre det glade bodskap om databerekningar i undervisninga. Takk også til Ilan Dehli Villanger i ForVei og studiekonsulent Grete Stavik-Døvle, for at de fekk meg over kneika. Ein stor takk til alle i ENT3R UiO, for alle opplevingane og erfaringane eg fekk med dykk.

Takk til Marte Julie Sætra for godt venskap, og for at du har lært meg at ein må tru på eigne ferdigheiter. Takk til Henrik Schou Røising for trygt og godt venskap, og fem fine år saman på Blindern. Du er god å ha. Takk til mamma og pappa, Lisa og Nora, for at de er mine bautaer i livet, og for at de alltid viser interesse og omsorg.

Så, til slutt. Kjære Mari [1]. Ord blir fattige. Denne masteren hadde ikkje blitt til utan deg, på alle mulege måtar. Vi klarte det!

The CPU intensive part of this work was performed on the Abel Cluster, owned by the University of Oslo and the Norwegian metacenter for High Performance Computing (NOTUR), and operated by the Research Computing Services group at USIT, the University of Oslo IT-department. The computing time was given by NOTUR allocation NN9284K, financed through the Research Council of Norway.

Eli Bæverfjord Rye
Blindern, 01.12.16

Contents

Introduction

Recent precision tests of the Standard Model (SM) of particle physics and the discovery of the Higgs boson have firmly established the validity of the SM at energies up to the electroweak scale and beyond. Despite these successes, there are many unanswered questions. The Standard Model is a model where the parameters are chosen to match the observations rather than coming from a higher theoretical principle. Thus, it is not believed to be the final theory of particle physics. Numerous theories for physics beyond the Standard Model have been proposed, and the perhaps most popular candidates are theories based on the idea of supersymmetry (SUSY).

In supersymmetry, each Standard Model particle has a superpartner "sparticle", which only differs from the particle by half a unit of spin. One of the motivations for supersymmetry is that it predics a candidate for the dark matter observed in the Universe. However, the main motivation is that it offers an explanation to the hierarchy problem of the Standard Model, and the resulting fine-tuning of the Higgs mass. Theories that require fine-tuned cancellations of large numbers in order to explain results are often thought to be theoretically unsatisfactory, or rather unnatural. This has led to the concept of naturalness, which can be interpreted as the heuristic rule that parameters in a fundamental physical theory should not be too fine-tuned.

The Large Hadron Collider (LHC) at CERN has since its start-up in 2008 generated around 5 fb^{-1} of collisions at a centre-of-mass energy $\sqrt{s} = 7$ TeV, over 20 fb^{-1} at $\sqrt{s} = 8$ TeV, and 39 fb^{-1} at $\sqrt{s} = 13$ TeV. This data set was sufficient for the discovery of the long sought Higgs boson in 2012, however, there has so far been no evidence for production of any supersymmetric particles. The question then becomes if some signs of supersymmetry can be found at future colliders.

When designing and selecting future collider projects, it is important to understand the physics potential of the different alternatives. In this thesis, we investigate the naturalness reach of the planned International Linear Collider (ILC) with energy options $\sqrt{s} = 0.5$ and 1 TeV in simple constrained supersymmetric models, and compare it to similar results for the already approved High-Luminosity Large Hadron Collider (HL-LHC), operating at $\sqrt{s} = 14$ TeV and collecting up to 3000 fb^{-1} of data, based on the results in [1]. The reach

is quantified both in terms of the range of naturalness covered, calculated from the Barbieri–Giudice measure, and in terms of the information gained about naturalness, quantified by the Kullback–Leibler divergence.

We begin by giving a basic review of the Standard Model in Chapter 1, before introducing supersymmetry in Chapter 2. The hierarchy problem and its supersymmetry solution is presented in Chapter 3, together with the concept of naturalness. Chapter 4 gives an introduction to the statistical concepts needed for this work, before we present the details of the simulations performed in Chapter 5. Our results are presented and discussed in Chapter 6, before we make our conclusions. The notation and conventions used in this thesis are given i Appendix A.

Chapter 1

The Standard Model of particle physics

The Standard Model of particle physics emobodies our current understanding of the fundamental constituents of the Universe, the *elementary particles*, and the interactions between them, the *forces*, where the forces themselves are actually described by the exchange of a certain type of elementary particles.

The Standard Model (SM) is undoubtedly one of the greatest triumphs of modern physics. Over the years, it has proven to be a very successful theory, and its highlight came when the ATLAS and CMS experiments at CERN discovered a Higgs boson consistent with Standard Model predictions in 2012 [2,3]. However, the Standard Model is not believed to be the final theory of particle physics. It is a model where the parameters are chosen to match observations rather than coming from a higher theoretical principle, and it fails to include the force of gravity. There are also some more technical problems with the SM, such that it does not contain dark matter, or offer an explanation to the hierarchy problem coming from the radiative loop corrections to the Higgs boson mass (which will be discussed in detail in Chapter 3).

In this chapter, the general principles behind the Standard Model will be given. The need for new physics will be explained in more detail at the end.

1.1 The Standard Model for dummies

There are two major categories for elementary particles: *bosons* and *fermions*. The fermions are responsible for matter, while the bosons are responsible for the forces of nature. There are four presently known fundamental forces:

- The electromagnetic force, which is mediated by massless *photons*.
- The weak force, which is mediated by massive W^+, W^- and Z^0 *bosons*.
- The strong force, which is mediated by massless *gluons*.

– Gravity, which may be mediated by massless *gravitons*. (The gravitons have not been confirmed experimentally.)

Only the three former forces are included in the Standard Model, due to difficulties encountered when trying to also include gravity. The SM is actually widely considered to be incompatible with the most successful theory of gravity to date, namely *general relativity*. This is one of the main reasons for believing that the SM is not the final theory of particle physics. However, since gravitational effects are expected to be negligible all the way up to the Planck scale, $\Lambda_P \sim 10^{18}$ GeV, the Standard Model is a highly predictive theory at low energies even though gravity is not included.

The fundamental forces are closely related to symmetries, and the fact that the bosons mediating the weak force are massive means that the corresponding symmetry is broken. In fact, one of the most important features of the Standard Model is the unification of the electromagnetic and weak interactions into a more fundamental *electroweak* force. It is due to *electroweak symmetry breaking*, explained by the *Higgs mechanism*, that they appear as two separate forces at low energies. This breaking is actually responsible for the masses of all elementary particles, which will be explained in more detail in Sec. 1.4, where we encounter the famous Higgs boson mentioned in the introduction of this chapter.

The elementary particles interact via some force if they carry the *charge* corresponding to the force:

– Only particles that are electrically charged interact via the electromagnetic force.
– Only particles with (weak) isospin interact via the weak force.[1]
– Only particles with color charge interact via the strong force.[2]

All of the known fermions carry isospin, and thus interact via the weak force. Further, the fermions are divided into two subcategories: *quarks* and *leptons*. Quarks are the building blocks of protons and neutrons, while leptons are for example electrons and neutrinos. Quarks carry color charge, and thus interact via the strong force, while leptons do not. In the SM, there are three *generations* of fermions, which each consists of two leptons and two quarks. This gives six lepton and six quark species, often referred to as *flavours*. Because of the confinement property of the strong force, quarks can actually only exist in "colorless" combinations collectively known as *hadrons*, meaning either in a combination of all three possible colors, called *baryons*, or in a combination of color-anticolor, called *mesons*. All ordinary atomic matter is built up of the lighter first generation of fermions, while the heavier fermions only appear as unstable products of particle interactions.

[1] The prefix "weak" will be omitted in the following. There is also another type of isospin, but this is not a fundamental charge, and will not be treated in this thesis.

[2] There are three different color charges, referred to as red, green and blue. The term "color charge" can be a bit confusing, as it has nothing to do with visual perception of color.

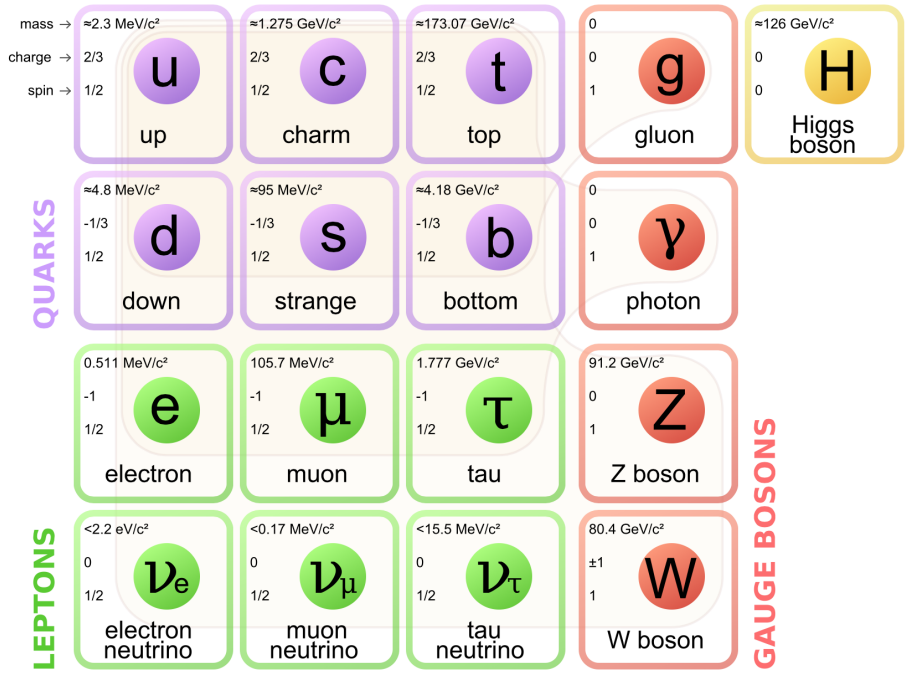

Figure 1.1: The particles of the Standard Model and their interactions. The first three columns show the three generations of fermions. The charge referred to in the figure is electric charge. Figure taken from [4].

In addition to the charges mentioned above, all fundamental particles carry an intrinsic property called *spin*, which can be seen as some kind of internal angular momentum. Fermions carry half-integer spin, whereas bosons carry integer spin. All SM fermions have spin-1/2. All SM bosons have spin-1 and are called vectors, except for the Higgs boson, which has spin-0 and is called a scalar.[3]

A schematic overview of the elementary particles in the Standard Model is shown in Fig. 1.1. Most particles have antiparticles distinct from the particles themselves. Antiparticles are particles with the same mass and spin, but opposite charges.[4] The antiparticle of the electron is called the *positron*, but in general there is no extra name, only a prefix "anti". For instance, the antiparticle of the up-quark is called the anti-up-quark. All of the neutral bosons, and possibly the neutrinos, are their own antiparticles.[5] The two charged W bosons are each others antiparticle.

The electromagnetic and strong interactions both conserve flavour. This

[3]The hypothetical graviton would have to have spin-2.

[4]Historically, the concept of antiparticles was introduced when trying to construct quantum theories consistent with special relativity.

[5]Although it is still an open question whether the neutrinos are *Majorana particles*, in which case they are identical to the corresponding antineutrinos, there are good reasons to believe they are.

means that a top-quark cannot change into a bottom-quark through emission of a photon or a gluon. On the other hand, the weak force does not conserve flavour in charged interactions, so a top-quark can indeed change into a bottom-quark through emission of a charged W boson. More generally, this does not only apply within the same generation — mixing of generations is quantified by the Cabibbo–Kobayashi–Maskawa (CKM) matrix for the quarks [5, 6], and the Pontecorvo–Maki–Nakagawa–Sakata (PMNS) matrix for the leptons [7, 8]. If the neutrinos are assumed to be massive (which they technically are not in the SM), the latter matrix can also explain the observed *neutrino oscillations*.[6]

1.2 Symmetries in particle physics

The previous section gave a somewhat superficial introduction to the ingredients of the Standard Model. A more detailed introduction to the underlying theory of the SM will be given in the coming sections, with a special emphasis on *symmetries*.

The theoretical framework of elementary particle physics is *quantum field theory* (QFT), which successfully combines two well-established concepts in physics: *quantum mechanics* (describes really small stuff) and *special relativity* (describes really fast stuff). The idea of QFT is to use fields rather than individual particles as the fundamental constituents of the theory. Particles are treated as excited states of the fields, and are therefore called field quanta.[7] Quantum mechanical interactions between particles are described by interaction terms between the corresponding quantum fields, which can be visualized and evaluated using *Feynman diagrams* (more about this in Sec. 1.5).

The starting point of a quantum field theory is the *Lagrangian density*, $\mathcal{L}$, which is a function of fields, $\psi_i(x)$, and their derivatives, $\partial_\mu \psi_i(x)$. Different fields represent different particles. The Lagrangian density (from now on simply called the "Lagrangian") is closely related to the fields' *equations of motion*, as the latter can be obtained from $\mathcal{L}$ through the Euler-Lagrange equation:

$$\frac{\partial \mathcal{L}}{\partial \psi_i} - \partial_\mu \left(\frac{\partial \mathcal{L}}{\partial(\partial_\mu \psi_i)} \right) = 0, \qquad i = 1, ..., N, \tag{1.1}$$

where the index i runs over all N fields contained in $\mathcal{L}$.

A *symmetry transformation* is a transformation that leaves the equations of motion for the fields of the theory invariant. This is guaranteed if the *action*,

[6] The neutrinos are assumed to be massless in the Standard Model. However, the experimentally established phenomenon of neutrino oscillation requires neutrinos to have nonzero masses.

[7] Since particles and fields are closely related in QFT, the two will be used interchangeably throughout this thesis. But it is important to know the difference.

defined by

$$S = \int d^4x\, \mathcal{L}, \tag{1.2}$$

is left invariant under the transformation. This is automatically fulfilled if the Lagrangian itself is invariant. The action also remains invariant if the Lagrangian only changes by a total derivative, $\mathcal{L} \to \mathcal{L}' = \mathcal{L} + \partial_\mu f(x)$, where $f(x)$ is a function of the fields, since we assume that all fields must vanish on the integration boundary.

1.2.1 Noether's theorem

One of the basic principles in physics is that the laws of physics are the same at all locations and all times. This principle is equivalent to a symmetry: the laws of physics are invariant when we change our viewpoint — either from one location to another, or from one time to another. For instance, the theory of special relativity is symmetric under boosts and rotations, as well as translations, in space and time.

In 1915, Emmy Noether proved that there is a deep connection between symmetries and conserved physical quantities [9, 10]. Noether's theorem states that *every differentiable symmetry of the action of a physical system has a corresponding conservation law*. In the example of special relativity, the conserved quantities corresponding to the symmetries under translations in space and time are the well-known momentum and energy, respectively. Noether's theorem is one of the most profound observations in theoretical physics.

1.2.2 Description by groups

It is often convenient to describe the symmetries of physical systems in terms of *groups*. Mathematically, a group G is a set of elements g_i, together with a binary operation $\bullet$, that satisfies the following properties $\forall g_i \in G$:

$$\begin{aligned}
&\text{i)} && g_i \bullet g_j \in G && \text{(closure)}, && (1.3)\\
&\text{ii)} && (g_i \bullet g_j) \bullet g_k = g_i \bullet (g_j \bullet g_k) && \text{(associativity)}, && (1.4)\\
&\text{iii)} && \exists\, e \in G \text{ such that } g_i \bullet e = e \bullet g_i = g_i && \text{(identity element)}, && (1.5)\\
&\text{iv)} && \exists\, g_i^{-1} \in G \text{ such that } g_i \bullet g_i^{-1} = g_i^{-1} \bullet g_i = e && \text{(inverse)}. && (1.6)
\end{aligned}$$

The set of all transformations that leave a given object invariant is called a *symmetry group*. In the example of special relativity introduced above, the object that is left invariant is the Minkowski metric, and the corresponding symmetry group is called the *Poincaré group*, which is assumed to be the fundamental symmetry group of spacetime.

For quantum field theories, there are actually two kinds of symmetries. Up until now, we have only discussed invariance of the Lagrangian under transformations of spacetime, such as rotation. But we can also have invariance under transformations of the fields themselves, which are called *internal symmetries*. The latter leads us to the principle of *gauge invariance*, which will be explained in detail in the next section. For now we only state that the particle interactions are related to internal symmetries, and that the corresponding conserved quantities implied by Noether's theorem are related to the charges of the different fundamental forces.

An important type of groups in this context are the $SU(n)$ groups, which we encounter on several occasions in the following. In the defining, *fundamental*, representation, the $SU(n)$ group is the set of all complex-valued and unitary $n \times n$ matrices with determinant 1.[8] The $SU(n)$ groups are so-called *Lie groups*, meaning that they describe continuous symmetries.

When working with groups, it is often more instructive to look at the corresponding *algebra*, which is expressed in terms of the *generators* of the group. The group generators are group elements that can produce all the elements in the group by repeated application of the generators on themselves and each other. With the generators of a Lie group denoted T_a, the corresponding *Lie algebra* can be written as

$$[T_a, T_b] = i f_{ab}{}^c T_c, \tag{1.7}$$

where f_{abc} is a set of (antisymmetric) numbers called *structure constants*. These structure constants uniquely determine the algebra. For $SU(n)$, there are $n^2 - 1$ generators, so $a, b, c = 1, ..., n^2 - 1$. For a general Lie group, the binary operator $[-, -]$, called a *Lie bracket*, must be specified, but for $SU(n)$ it is just the commutator

$$[T_a, T_b] \equiv T_a T_b - T_b T_a. \tag{1.8}$$

For $SU(2)$, the fundamental representation of the generators are proportional to the three Pauli matrices σ_i, and for $SU(3)$ they are proportional to the eight Gell-Mann matrices λ_i. For further details of notation, see Appendix A.

1.3 The gauge principle

We became familiar with the concept of Lagrangians in the previous section, but we did not discuss exactly how they are constructed. A prescription known as the *gauge principle* has proven to be very successful for obtaining theories for elementary particles. The term *gauge* refers to redundant degrees of freedom in

[8] Group elements, and the objects they act upon, can be given in several different *representations*. For a $SU(n)$ group, the two most important representations are the defining, or fundamental, representation, and the adjoint representation.

the Lagrangian, meaning that they have no observable consequences.[9] We can require that the Lagrangian should remain unchanged when transforming between different values of the gauge degrees of freedom. Simpler put, the Lagrangian should be gauge independent. A very important feature of such gauge theories is that they should be *renormalizable*, i.e. that all observables have finite values (more about this in Sec. 1.5).

The gauge principle is explained in the following. We start out with a Lagrangian containing the free, i.e. non-interacting, fermion fields, and identify *global* transformations, of these fields that leave the Lagrangian unchanged.[10] We then promote these transformations to *local*, or gauge, transformations, and demand that the Lagrangian should still be invariant. This latter criterion forces us to introduce spin-1 (vector) fields, which is where the bosons come into play.

The set of gauge transformations that leave the Lagrangian invariant form a *gauge group*. The Standard Model is based on invariance under three such groups, collectively known as the Standard Model gauge group: $SU(3)_C \times SU(2)_L \times U(1)_Y$.[11] The two former groups can be recognized from the previous section, where we stated that the $SU(n)$ groups are related to internal symmetries and particle interactions. In fact, $SU(3)_C$ is the symmetry group of the strong force, or more precisely, *quantum chromodynamics* (QCD), which is the quantum field theory of the strong interaction. The conserved quantity implied by Noether's theorem is in this case the color charge introduced in Sec. 1.1, referred to by the subscript C. Further, $SU(2)_L$ is the symmetry group of the weak force, with isospin I as the conserved quantity. In this case, however, the subscript L refers to the fact that only *left-chiral* particles (and antiparticles of *right-chiral* particles) are charged under this force. We will return to this topic in Sec. 1.3.3.

Finally, the $U(1)_Y$ symmetry group is a bit simpler. The conserved quantity is in this case *weak hypercharge* Y, which is related to electric charge Q (in elementary charge units) and the third component of the weak isospin I_3 through

$$Y = 2(Q - I_3). \tag{1.9}$$

As briefly mentioned in Sec. 1.1, one of the cornerstones of the Standard Model is that it unifies the electromagnetic and weak interactions into a more fundamental electroweak interaction. This is often referred to as the *Glashow–Weinberg–Salam model*, and is described by the combined gauge group $SU(2)_L \times U(1)_Y$. However, because of electroweak symmetry breaking, needed to give all of the Standard Model particles their masses, this group is broken down from $SU(2)_L \times U(1)_Y$ to $U(1)_{\text{em}}$, so that the weak and electromagnetic interactions appear as two different

[9] In physics, a degree of freedom is an independent parameter in the formal description of the state of a physical system.

[10] A global transformation is a transformation that is independent of the coordinate x.

[11] Multiplication here shows the factorization of these transformations, i.e. they act independtly as if on separate coordinates of a vector.

forces at low energies. The electroweak symmetry breaking will be described in more detail in Sec. 1.4.

The $U(1)_{\text{em}}$ symmetry group describes *quantum electrodynamics* (QED), the quantum field theory of the electromagnetic interaction. The corresponding conserved quantity is the well-known electric charge. QED describes interactions of photons with charged fermions, and is the simplest of the quantum field gauge theories. We will illustrate the gauge principle for this theory below.[12]

1.3.1 Abelian gauge groups

Analogous to the $SU(n)$ group, the $U(n)$ group consists of all complex and unitary $n \times n$ matrices.[13] In the simple case of $n = 1$, all of the group elements commute with each other, which is the definiton of an *Abelian* group. In this subsection, we will apply the gauge principle to the Abelian $U(1)_{\text{em}}$ symmetry group of QED and see that it necessitates the existence of photons.

Fermions are described by so-called *Dirac spinor fields*, and the basic Dirac Lagrangian for such a free field $\psi(x)$ is

$$\mathcal{L}_D = \bar{\psi}(x)(i\gamma^\mu \partial_\mu - m)\psi(x), \tag{1.10}$$

where γ^μ are the 4×4 Dirac gamma matrices, $\bar{\psi} \equiv \psi^\dagger \gamma^0$, and m is the mass of the fermion. The Dirac spinor fields must have four components in order to match the dimension of the Dirac gamma matrices. These four components describe both the particle and the antiparticle, with two possible spin states for each of them.[14] By application of the Euler-Lagrange equation in Eq. (1.1), the Lagrangian in Eq. (1.10) reproduces the Dirac equation of relativistic quantum mechanics.

According to the gauge principle, we now want to identify global transformations of the Dirac spinor field $\psi(x)$ that leave $\mathcal{L}_D$ invariant. The phase transformations

$$\psi(x) \to \psi'(x) = e^{-ig\alpha}\psi(x) \tag{1.11}$$

fulfill this criterion, where α is an arbitrary real number, and g is the charge of the field under the symmetry, i.e. electric charge in the case of QED. The charge g is also often referred to as the field's coupling strength or coupling constant, since it is the normalizing factor in the terms in the Lagrangian coupling

[12] Historically, the gauge principle was inspired by QED, not the other way around.

[13] The *SU* in $SU(n)$ stands for *special unitary*, where the term *special* refers to the fact that the group matrices have determinant 1. The $SU(n)$ groups are therefore subgroups of the more general $U(n)$, since the latter have no determinant requirements.

[14] All fermions have spin-1/2, but they exist in two different *spin states*, either with spin $+1/2$ or with spin $-1/2$.

fermions to gauge bosons.[15] This will become evident below. These (global) phase transformations constitute the group of 1×1 "matrices" called $U(1)$.

The next step is to make the above transformations local:

$$\psi(x) \to \psi'(x) = e^{-ig\alpha(x)}\psi(x), \tag{1.12}$$

where $\alpha(x)$ now is an arbitrary real and differentiable function which depends on spacetime, making it local. Due to the derivative ∂_μ in Eq. (1.10), $\mathcal{L}_D$ is *not* invariant under these local transformations:

$$\begin{aligned} \mathcal{L}_D \to \mathcal{L}'_D &= \bar{\psi}'(x)(i\gamma^\mu\partial_\mu - m)\psi'(x) \\ &= \bar{\psi}(x)e^{ig\alpha(x)}(i\gamma^\mu\partial_\mu - m)e^{-ig\alpha(x)}\psi(x) \\ &= \bar{\psi}(x)(i\gamma^\mu[\partial_\mu - ig\partial_\mu\alpha(x)] - m)\psi(x) \\ &\neq \mathcal{L}_D. \end{aligned} \tag{1.13}$$

In order to restore the invariance, we start by substituting the derivative ∂_μ in Eq. (1.10) with the *covariant derivative*, defined by

$$D_\mu \equiv \partial_\mu + igA_\mu(x), \tag{1.14}$$

where a spin-1 (vector) field $A_\mu(x)$ has been introduced. When putting this covariant derivative into the Dirac Lagrangian in Eq. (1.10), we see that we ultimately need

$$D_\mu\psi(x) \to D'_\mu\psi'(x) = D_\mu\psi(x) \tag{1.15}$$

for the Lagrangian to be invariant, leading to a requirement on the gauge transformation of $A_\mu(x)$ itself. By comparing the definition of D_μ with the term $-ig\partial_\mu\alpha(x)$ in Eq. (1.13) that breaks the invariance of $\mathcal{L}_D$, we find that $A_\mu(x)$ must transform according to

$$A_\mu(x) \to A'_\mu(x) = A_\mu(x) + \partial_\mu\alpha(x). \tag{1.16}$$

This new spin-1 field $A_\mu(x)$ is called a gauge boson field, which in the case of QED is the photon. This field must also have its own free field term in the Lagrangian, which for a vector field is given by the Proca Lagrangian:

$$\mathcal{L}_{\text{Proca}} = -\frac{1}{4}F_{\mu\nu}F^{\mu\nu} + \frac{1}{2}m^2A_\mu(x)A^\mu(x), \tag{1.17}$$

where the electromagnetic *field strength tensor* $F_{\mu\nu}$ is defined as

$$F_{\mu\nu} \equiv \partial_\mu A_\nu(x) - \partial_\nu A_\mu(x). \tag{1.18}$$

[15] The term *coupling constant* is also used in a broader sense, meaning the constant of any Lagrangian term that gives rise to a coupling vertex.

Only the first (kinetic) term in Eq. (1.17) is invariant under the transformation in Eq. (1.16), so the second (mass) term can not be included.

We have thus arrived at the complete QED Lagrangian:

$$\begin{aligned}\mathcal{L}_{\text{QED}} &= \bar{\psi}(x)(i\gamma^\mu D_\mu - m)\psi(x) - \frac{1}{4}F_{\mu\nu}F^{\mu\nu} \\ &= \bar{\psi}(x)(i\gamma^\mu \partial_\mu - m)\psi(x) - \frac{1}{4}F_{\mu\nu}F^{\mu\nu} - g\bar{\psi}(x)\gamma^\mu\psi(x)A_\mu(x),\end{aligned} \tag{1.19}$$

which is invariant under the coupled gauge transformations in Eqs. (1.12) and (1.16). We see that the last term couples the fermion and gauge fields, giving rise to interactions between them.

1.3.2 Non-Abelian gauge groups

For non-Abelian groups, i.e. groups with non-commuting elements, the gauge principle gets a bit more complicated. We get some additional terms due to the non-commuting property. This is the case for both $SU(3)_C$, describing QCD, and $SU(2)_L$, describing the weak interaction. We will not go through the full gauge principle for such groups, but rather point out the main differences compared to the simpler Abelian case.

Similar to the Abelian case, the $SU(n)$ gauge transformations of a Dirac spinor field $\psi(x)$ can be expressed as

$$\psi(x) \to \psi'(x) = e^{-ig\alpha^a(x)T_a}\psi(x), \tag{1.20}$$

where the (non-commuting) generators T_a of the $SU(n)$ group are now included. In this case, there are as many *transformation parameters* $\alpha^a(x)$ as generators of the group. For $SU(2)$, the index a runs from 1 to 3, while for $SU(3)$ it runs from 1 to 8, corresponding to their respective number of generators $(n^2 - 1)$.

The covariant derivate needed to restore gauge invariance of the Lagrangian now takes the form

$$D_\mu \equiv \partial_\mu + igA^a_\mu(x)T_a, \tag{1.21}$$

where we see that as many gauge boson fields $A_\mu(x)$ as group generators have been introduced. These have to transform according to

$$A^a_\mu(x) \to A'^{\,a}_\mu(x) = A^a_\mu(x) + \partial_\mu\alpha^a(x) + gf^a{}_{bc}\alpha^b(x)A^c_\mu(x), \tag{1.22}$$

where f_{abc} are the structure constants of the $SU(n)$ group given by the Lie algebra in Eqs. (1.7) and (1.8), and the last term is a consequence of the non-commuting property of the group generators.

As for the Abelian case, the gauge bosons need their own free term in the Lagrangian, given by the Proca Lagrangian in Eq. (1.17). However, also the field

strength tensor gets an additional term due to the non-commuting property of the generators:

$$F^a_{\mu\nu} = \partial_\mu A^a_\nu(x) - \partial_\nu A^a_\mu(x) + g f^a{}_{bc} A^b_\mu(x) A^c_\nu(x), \tag{1.23}$$

which gives rise to self-interactions between the gauge bosons.

For the full Standard Model gauge group $SU(3)_C \times SU(2)_L \times U(1)_Y$, the covariant derivative takes the form

$$D_\mu = \partial_\mu + i g_s \frac{\lambda_a}{2} C^a_\mu(x) + i g \frac{\sigma_a}{2} W^a_\mu(x) + i \frac{1}{2} g' Y B_\mu(x), \tag{1.24}$$

where $C^a_\mu(x)$, $W^a_\mu(x)$ and $B_\mu(x)$ are the gauge fields, and g_s, g and g' the coupling constants, of $SU(3)_C$, $SU(2)_L$ and $U(1)_Y$, respectively. As a convention, the hypercharge Y is assigned in units of $\frac{1}{2}g'$. The generators of $SU(3)_C$ and $SU(2)_L$ are defined as $1/2$ times the Gell-Mann (λ_a) and Pauli (σ_a) matrices, respectively.

The gauge fields $W^a_\mu(x)$ and $B_\mu(x)$ introduced above do not correspond to the physical gauge bosons mediating the weak and electromagnetic interactions directly. In Sec. 1.4, we will see how the electroweak symmetry breaking mixes these fields by linear combinations, so that the physical bosons $W^\pm$, Z^0 and γ are obtained. This is not the case for the strong interaction, where the eight gauge fields $C^a_\mu(x)$ correspond to the mediating gluons directly.

1.3.3 Gauge multiplets

In the above discussion on the gauge principle for non-Abelian theories, we ignored the fact that the fermion fields have to be put into vectors in order to be acted upon by the $SU(n)$ transformations. For instance, since the $SU(2)$ transformations are defined in terms of 2×2 matrices (in the fundamental representation), they need a two-dimensional vector to act upon. Analogously, the $SU(3)$ transformations need to act upon a three-dimensional vector. These vectors are referred to as $SU(2)$ *doublets* and $SU(3)$ *triplets*.

In order to explain observations of parity (spatial inversion) violation of the weak interaction, it is defined as a *chiral* theory. Using projection operators P_L and P_R, defined as

$$P_L = \frac{1}{2}(1 - \gamma^5) \quad \text{and} \quad P_R = \frac{1}{2}(1 + \gamma^5), \tag{1.25}$$

a Dirac fermion field $\psi(x)$ can be separated into a *left-chiral* and a *right-chiral* part:

$$\psi(x) = P_L \psi(x) + P_R \psi(x) \equiv \psi_L(x) + \psi_R(x). \tag{1.26}$$

As briefly mentioned in Sec. 1.3, only the left-chiral part of a fermion is charged under the weak force.

For the weak force, described by the $SU(2)_L$ gauge group, it is thus the left-chiral parts of fermion fields that are put into doublets. For instance, for the first generation of quarks we construct the $SU(2)_L$ doublet

$$q_L(x) = \begin{pmatrix} u_L(x) \\ d_L(x) \end{pmatrix}, \tag{1.27}$$

while the right-chiral parts $u_R(x)$ and $d_R(x)$ are $SU(2)_L$ *singlets*, meaning that they are not affected by the weak force. Analogously, for the first generation of leptons we construct the $SU(2)_L$ doublet

$$\ell_L(x) = \begin{pmatrix} \nu_{eL}(x) \\ e_L(x) \end{pmatrix}, \tag{1.28}$$

while the right-chiral parts $\nu_{eR}(x)$ and $e_R(x)$ yet again are $SU(2)_L$ singlets. In fact, right-chiral neutrinos are actually singlets under the full Standard Model gauge group, meaning that they are not charged under any of the SM forces. If they exist, they are thus difficult to detect. They are not included in the Standard Model.

Quarks are the only fermions that are charged under the strong force, described by the $SU(3)_C$ gauge group. Leptons are thus $SU(3)_C$ singlets. In Sec. 1.1, it was briefly mentioned that there are three different quark colors. For each of the six quark flavours, we therefore construct a $SU(3)_C$ triplet

$$q_C(x) = \begin{pmatrix} q_r(x) \\ q_g(x) \\ q_b(x) \end{pmatrix}, \tag{1.29}$$

containing the three different color components of the quark field.

1.4 The Higgs mechanism

In the above discussion on the gauge principle, the bosons had to be treated massless in order for the Lagrangian to be gauge invariant. This is not a problem for QED and QCD, where the gauge bosons indeed are assumed to be massless, but it is in contradiction with observations of quite massive $W^{\pm}$ and Z^0 bosons mediating the weak force, of nearly 100 GeV each. In order to get past this discrepancy, we need a gauge invariant way of acquiring masses for these particles. It appears that this can be obtained by introducing a new complex scalar field doublet $\Phi(x) = (\phi_a(x), \phi_b(x))^T$ into the Lagrangian. This mechanism was first proposed by Anderson back in 1962 [11], and generalised to the relativistic case of the Standard Model by three independent groups in 1964: Guralnik, Hagen and Kipple [12], Brout and Englert [13], and Higgs [14]. It has become known as the *Higgs mechanism*.

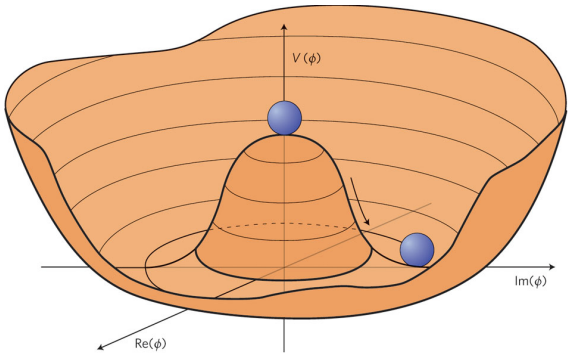

Figure 1.2: Illustration of the "Mexican hat" Higgs potential with $\mu^2 < 0$, in the case of only one complex scalar field ϕ. Figure taken from [15].

By introducing the Higgs doublet field $\Phi(x)$, the following $SU(2)_L \times U(1)_Y$ invariant terms are added to the full Lagrangian:

$$\mathcal{L}_{\mathcal{H}} = |D_\mu \Phi(x)|^2 - \mu^2 |\Phi(x)|^2 - \lambda |\Phi(x)|^4, \tag{1.30}$$

where the latter two constitute the so-called *Higgs potential*, with $\mu^2, \lambda \in \mathbb{R}$, and the covariant derivative in this case is given by

$$D_\mu = \partial_\mu + ig\frac{\sigma_a}{2}W_\mu^a(x) + i\frac{1}{2}g'YB_\mu(x), \tag{1.31}$$

showing that the Higgs couples to the electroweak sector.

It will become evident below that it is the properties of the *vacuum state* (the lowest energy state) $\Phi_0 = (\phi_{a0}, \phi_{b0})^T$ for this Higgs field, corresponding to the minimum of the Higgs potential, that facilitate the electroweak symmetry breaking and give the weak bosons their masses. In order to have such a vacuum state at all, the potential must be bounded from below, i.e. have a finite minimum. This introduces a requirement on one of the potential parameters, namely $\lambda > 0$. However, no such requirement is introduced for μ^2.

If μ^2 is assumed to be positive, the potential has a unique minimum for $\phi_{a0} = \phi_{b0} = 0$. On the other hand, if μ^2 is assumed to be negative, the potential takes the form of a "Mexican hat": it has a circle of degenerate minima for non-zero field values, defined by

$$|\Phi_0|^2 = |\phi_{a0}|^2 + |\phi_{b0}|^2 = \frac{-\mu^2}{2\lambda} \equiv \frac{v^2}{2}, \tag{1.32}$$

where the constant v is referred to as the (non-zero) *vacuum expectation value* (vev) of the Higgs field. An illustration of the analogous potential in the case of only one complex scalar field is illustrated in Fig. 1.2. The *physical* vacuum state will correspond to a particular point on this circle, breaking the underlying $SU(2)_L \times U(1)_Y$ symmetry of the Lagrangian. This is known as *spontaneous*

symmetry breaking, and is the key ingredient for obtaining the missing masses in a gauge invariant way.

Without loss of generality, the vacuum state Φ_0 can be chosen to be

$$\Phi_0 = \frac{1}{\sqrt{2}} \begin{pmatrix} 0 \\ v \end{pmatrix}. \tag{1.33}$$

The particle states, described by excitations of the field, can be obtained by considering *perturbations* of the field around this vacuum state:

$$\Phi(x) = \frac{1}{\sqrt{2}} \begin{pmatrix} \eta_1(x) + i\eta_2(x) \\ v + h(x) + i\eta_3(x) \end{pmatrix}, \tag{1.34}$$

where $h(x)$ and $\eta_i(x)$ are four real scalar fields. Expressing the Lagrangian in Eq. (1.30) in terms of these fields gives rise to a multitude of terms, where several of the terms containing the $\eta_i(x)$ fields are problematic. It appears that these field are "unphysical", meaning that they do not correspond to physical particles.

Since we have a gauge invariant theory — it is the vacuum state that breaks the symmetry — the Lagrangian itself is symmetric), we are free to perform a gauge transformation of $\Phi(x)$ such that the $\eta_i(x)$ fields vanish:

$$\Phi(x) \to \Phi'(x) = \frac{1}{\sqrt{2}} \begin{pmatrix} 0 \\ v + h(x) \end{pmatrix}. \tag{1.35}$$

This particular gauge is known as *unitary gauge*, and the remaining real scalar field $h(x)$ corresponds to the famous Higgs boson. Of course, also the gauge fields contained in the covariant derivative in Eq. (1.31) must be transformed according to their respective transformation properties: $W^a_\mu(x) \to W'^a_\mu(x)$, $B_\mu(x) \to B'_\mu(x)$.

But what about the missing masses? It is the kinetic term $|D_\mu \Phi(x)|^2$ in Eq. (1.30) that contains the gauge fields we want to make massive. By writing out this term in the unitary gauge, it becomes evident that mass terms for these fields, i.e. terms that are quadratic in the fields, indeed have appeared:

$$|D_\mu \Phi|^2 \supset \frac{v^2}{8} g^2 \left(W^1_\mu W^{\mu 1} + W^2_\mu W^{\mu 2}\right) + \frac{v^2}{8} \left(g W^3_\mu - g' B_\mu\right) \left(g W^{\mu 3} - g' B^\mu\right), \tag{1.36}$$

where we for readability have omitted the "transformation primes" and the x-dependecy of the fields. The interpretation is that the three degrees of freedom contained in the real scalar fields $\eta_i(x)$ that are not present anymore are absorbed into the $W^a_\mu(x)$ and $B_\mu(x)$ fields in the gauge transformation, giving them the extra degree of freedom required for massive gauge bosons.

The gauge fields are mixed together in the above expression, which means that their physical *mass eigentstates* differ from their *gauge eigenstates*. The physical gauge bosons are given by the linear combinations

$$W^\pm_\mu = \frac{1}{\sqrt{2}} \left(W^1_\mu \mp i W^2_\mu\right), \quad Z^0_\mu = \frac{g W^3_\mu - g' B_\mu}{\sqrt{g^2 + g'^2}}, \quad A_\mu = \frac{g' W^3_\mu + g B_\mu}{\sqrt{g^2 + g'^2}}, \tag{1.37}$$

with masses from Eq. 1.36:

$$m_W = \frac{1}{2}gv, \qquad m_Z = \frac{1}{2}\sqrt{g^2 + g'^2}v, \qquad m_A = 0. \tag{1.38}$$

The fact that the photon, described by the $A_\mu(x)$ field, is massless also after the symmetry breaking means that there can be a remaining $U(1)_{\text{em}}$ symmetry. The corresponding conserved quantity is the electric charge, which has to be conserved in all Standard Model processes.

To summarize: by introducing a new complex scalar field doublet $\Phi(x)$ with a non-vanishing vacuum expectation value v, the electroweak $SU(2)_L \times U(1)_Y$ symmetry of the Standard Model is "spontaneously" broken down to the $U(1)_{\text{em}}$ symmetry of QED. If this is combined with a particular gauge transformation, three of the four degrees of freedom originally contained in $\Phi(x)$ can be "converted" into masses for the $W^\pm$ and Z^0 bosons of the weak force. Since these masses have been measured to be almost 100 GeV, the weak interaction is suppressed at energies below this scale.[16] This is why the electromagnetic and weak interactions appear as to separate forces at low energies. Finally, the last degree of freedom left in $\Phi(x)$ predicts the existence of the famous Higgs boson, whose mass term can be extracted from the Higgs potential:

$$m_h = \sqrt{-2\mu^2}. \tag{1.39}$$

1.4.1 Fermion masses

In Sec. 1.3.1, we saw that the fermionic mass term of the QED Lagrangian was $U(1)_{\text{em}}$ gauge invariant, whereas this was not the case for the hypotethical photon mass term. In the following, we tacitly assumed that this was valid also for the weak and strong interactions: fermions can be massive, while bosons initially must be treated massless. Above, we learned how the Higgs mechanism introduces boson masses in a gauge invariant way, fixing the apparent problem of observing massive weak bosons. So far, so good. However, due to electroweak unification, not even fermions are allowed to be massive initially.

By using the properties of the projection operators P_L and P_R given in Eq. (1.25), the Dirac Lagrangian can be expressed in terms of the chiral components of the fermion field:

$$\mathcal{L}_D = \bar{\psi}_L i\gamma^\mu \partial_\mu \psi_L + \bar{\psi}_R i\gamma^\mu \partial_\mu \psi_R - m(\bar{\psi}_L \psi_R + \bar{\psi}_R \psi_L), \tag{1.40}$$

where we have omitted the x-dependency for readability. From this, we see that the first, kinetic, term separates the two chiral components of the fermion field. In the mass term, however, the left- and right-chiral components have been

[16] The masses of the W and Z bosons are 80.4 GeV and 91.2 GeV, respectively.

mixed. Since the $SU(2)_L$ transformations only act on the left-chiral component, this mass term is not gauge invariant:

$$m(\bar{\psi}_L\psi_R + \bar{\psi}_R\psi_L) \neq m(\bar{\psi'}_L\psi_R + \bar{\psi}_R\psi'_L), \tag{1.41}$$

where the prime represents a $SU(2)_L$ transformation. This means that also fermions initially need to be treated as massless in the Standard Model.

It turns out that the Higgs mechanism also provides a resolution to the fermion mass problem. Without going into much detail, we note that fermion masses can be introduced into the Lagrangian through so-called *Yukawa terms* of the form $\bar{\ell}_L\Phi e_R$ and its hermitian conjugate, where ℓ_L is a left-handed $SU(2)_L$ doublet and e_R is a right-handed $SU(2)_L$ singlet, see Eq. (1.28). That such terms are gauge invariant can be seen from

$$\begin{aligned}\bar{\ell}_L\Phi e_R \to \bar{\ell'}_L\Phi' e'_R &= \bar{\ell}_L U^\dagger U\Phi e_R \\ &= \bar{\ell}_L\Phi e_R,\end{aligned} \tag{1.42}$$

where U represents a $SU(2)_L$ transformation.

By inserting the vacuum state in Eq. (1.33) into this term, the electron mass term appears:

$$\begin{aligned}\mathcal{L}_e &\supset -y_e\bar{\ell}_L\Phi e_R \\ &= -\frac{y_e}{\sqrt{2}}\begin{pmatrix}\nu_{eL} & \bar{e}_L\end{pmatrix}\begin{pmatrix}0\\ v\end{pmatrix}e_R \\ &= -\frac{y_e v}{\sqrt{2}}\bar{e}_L e_R,\end{aligned} \tag{1.43}$$

and similarly for the hermitian conjugate term. From this, we can identify the electron mass as

$$m_e = \frac{y_e v}{\sqrt{2}}, \tag{1.44}$$

where the *Yukawa coupling* y_e gives the coupling strength of the electron to the Higgs boson.

1.5 Feynman calculus and renormalization

There are very few problems in the framework of the Standard Model that can be solved exactly. Instead, physical observables, such as *cross sections* σ and *decay widths* Γ, are calculated in terms of *interaction amplitudes* $\mathcal{M}$, using *perturbation theory*. In perturbation theory, these quantities can be expanded as infinite sums of terms of increasing complexity and decreasing importance, in terms of powers of some small parameter. It is often sufficient to only evaluate the first few terms.

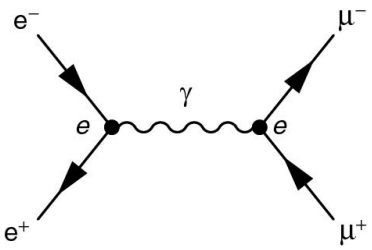

(a) Leading order (LO).

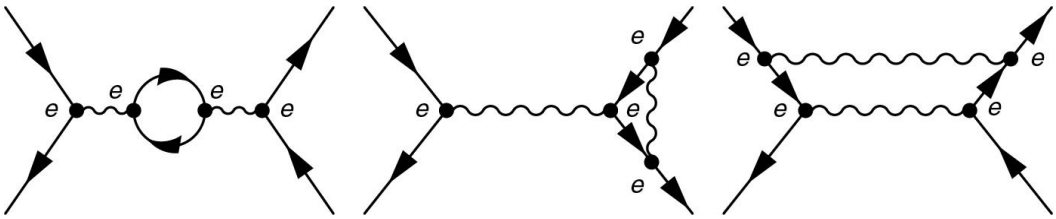

(b) Next-to-leading order (NLO).

Figure 1.3: The leading order (a) and some of the next-to-leading order (b) Feynman diagrams for the QED process $e^+e^- \to \mu^+\mu^-$. Figures taken from [17].

1.5.1 Feynman calculus

Richard Feynman introduced the concept of *Feynman diagrams* already in 1949 [16], which represents these terms graphically. As an example, some of the Feynman diagrams for the QED process $e^+e^- \to \mu^+\mu^-$ are shown in Fig. 1.3. Subfigure (a) shows the leading order (LO) diagram, while (b) shows three of the next-to-leading order (NLO) diagrams. Each element of these diagrams is associated with a factor that contributes to the interaction amplitude.

In Fig. 1.3(a), there are two QED interaction *vertices*, that each contribute a factor $ie\gamma^\mu$. This means that the absolute square of the amplitude $|\mathcal{M}|^2$ for this diagram will be proportional to e^4, or equivalently α^2, where α is the dimensionless fine-structure constant,

$$\alpha = \frac{e^2}{4\pi}. \tag{1.45}$$

This is the small parameter in the perturbation theory.

Similarly, each of the NLO diagrams in Fig. 1.3(b) has a factor of α for each of the four vertices, and hence $|\mathcal{M}|^2 \propto \alpha^4$. The *total* squared amplitude is the sum of all individual amplitudes giving the same final state.[17] The physical

[17]Each pair of terms at a specific order can interfere either positively or negatively.

observables are then obtained by integrating $|\mathcal{M}|^2$ over all possible spin and momentum configurations of the system.

1.5.2 Renormalization

The subleading Feynman diagrams in Fig. 1.3(b) contain closed loops, and since the momentum inside these loops is undetermined, we have to integrate over all possible momenta. These integrals diverge, which is physically unacceptable. However, this can be dealt with using *renormalization*.

The first step towards a finite theory is to parametrize the divergence. This is called *regularization*, and there are several different ways of doing it. For instance, with *cut-off regularization*, the integrals are only evaluated up to a finite cut-off scale Λ:

$$\int_0^\infty d^4k \to \int_0^\Lambda d^4k. \tag{1.46}$$

The argument is that the Standard Model is not valid at very high energies, where we know we need a yet to be discovered quantum theory of gravitation. We can thus limit the integrals to energies below this. This type of regularization will be applied to the Higgs boson mass loop corrections discussed in Sec. 3.1.

Another method is *dimensional regularization*, where the four spacetime dimensions are substituted with $d = 4 - \epsilon$, where ϵ is a small parameter:

$$\int_0^\infty d^4k \to \int_0^\infty d^dk. \tag{1.47}$$

This is mathematically well-defined, and the physical limit is found when ϵ goes to zero.

When the divergences have been parametrized, the next step is to get rid of the terms that blow up, and identify the physical quantities. As an example, consider the left-most diagram in Fig. 1.3(b), which has a loop in the photon propagator. After dimensional regularization of the correponding integral, we end up with terms that are proportional to $1/\epsilon$, which goes to infinity when ϵ goes to zero.

Renormalization is the claim that such infinities is part of the *bare* physical constants in the Lagrangian. A bare constant is not an observable quantity. What is observed is the renormalized constant, in this case the electron charge $e = e_0 + \delta e$, where e_0 is the bare charge and δe is an infinite shift that cancels the divergence. The infinities are thus absorbed into unobservable parameters of the theory.

All the coupling constants of the Standard Model are renormalized. The renormalization introduces an energy dependence, since the shift comes from loop corrections that depend on the energy of the process. For instance, the observed value of electron charge depends on what scale μ the observation takes

place, $e(\mu)$. The fact that the coupling "contants" are not constant is referred to as *running of the coupling constants*. The evolution of the couplings with energy is described by so-called *renormalization group equations* (RGEs). More specifically, these include so-called *beta functions* that describe the behaviour of a Lagrangian parameter λ as a function of the energy scale μ away from the value where it was defined, often denoted μ_0:

$$\beta_\lambda \equiv \mu \frac{\partial \lambda}{\partial \mu}. \tag{1.48}$$

1.6 Shortcomings of the Standard Model

Despite its tremendous success, the Standard Model is not believed to be the final theory of particle physics. As briefly mentioned in Sec. 1.1, it does not include the fourth fundamental force, namely gravity, and thus fails as a "theory of everything". There are also several other motivations for looking for physics beyond the Standard Model.

For instance, it is widely believed that the Standard Model is only an effective low-energy model of a more fundamental high-energy model, i.e. that the three interactions of the Standard Model unite at a higher energy and act as a single interaction under some larger gauge group. In such *Grand Unified Theories* (GUTs), the three Standard Model couplings should unite at a high energy scale $\Lambda_{\text{GUT}} \sim 10^{16}$ GeV. However, when the three couplings are evolved to higher energies using RGEs, they fail to intersect. Although this is not a direct problem for the Standard Model itself, it is viewed by many as an indication for physics beyond the Standard Model.

Further, the Standard Model has no candidate for dark matter. The existence and properties of dark matter are inferred from its gravitational effects on visible matter and gravitational lensing of background radiation. For instance, stars in the periphery of spiral galaxies are rotating so fast that the galaxies would fly apart if the gravity of their constituent stars and gas is all that is holding them together. Since this is not happening, a huge amount of unseen mass must be holding them together. This is known as the galaxy rotation problem, and attempts to explain it was what led to the theory of dark matter in the first place [18]. Dark matter is believed to make up $\sim 27\%$ of the mass-energy content of the universe, and the big question is then what this dark matter is. The most widely accepted theory is that it is composed of weakly interacting massive particles (WIMPs) that interact only through gravity and the weak force. The neutrinos, being both massive and weakly interacting, is the only Standard Model candidate for particle dark matter. However, the neutrinos are very low in mass and can only account for a small fraction of the total amount of dark matter. The existence of dark matter thus hints toward a new type of matter not described by the Standard Model.

There is also a more technical problem with the Standard Model. Quantum loops in the Higgs boson propagator contribute to the Higgs boson mass. These corrections are quadratic in the mass scale Λ, which means that if the SM is part of a theory that is valid up to very high energies, such as that of the Grand Unified Theory (GUT) $\Lambda_{\mathrm{GUT}}\,(\sim 10^{16}$ GeV), or the Planck scale $\Lambda_P\,(\sim 10^{18})$ GeV, these corrections become very large. It is thus difficult to keep the Higgs mass at the electroweak scale of 10^2 GeV. This is known as the hierarchy problem, and will be explained in more detail in Chapter 3.

Other problems include the mechanism for (small) neutrino masses not included in the Standard Model, and the asymmetry between particles and antiparticles observed in the Universe. Although this "list" of shortcomings of the Standard Model is far from exhaustive, it is more than enough to justify the need for new physics. There are numerous proposed theories for physics beyond the Standard Model, and the perhaps most popular candidates are based on supersymmetry, which will be the topic of the next chapter.

Chapter 2

Supersymmetry

The need for theories that go beyond the Standard Model was motivated in Section 1.6. Supersymmetry is a proposed extension to the Standard Model that offers a resolution to some of the problems described there. In Sec. 2.9, we will see how it successfully unifies the Standard Model coupling constants at a high energy scale, while we in Chapter 3 will see how it offers a solution to the hierarchy problem. It also includes a candidate for dark matter.

We begin this chapter by presenting the general principle behind supersymmetry. Some phenomenology relevant to the thesis is also given. The particular supersymmetry models that will be studied in the rest of this thesis is discussed at the end.

2.1 Supersymmetry for dummies

Supersymmetry (SUSY) proposes a symmetry between fermions and bosons. Each Standard Model particle has a superpartner "sparticle", which only differs from the particle by half a unit of spin. All other quantum numbers are the same. This can be illustrated schematically as

$$Q\left|\text{fermion}\right\rangle = \left|\text{boson}\right\rangle, \qquad Q\left|\text{boson}\right\rangle = \left|\text{fermion}\right\rangle, \tag{2.1}$$

where Q is a supersymmetry operator that alters the spin by $1/2$. A SM fermion (spin-$1/2$) transforms under Q to a scalar superpartner (spin-0), while a SM vector boson (spin-1) transforms to a fermion superpartner (spin-$1/2$). The Higgs scalar boson (spin-0) also transforms to a fermion superpartner (spin-$1/2$).

The name *sparticle* is used above as a general label for any supersymmetric particle. The naming convention for the bosonic superpartners of the SM fermions is to add the prefix "s-" to the name of the SM particle. For instance, the superpartner of the electron is the *selectron*. For the femionic superpartners of the SM bosons one uses the suffix "-ino" together with the boson name. For instance, the superpartner of the W boson is the *wino*. A tilde ($\tilde{}$) is used

to denote supersymmetric particles, e.g. the above mentioned selectron has the symbol $\tilde{e}$.

Two important observations can be made. First, there are no two SM particles that differ in spin by 1/2, with the remaining quantum numbers being equal. This means that supersymmetry predicts the existence of a multitude of new particles. Second, if supersymmetry was an exact symmetry of nature, the sparticles would have had the same masses as the particles, which means that they already should have been discovered. Therefore, if supersymmetry exists, it is a broken symmetry, and the mass scale of the sparticles is not known *a priori*. However, there are theoretical arguments that favour a relatively low mass scale of $\mathcal{O}(1\text{TeV})$, more about this in Sec. 3.1.

2.2 Extending the Poincaré group

The previous section gave a short introduction to the general concept of supersymmetry. But where does it come from and what is the theory behind it? Let us start at the beginning.

In Any physical theory obeying special relativity must be invariant under the *Poincaré group*, also known as the spacetime symmetry group. This is the group of all Lorentz boost and rotations as well as translations. More explicitly, it is defined as the group of all transformations of the form

$$x^\mu \to x^{\mu\prime} = \Lambda^\mu{}_\nu x^\nu + a^\mu, \tag{2.2}$$

that leaves the spacetime interval $(x-y)^2$ invariant. Here, x^μ denotes a coordinate four-vector, $\Lambda^\mu{}_\nu$ denotes a Lorentz transformation, while a^μ denotes a constant translation. The generators of Lorentz boosts and rotations, $M_{\mu\nu}$, and the generators of translations, P_μ, satisfy the *Poincaré algebra*:

$$[P_\mu, P_\nu] = 0, \tag{2.3}$$
$$[M_{\mu\nu}, P_\rho] = -i(g_{\mu\rho}P_\nu - g_{\nu\rho}P_\mu), \tag{2.4}$$
$$[M_{\mu\nu}, M_{\rho\sigma}] = -i(g_{\mu\rho}M_{\nu\sigma} - g_{\mu\sigma}M_{\nu\rho} - g_{\nu\rho}M_{\mu\sigma} + g_{\nu\sigma}M_{\mu\rho}), \tag{2.5}$$

which is a Lie algebra. Further, these generators commute with the generators of the internal gauge symmetries of the SM, i.e. the generators B_i of the SM gauge groups all have

$$[P_\mu, B_i] = [M_{\mu\nu}, B_i] = 0. \tag{2.6}$$

Supersymmetry came around as a result of an attempt to extend the external spacetime symmetries to also include the internal gauge symmetries in a *non-trivial* way. That is, without all the generators of the internal gauge symmetries commuting with the spacetime symmetry generators. In 1967, Coleman and Mandula [19] showed that there exists no Lie algebra based extension of the Poincaré

algebra that fulfills this criterion. However, Haag, Lopuszanski and Sohnius [20] did not give up on the idea of an unification of internal and external symmetries. In 1975, they showed that a non-trivial extension can be obtained by allowing *anti*commutators in Lie algebras, by introducing the concept of *superalgebras*.

A superalgebra, or *graded* Lie algebra, L, is a direct sum of two Lie algebras L_0 and L_1, $L = L_0 \oplus L_1$, with a special binary operation $\bullet$ called *grading*. For $x_i \in L_i$, the grading is given by

$$x_i \bullet x_j = x_k \in L_{i+j \bmod 2}, \tag{2.7}$$

which means that $x_0 \bullet x_0 \in L_0$, $x_1 \bullet x_1 \in L_0$ and $x_0 \bullet x_1 \in L_1$.

By combining the Poincaré algebra with an algebra spanned by a set of four new operators Q_a, $a = 1, 2, 3, 4$, called *Majorana spinor charges*, Haag *et al.* came up with the supersymmetric extension of the Poincaré algebra — the *super-Poincaré algebra* (often simply called the superalgebra, which can be a bit confusing). Represented in terms of two-component Weyl spinors Q_A (which will be defined shortly) and their hermitian conjugates $\bar{Q}_{\dot{A}}$, instead of the four-component Majorana spinor charges, the superalgebra is given by the Poincaré algebra plus the (anti)commutation relations

$$\{Q_A, Q_B\} = \{\bar{Q}_{\dot{A}}, \bar{Q}_{\dot{B}}\} = 0, \tag{2.8}$$

$$\{Q_A, \bar{Q}_{\dot{B}}\} = 2\sigma^{\mu}_{A\dot{B}} P_\mu, \tag{2.9}$$

$$[Q_A, P_\mu] = [\bar{Q}_{\dot{A}}, P_\mu] = 0, \tag{2.10}$$

$$[Q_A, M^{\mu\nu}] = \sigma^{\mu\nu B}_{A} Q_B, \tag{2.11}$$

where $\sigma^{\mu\nu} = \frac{i}{4}(\sigma^\mu \bar{\sigma}^\nu - \sigma^\nu \bar{\sigma}^\mu)$, with $\sigma^\mu = (\mathbb{1}_{2\times 2}, \sigma^i)$ (σ^i are the usual two-dimensional Pauli matrices). For the Weyl spinors, $A, B = 1, 2$ and $\dot{A}, \dot{B} = 1, 2$ are distinct indices. The transformations corresponding to the superalgebra are called *supersymmetry transformations*.

Symbolically, the relation between the Majorana spinors and Weyl spinors is

$$Q_a = \begin{pmatrix} Q_A \\ \bar{Q}^{\dot{A}} \end{pmatrix}. \tag{2.12}$$

The fermion fields transforming under the Poincaré group are usually represented as four-component Dirac/Majorana spinors. However, since it can be shown that the Poincaré group is homomorphic to the special linear group $SL(2, \mathbb{C})$, the representations of this group can be used instead. The $SL(2, \mathbb{C})$ group has two inequivalent fundamental representations, with one two-component Weyl spinor each. They are called left- and right-handed Weyl spinors, and are written as ξ_A and $\bar{\eta}_{\dot{A}}$, respectively. For the special case of Majorana fermions, we have $\xi_A = \eta_A$, as in Eq. (2.12).

It should be noted that supersymmetry as defined by Eqs. (2.8) – (2.11) actually does not fulfill the original goal of unifying the internal gauge and external

spacetime symmetries. However, the superalgebra can be extended by introducing more Majorana spinor charges, labeled Q_a^α, where $\alpha = 1, ..., N$. The internal symmetries can appear for $N > 1$ supersymmetries, but they introduce an extensive number of extra particles, and do not seem to be realised in nature.

From the above, it is clear that supersymmetry did in fact come around as an "accident". Since it has some interesting features, physicists decided to explore it some more, even though it did not fulfill its intended purpose. For instance, it can be shown that supersymmetry is the largest possible extension of the Poincaré group.

2.3 Superfields

As already mentioned, supersymmetry introduces several new particles. But where exactly do they enter into the picture? This is best explained by the superfield formalism, which is introduced next.

In the previous section, it was stated that the transformations corresponding to the action of the operators in the superalgebra are called supersymmetry transformations. The objects (particles) transforming under these transformations can be represented by so-called *superfields*, which are functions of the *superspace* coordinates. Simpler put; superspace is a coordinate system where supersymmetry transformations are manifest.

Technically, superspace is an eight-dimensional manifold with coordinates

$$z^\pi = (x^\mu, \theta^A, \bar{\theta}^{\dot{A}}), \tag{2.13}$$

where x^μ are the ordinary Minkowski coordinates, and θ^A and $\bar{\theta}^{\dot{A}}$, $A = 1, 2$ and $\dot{A} = 1, 2$, are four anticommuting *Grassman numbers*. This notation may seem familiar, which is no accident: these Grassman numbers correspond to Weyl spinors, which was introduced above. Because of the anticommutativity, any Grassman number squared vanishes (no contraction implied):

$$\theta_A^2 = \theta_A \theta_A = -\theta_A \theta_A = 0, \tag{2.14}$$

which means that a function of a Grassman number, $f(\theta_A)$, has an all-order expansion given by

$$f(\theta_A) = a + b\theta_A. \tag{2.15}$$

Further, Grassman numbers also have the properties

$$\theta^A \equiv \theta\theta \equiv \theta^A \theta_A = -2\theta_1 \theta_2, \tag{2.16}$$

$$\bar{\theta}^2 \equiv \bar{\theta}\bar{\theta} \equiv \bar{\theta}_{\dot{A}} \bar{\theta}^{\dot{A}} = 2\bar{\theta}^{\dot{1}} \bar{\theta}^{\dot{2}}. \tag{2.17}$$

Table 2.1: Component field content of a general superfield.

Component field	Type	D.o.f.
$f(x), m(x), n(x)$	Complex (pseudo) scalar	2
$\psi_A(x), \phi_A(x)$	Left-handed Weyl spinor	4
$\bar{\chi}^{\dot{A}}(x), \bar{\lambda}^{\dot{A}}(x)$	Right-handed Weyl spinor	4
$V_\mu(x)$	Lorentz four-vector	8
$d(x)$	Complex scalar	2

It can be shown that Eq. (2.15) enables that a superfield Φ generally may be written as

$$\begin{aligned}\Phi(x,\theta,\bar{\theta}) =& f(x) + \theta^A\phi_A(x) + \bar{\theta}_{\dot{A}}\bar{\chi}^{\dot{A}}(x) + \theta\theta m(x) + \bar{\theta}\bar{\theta}n(x) \\ &+ \theta\sigma^\mu\bar{\theta}V_\mu(x) + \theta\theta\bar{\theta}_{\dot{A}}\bar{\lambda}^{\dot{A}} + \bar{\theta}\bar{\theta}\theta^A\psi_A(x) + \theta\theta\bar{\theta}\bar{\theta}d(x).\end{aligned} \tag{2.18}$$

The properties of the component fields in this superfield are listed in Table 2.1.

It was stated above that the particles transforming under supersymmetry transformations can be represented by superfields. However, the superfields used to represent physical particles are not general superfields, like the one in Eq. (2.18), but rather so-called scalar and vector superfields, which have fewer degrees of freedom. They correspond to the *irreducible representations* of the superalgebra, and need to be recovered from the general superfield by some rather *ad hoc* restrictions.

2.3.1 Scalar superfields

The restrictions for scalar superfields involves covariant derivatives. Covariant derivatives are introduced in gauge theories to make the Lagrangian invariant under gauge transformations, as seen in Sec. 1.3. Similarly, it would have been nice to have a derivative that is invariant under supersymmetry transformations, i.e. that commutes with the supersymmetry operators. The following derivatives fulfills this criterion:

$$D_A \equiv \partial_A + i(\sigma^\mu\bar{\theta})_A\partial_\mu, \tag{2.19}$$

$$\bar{D}_{\dot{A}} \equiv -\partial_{\dot{A}} - i(\theta\sigma^\mu)_{\dot{A}}\partial_\mu. \tag{2.20}$$

A left-handed scalar superfield is then defined by the constraint

$$\bar{D}_{\dot{A}}\Phi = 0. \tag{2.21}$$

By change of variable, $y^\mu = x^\mu + i\theta\sigma^\mu\bar{\theta}$, the covariant derivative $\bar{D}_{\dot{A}}$ becomes

$$\bar{D}_{\dot{A}} = -\partial_{\dot{A}} \equiv -\frac{\partial}{\partial\bar{\theta}_{\dot{A}}}, \tag{2.22}$$

which means that a left-handed scalar superfield needs to be independent of $\bar{\theta}$ in this new set of coordinates, giving

$$\Phi(y,\theta) = A(y) + \sqrt{2}\theta\psi(y) + \theta\theta F(y), \tag{2.23}$$

where A and F are complex scalars and ψ is a left-handed Weyl spinor.

The field F is called an auxillary field, because it can be eliminated by applying the equations of motion. This can be seen by undoing the coordinate change, where it becomes clear that there is no derivative term for the F-field. The equations of motion also remove two of the (fermionic) degrees of freedom contained in the left-handed Weyl spinor ψ_A. A left-handed scalar superfield is thus left with two scalar (bosonic) degrees of freedom and two fermionic degrees of freedom.

The hermitian conjugate of a left-handed scalar superfield is called a right-handed scalar superfield, and satisfies the constraint

$$D_A\Phi^\dagger = 0. \tag{2.24}$$

By following a similar procedure as for left-handed scalar superfields, it can be shown that a right-handed scalar superfield also contains two scalar and two fermionic degrees of freedom, where the latter are contained in a right-handed Weyl spinor $\psi^{\dot{A}}$.

2.3.2 Vector superfields

For vector superfields, the restriction is a bit different. A vector superfield is defined by the contraint

$$\Phi^\dagger = \Phi, \tag{2.25}$$

which means that a general vector superfield can be written as

$$\begin{aligned}\Phi(x,\theta,\bar{\theta}) =& f(x) + \theta^A\phi_A(x) + \bar{\theta}_{\dot{A}}\bar{\phi}^{\dot{A}}(x) + \theta\theta m(x) + \bar{\theta}\bar{\theta}m^*(x) \\ &+ \theta\sigma^\mu\bar{\theta}V_\mu(x) + \theta\theta\bar{\theta}_{\dot{A}}\bar{\lambda}^{\dot{A}} + \bar{\theta}\bar{\theta}\theta^A\lambda_A(x) + \theta\theta\bar{\theta}\bar{\theta}d(x).\end{aligned} \tag{2.26}$$

Here, the scalar fields $f(x)$ and $d(x)$, as well as the four-vector $V_\mu(x)$, are required to be real, which halves their amount of degrees of freedom. Further, this vector superfield contains auxillary degrees of freedom, which can be removed with a *supergauge transformation* (a generalisation of the standard gauge transformation). One particular choice of gauge that removes all the auxillary degrees of

freedom is the *Wess-Zumino gauge*. In this gauge, a vector superfield can be written as

$$V_{WZ}(x,\theta,\bar{\theta}) = (\theta\sigma^{\mu}\bar{\theta})[V_{\mu}(x) + i\partial_{\mu}(A(x) - A^{*}(x))] + \theta\theta\bar{\theta}_{\dot{A}}\bar{\lambda}^{\dot{A}}(x) + \bar{\theta}\bar{\theta}\theta^{A}\lambda_{A}(x) + \theta\theta\bar{\theta}\bar{\theta}d(x), \tag{2.27}$$

where $A(x)$ is a complex scalar field obeying $A(x) + A^{*}(x) = -f(x)$. This vector superfield contains one real scalar degree of freedom from $d(x)$, three gauge degrees of freedom from $[V_{\mu}(x) + i\partial_{\mu}(A(x) - A^{*}(x))]$, and four fermionic degrees of freedom from the Weyl spinors $\lambda(x)$ and $\bar{\lambda}(x)$.[1]

2.3.3 Relation to physical particles

It was stated above that physical particles are represented by scalar and vector superfields. But the superfields do not correspond to individual particles directly. Instead, it is a matter of degrees of freedom, which is explained below.

A two-component Weyl spinor cannot on its own describe a four-component Dirac spinor. To construct a Dirac fermion, two different Weyl spinors of opposite handedness are needed. This gives the four fermionic degrees of freedom required by a Dirac fermion and its antiparticle. Since each scalar superfield contains two bosonic degrees of freedom in addition to a Weyl spinor (after the equations of motion have been applied), two scalar particle-antiparticle pairs are introduced as well when constructing a Dirac fermion. They are the supersymmetric partners of a Dirac fermion, called *sfermions*.

To construct the SM gauge bosons, vector superfields are needed. After the equations of motion have been applied, each vector superfield contains a massless vector boson with two bosonic degrees of freedom, and two Weyl spinors of opposite handedness with two fermionic degrees of freedom.[2] We need one vector superfield for each SM gauge boson, giving a lot of "excessive" Weyl spinors. These combine into the supersymmetric fermionic superpartners of the SM gauge bosons, called *gauginos*, one for each gauge boson.

From this it is clear that supersymmetry indeed introduces many new particles. We will return to this in Sec. 2.6, where a specific supersymmetric model is presented.

[1] $V_{\mu}(x)$ has four degrees of freedom, but one of them can be eliminated by the remaining gauge freedom in the choice of $A(x) - A^{*}(x)$, which is the ordinary gauge freedom of a $U(1)$ field theory.

[2] For vector superfields, λ_{A} and $\lambda^{\dot{A}}$ have the same two degrees of freedom, since they are related through hermitian conjugation.

2.4 The unbroken supersymmetric Lagrangian

In the previous sections, we have learned where supersymmetry comes from, and how the extra particles come into play. The next step is to construct a viable model that is invariant under supersymmetry transformations, in the same way as the Standard Model is invariant under Poincaré transformations.

The starting point is as usual the Lagrangian. We recall that a symmetry transformations leaves the action invariant, which is automatically fulfilled it the Lagrangian only changes by a total derivative. The supersymmetry Lagrangian is constructed from superfields, and it can be shown that the highest order (in θ and $\bar{\theta}$) component fields always have this property for both scalar and vector superfields, as well as their products. Invariance of the action under supersymmetry transformations can therefore be ensured by a redefinition of the Lagrangian such that

$$S = \int d^4x \int d^4\theta \, \mathcal{L}, \tag{2.28}$$

where the last integral is over the four Grassman numbers introduced with superspace.[3] Here, the last integral isolates the allowed terms because of the calculus properties of Grassman numbers.[4] The supersymmetry Lagrangian can therefore generically be written as

$$\mathcal{L} = \mathcal{L}_{\theta\theta\bar{\theta}\bar{\theta}} + \theta\theta\mathcal{L}_{\bar{\theta}\bar{\theta}} + \bar{\theta}\bar{\theta}\mathcal{L}_{\theta\theta}, \tag{2.29}$$

where the indices indicate the highest power of $\theta, \bar{\theta}$ in the term.

The fact that the theory has to be renormalizable puts further restrictions on the fields in $\mathcal{L}$. Renormalizability forbids terms where the combined mass dimension of the factors is greater than four, including the leading Grassman numbers in Eq. (2.29) and the differential $d^4\theta$ in Eq. (2.28). We can thus have at most three powers of scalar superfields Φ in the Lagrangian. The general supersymmetry Lagrangian can therefore be written in terms of scalar superfields as

$$\mathcal{L} = \Phi_i^\dagger \Phi_i + \bar{\theta}\bar{\theta} W[\Phi] + \theta\theta W[\Phi^\dagger], \tag{2.30}$$

where $\Phi_i^\dagger \Phi_i$ is called the kinetic term, and W is the so-called *superpotential*, given by

$$W[\Phi] = g_i \Phi_i + m_{ij} \Phi_i \Phi_j + \lambda_{ijk} \Phi_i \Phi_j \Phi_k. \tag{2.31}$$

2.4.1 Supergauge

In the same way as the Standard Model Lagrangian, the supersymmetry Lagrangian introduced above section has be gauge invariant. In this subsection, we

[3] Note that this alters the dimension of $\mathcal{L}$, since the Grassman numbers have dimension $[\theta] = [\bar{\theta}] = M^{-1/2}$.

[4] Integration over Grassman numbers is defined so that $\int d^4\theta (\theta\theta)(\bar{\theta}\bar{\theta}) = 1$, while any other power of θ and $\bar{\theta}$ gives zero.

impose *supergauge* transformations on the superfields and see what consequenses that implies.

The supergauge transformation on a left-handed scalar superfield under a gauge group G is defined as

$$\Phi \to \Phi' = e^{-iq\Lambda^a T_a}\Phi, \tag{2.32}$$

where T_a are the group generators, q is the charge of Φ under G, and the parameters of the gauge transformation Λ_a can be shown to be left-handed scalar superfields themselves. The supergauge transformation on a right-handed scalar superfields is similar.[5]

Requiring gauge invariance of the superpotential W puts great restrictions on the form of the superpotential and the charge assignments of the superfields. We will not go into detail on this in this thesis. To make the kinetic term gauge invariant, gauge compensating vector superfields V^a, with the appropriate gauge transformations, are introduced through a modification of the kinetic term,

$$\Phi^\dagger e^{qV^a T_a}\Phi. \tag{2.33}$$

The kinetic term then transforms as

$$\Phi^\dagger e^{qV^a T_a}\Phi \to \Phi'^\dagger e^{qV'^a T_a}\Phi' = \Phi^\dagger e^{iq\Lambda^{a\dagger} T_a} e^{qV'^a T_a} e^{-iq\Lambda^a T_a}\Phi, \tag{2.34}$$

which is invariant if the vector superfields transform as

$$e^{qV'^a T_a} = e^{-iq\Lambda^{a\dagger} T_a} e^{qV^a T_a} e^{iq\Lambda^a T_a}. \tag{2.35}$$

2.4.2 Supersymmetric field strength

We now have a general Lagrangian that is invariant under both supersymmetry and gauge transformations. But there is still one thing missing — we need to include field strength terms for the gauge fields.

Supersymmetric field strength is defined by

$$W_A \equiv -\frac{1}{4}\bar{D}\bar{D}e^{-V^a T_a} D_A e^{V^a T_a}, \tag{2.36}$$

$$\bar{W}_{\dot{A}} \equiv -\frac{1}{4} D D e^{-V^a T_a} \bar{D}_{\dot{A}} e^{V^a T_a}, \tag{2.37}$$

where W_A and $\bar{W}_{\dot{A}}$ are left- and right-handed scalar superfields, respectively. A gauge invariant combination of these are needed in the Lagrangian. It can be shown that the trace,

$$\mathrm{Tr}[W^A W_A], \tag{2.38}$$

[5]Here, the gauge transformation parameters $\Lambda^\dagger$ are right-handed scalar superfields.

fulfills this criterion.

If W_A is expanded in component fields, we find that it contains the ordinary Standard Model field strength tensor,

$$F^a_{\mu\nu} = \partial_\mu V^a_\nu - \partial_\nu V^a_\mu + q f_{bc}{}^a V^b_\mu V^c_\nu, \tag{2.39}$$

and that the trace contains the Standard Model field strength terms $F^a_{\mu\nu}F^{\mu\nu a}$.

2.4.3 General supersymmetric Lagrangian

Gathering all the ingredients gives an expression for the most general supersymmetric Lagrangian:

$$\mathcal{L} = \Phi^\dagger e^{qV^a T_a}\Phi + \bar\theta\bar\theta W[\Phi] + \theta\theta W[\Phi^\dagger] + \frac{1}{2T(R)}\bar\theta\bar\theta \mathrm{Tr}[W^A W_A], \tag{2.40}$$

where $T(R)$ is a normalization constant for the chosen representation of the gauge group called the *Dynkin index*.

2.5 Supersymmety breaking

As noted already in Sec. 2.1, supersymmetry must be a broken symmetry in order to produce the mass differences between the Standard Model and supersymmetry particles required by experiment. This property is not contained in the expression for the general supersymmetry Lagrangian we ended up with in the previous section, Eq. (2.40), so we need to do something about that.

Supersymmetry is expected to be broken *spontaneously*. This means that the Lagrangian itself is invariant under supersymmetry transformations, but the vacuum state is not. In this case, the properties of the vacuum can supply the extra mass of the supersymmetry particles compared to their SM partners. This is analogous to the Standard Model, where the initially massless gauge bosons acquire mass through the Higgs mechanism.

A common assumption is that the supersymmetry breaking takes place in a *hidden sector* at some high energy scale that we do not have access to. By hidden, we mean that fields in this sector have very small or no direct couplings to the fields in our visible sector. The effects of a non-zero *vacuum expectation value* (vev) in the hidden sector are mediated down to the visible sector through some interaction that is common to both sectors. There are several alternative models for how exactly this takes place, and we will mention one of the most popular.In Planck-scale Mediated Supersymmetry Breaking (PMSB), some gravity mechanism at the Planck scale, $\Lambda_P \sim 10^{18}$ GeV is assumed to mediate the supersymmetry breaking from the hidden sector down to the visible sector.

PMSB is assumed to be the supersymmetry breaking mechanism in the Constained Supersymmetric Standard Model (CMSSM), which will be introduced in Sec. 2.10.

In practice, in cases where the underlying symmetry-breaking mechanism is unknown (as for supersymmetry) it is common to use an effective phenomenological theory constructed from an originally symmetric (non-broken) theory, by adding terms that explicitly breaks the symmetry. This is known as *explicit symmetry breaking*. However, we cannot simply add arbitrary terms to the Lagrangian. Only so-called *soft terms*, with couplings of mass dimension one or higher, are allowed. Terms with smaller mass dimension can lead to divergences in loop contributions to scalar masses that are quadratic or worse. We will return to this in Sec. 3.1. The allowed supersymmetry breaking terms are in superfield notation written as

$$\begin{aligned}\mathcal{L}_{\text{soft}} = &-\frac{1}{4T(R)}M\theta\theta\bar{\theta}\bar{\theta}\text{Tr}[W^A W_A] - \frac{1}{6}a_{ijk}\theta\theta\bar{\theta}\bar{\theta}\Phi_i\Phi_j\Phi_k \\ &-\frac{1}{2}b_{ij}\theta\theta\bar{\theta}\bar{\theta}\Phi_i\Phi_j - t_i\theta\theta\bar{\theta}\bar{\theta}\Phi_i + \text{h.c.} \\ &- m_{ij}^2\theta\theta\bar{\theta}\bar{\theta}\Phi_i^\dagger\Phi_j.\end{aligned} \tag{2.41}$$

Only the lowest order component fields of the superfields contribute, due to the factor of $\theta\theta\bar{\theta}\bar{\theta}$ in each term.

The above terms are not necessarily gauge invariant. Requiring gauge invariance puts restrictions on the allowed terms, in the same way as it did for the superpotential. However, it turns out that the soft terms are responsible for most of the parameters in supersymmetric theories. This will become clear in the next section, where a specific theory is constructed.

In terms of component fields, the soft terms can be written as

$$\mathcal{L}_{\text{soft}} = -\frac{1}{2}M\lambda^A\lambda_A - \left(\frac{1}{6}a_{ijk}A_iA_jA_k + \frac{1}{2}b_{ij}A_iA_j + t_iA_i + \text{c.c.}\right) - m_{ij}^2A_i^*A_j, \tag{2.42}$$

where λ_A are Weyl spinor fields and A_i are scalar fields. This shows that the soft terms give masses to both the scalar and the fermionic superpartners of the SM particles.

2.6 The Minimal Supersymmetric Standard Model

The Minimal Supersymmetric Standard Model (MSSM) is based on the minimal extension of the Poincaré algebra, namely $N = 1$ supersymmetry. It is the supersymmetric model with the smallest field content consistent with the Standard

Model. In this section, it will be constructed from superfields following the recipe of the previous sections.

As explained in Sec. 2.3.3, two Weyl spinors of opposite handedness (from different superfields) are needed to construct a Dirac fermion and its antiparticle. Since each scalar superfield ultimately has two bosonic degrees of freedom in addition to a Weyl spinor, we also get four scalars — two particle-antiparticle pairs — from constructing a Standard Model fermion. They are the bosonic superpartners of the SM fermions, collectively called *sfermions*.

For the leptons, we introduce the scalar superfields

$$L_i = \begin{pmatrix} \nu_i \\ l_i \end{pmatrix} \quad \text{and} \quad \bar{E}_i, \tag{2.43}$$

where l_i and $\bar{E}_i$ are for the charged leptons, ν_i is for the (left-handed) neutrinos and i is the generation index. The $\bar{E}_i$ superfield contains the part of the anti-(s)electrons that do not couple to $SU(2)_L$, while l_i and ν_i are placed in $SU(2)_L$ doublets L_i. From these three fields (and their hermitian conjugates), all of the Standard Model leptons and their bosonic superpartners, called *sleptons*, are constructed.

Similarly, for up- and down-type quarks we introduce the scalar superfields

$$Q_i = \begin{pmatrix} u_i \\ d_i \end{pmatrix}, \quad \bar{U}_i \quad \text{and} \quad \bar{D}_i. \tag{2.44}$$

From these four fields and their hermitian conjugates, all of the Standard Model quarks as well as their bosonic superpartners, called *squarks*, are constructed.

For the gauge bosons we need to introduce vector superfields. As already noted in Sec. 2.3.3, each vector superfield contains one massless vector boson and two Weyl spinors of opposite handedness. One vector superfield V^a per generator T_a of the gauge groups $SU(3)_C$, $SU(2)_L$ and $U(1)_Y$ contained in the SM are needed to obey (super)gauge invariance. They are denoted

$$C^a, \quad W^a \quad \text{and} \quad B^0, \tag{2.45}$$

respectively. Altogether, these $8+3+1=12$ vector superfields give the g, $W^{1,2,3}$ and B^0 gauge bosons of the SM (before the Higgs mechanism), as well as their fermionic superpartners. The latter are referred to as the gluino, wino and bino, and are denoted by $\tilde{g}$, $\tilde{W}^a$ and $\tilde{B}^0$, respectively.

In the MSSM, two Higgs superfield $SU(2)_L$ doublets are needed in order to give mass to both up- and down-type quarks. In the Standard Model, one doublet can be used for both types by rotating its components using the $SU(2)_L$ generators, but this cannot be done in the MSSM, as it would mix left- and right-handed superfields in the superpotential. The two Higgs doublets are

$$H_u = \begin{pmatrix} H_u^+ \\ H_u^0 \end{pmatrix} \quad \text{and} \quad H_d = \begin{pmatrix} H_d^0 \\ H_d^- \end{pmatrix}, \tag{2.46}$$

where the sign indicates electric charge of the component superfields. These four left-handed scalar superfields introduce altogether four Weyl spinors and eight bosonic degrees of freedom. Three of the latter are absorbed into mass terms for the $W^{\pm}$ and Z^0 bosons through the Higgs mechanism, leaving five physical scalar degrees of freedom that are manifest through the mass eigenstates h^0, H^0, A^0 and $H^{\pm}$. The Weyl spinors combine into so-called *higgsinos*.

We have now introduced all the superfields needed to reconstruct the Standard Model content, and are ready to write down the Lagrangian. From Secs. 2.4 and 2.5, it is clear that the total MSSM Lagrangian has to include kinetic terms, superpotential terms, supersymmetric field strength terms and soft supersymmetry breaking terms:

$$\mathcal{L}_{\text{MSSM}} = \mathcal{L}_{\text{kin}} + \mathcal{L}_W + \mathcal{L}_V + \mathcal{L}_{\text{soft}}. \tag{2.47}$$

The kinetic terms are given by

$$\begin{aligned}\mathcal{L}_{\text{kin}} =& L_i^\dagger e^{\frac{1}{2}g\sigma W - \frac{1}{2}g'B} L_i + Q_i^\dagger e^{\frac{1}{2}g_s\lambda C + \frac{1}{2}g\sigma W + \frac{1}{3}\cdot\frac{1}{2}g'B} Q_i \\ &+ \bar{U}_i^\dagger e^{\frac{1}{2}g_s\lambda C - \frac{4}{3}\cdot\frac{1}{2}g'B}\bar{U}_i + \bar{D}_i^\dagger e^{\frac{1}{2}g_s\lambda C + \frac{2}{3}\cdot\frac{1}{2}g'B}\bar{D}_i \\ &+ \bar{E}_i^\dagger e^{2\cdot\frac{1}{2}g'B}\bar{E}_i + H_u^\dagger e^{\frac{1}{2}g\sigma W + \frac{1}{2}g'B} H_u + H_d^\dagger e^{\frac{1}{2}g\sigma W - \frac{1}{2}g'B} H_d.\end{aligned} \tag{2.48}$$

where g_s, g and g' are the coupling constants of $SU(3)_C$, $SU(2)_L$ and $U(1)_Y$, respectively.

The supersymmetric field strength terms are

$$\mathcal{L}_{\mathcal{V}} = \frac{1}{2}\text{Tr}[W^A W_A]\bar{\theta}\bar{\theta} + \frac{1}{2}\text{Tr}[C^A C_A]\bar{\theta}\bar{\theta} + \frac{1}{4}B^A B_A \bar{\theta}\bar{\theta} + \text{h.c.}, \tag{2.49}$$

where the field strengths are given by

$$W_A = -\frac{1}{4}\bar{D}\bar{D}e^{-W}D_A e^W, \quad W = \frac{1}{2}g\sigma^a W^a, \tag{2.50}$$

$$C_A = -\frac{1}{4}\bar{D}\bar{D}e^{-C}D_A e^C, \quad C = \frac{1}{2}g_s\lambda^a C^a, \tag{2.51}$$

$$B_A = -\frac{1}{4}\bar{D}\bar{D}D_A B, \quad B = \frac{1}{2}g'B^0. \tag{2.52}$$

For the superpotential, the terms that preserve gauge invariance are

$$\begin{aligned}W =& \mu H_u H_d + \mu_i' L_i H_u + y_{ij}^e L_i H_d \bar{E}_j + y_{ij}^u Q_i H_u \bar{U}_j + y_{ij}^d Q_i H_d \bar{D}_j \\ &+ \lambda_{ijk} L_i L_j \bar{E}_k + \lambda_{ijk}' L_i Q_j \bar{D}_k + \lambda_{ijk}'' \bar{U}_i \bar{D}_j \bar{D}_k,\end{aligned} \tag{2.53}$$

where $H_u H_d$ is shorthand for $H_u^T i\sigma_2 H_d$, and similarly for the other doublet pairs. The $i\sigma_2$ construction preserves $SU(2)_L$ invariance.

The soft supersymmetry breaking terms $\mathcal{L}_{\text{soft}}$ are presented below, after the concept of *R-parity* has been introduced.

2.6.1 R-parity

There are no renormalizable terms in the Standard Model Lagrangian that violate conservation of baryon number B and lepton number L, and indeed, no B or L violating processes have been observed experimentally. In the MSSM, with only general requirements of gauge and supersymmetry invariance, B and L are no longer conserved. The terms LH_u, $LL\bar{E}$ and $LQ\bar{D}$ in the superpotential violate lepton number conservation, while the term $\bar{U}\bar{D}\bar{D}$ violate baryon number conservation. This can lead to unacceptable predictions, e.g. rapid proton decay. Since the experimental lower limit of the proton lifetime is $\tau_{\text{proton}} > 10^{33}$ years [21], the couplings of the B and L violating terms need to be suppressed.

This can be done by setting all such terms to zero by hand, by assuming that some unknown mechanism suppresses them. However, a more elegant way is to introduce a new symmetry. The latter is done in the MSSM, by requiring that all the interactions conserve the discrete and multiplicative R-parity, which is defined as

$$P_R \equiv (-1)^{3(B-L)+2s}, \tag{2.54}$$

where s is particle spin. From this it follows that all SM particles and the additional Higgs bosons of the MSSM have $P_R = +1$, while all sparticles have $P_R = -1$.

Three important consequences follow from the fact that R-parity is required to be conserved in the MSSM:

- When produced from SM particles, sparticles can occur in pairs only.
- Sparticles decay into an odd number of lighter sparticles (most often just one).
- The lightest sparticle (LSP) has to be absolutely stable since it has nothing to decay into, which means that all sparticle decay chains end with the LSP.

From the above, it follows that supersymmetric particles typically will decay in *cascades* down to the LSP, emitting multiple Standard Model particles along the way. It also means that the LSP has to be invisible to detectors, or else it would have been observed already. Which again means that the LSP has to interact weakly (at most), and thus has to be both color and electrically neutral. It is therefore a good candidate for particle dark matter discussed in Section 1.6.

With R-parity conservation, the B or L violating terms mentioned at the beginning of this subsection are all excluded from the superpotential. In addition, requiring both R-parity conservation and gauge invariance, the possible soft

supersymmetry breaking terms in the MSSM are, in component fields,

$$\begin{aligned}\mathcal{L}_{\text{soft}} =& \left(-\frac{1}{2}M_1\tilde{B}\tilde{B} - \frac{1}{2}M_2\tilde{W}^a\tilde{W}^a - \frac{1}{2}M_3\tilde{g}^a\tilde{g}^a + \text{c.c.}\right) \\ &+ \left(-bH_uH_d - a^e_{ij}\tilde{L}_iH_d\tilde{e}^*_{jR} - a^u_{ij}\tilde{Q}_iH_u\tilde{u}^*_{jR} - a^d_{ij}\tilde{Q}_iH_d\tilde{d}^*_{jR} + \text{c.c.}\right) \\ &- (m^L_{ij})^2\tilde{L}^\dagger_i\tilde{L}_j - (m^e_{ij})^2\tilde{e}^*_{iR}\tilde{e}_{jR} - (m^Q_{ij})^2\tilde{Q}^\dagger_i\tilde{Q}_j - (m^u_{ij})^2\tilde{u}^*_{iR}\tilde{u}_{jR} \\ &- (m^d_{ij})^2\tilde{d}^*_{iR}\tilde{d}_{jR} - m^2_{H_u}H^\dagger_uH_u - m^2_{H_d}H^\dagger_dH_d.\end{aligned} \tag{2.55}$$

After removing all "excessive" freedom through possible field redefinitions, it becomes clear that the MSSM introduces in total 105 new parameters in addition to the SM parameters. The superpotential parameter μ is the only one that does not come from the soft breaking terms.

2.7 Radiative electroweak symmetry breaking

In the Standard Model, the massive vector bosons (and also the fermions) acquire mass through electroweak symmetry breaking (the Higgs mechanism), describen in Sec. 1.4. In the MSSM, the soft terms are accountable for boosting the sparticle masses, but electroweak symmetry breaking is still needed. The corresponding mechanism in the MSSM is called *radiative* electroweak symmetry breaking.

In the MSSM, the scalar Higgs potential is, in terms of component fields,

$$\begin{aligned}V(H_u, H_d) =& |\mu|^2\left(|H^0_u|^2 + |H^+_u|^2 + |H^0_d|^2 + |H^-_d|^2\right) \\ &+ \frac{1}{8}\left(g^2 + g'^2\right)\left(|H^0_u|^2 + |H^+_u|^2 - |H^0_d|^2 - |H^-_d|^2\right)^2 \\ &+ \frac{1}{2}g^2|H^+_uH^{0*}_d + H^0_uH^{-*}_d|^2 \\ &+ m^2_{H_u}\left(|H^0_u|^2 + |H^+_u|^2\right) + m^2_{H_d}\left(|H^0_d|^2 + |H^-_d|^2\right) \\ &+ \left[b\left(H^+_uH^-_d - H^0_uH^+_d\right) + \text{c.c.}\right],\end{aligned} \tag{2.56}$$

where μ is the superpotential parameter, b, m_{H_u} and m_{H_d} are parameters from the soft breaking terms, and g and g' are the $SU(2)_L$ and $U(1)_Y$ couplings, respectively. This potential has eight degrees of freedom from the four complex scalar fields H^+_u, H^0_u, H^-_d and H^0_d.

In the same way as in the Standard Model, we now want to break $SU(2)_L \times U(1)_Y$ down to $U(1)_{\text{em}}$ in order to give masses to the SM gauge bosons and fermions. To do this, three properties are needed for the scalar Higgs potential:

- It has to be bounded from below.
- It has to have a minimum for non-zero field values.
- This minimum must have a remaining $U(1)_{\text{em}}$ symmetry.

The latter can be obtained by using $SU(2)_L$ gauge freedom to set $H_u^+ = 0$ at the minimum of the potential. One can show that this also leads to $H_d^- = 0$, since $\partial V/\partial H_u^+ = 0$ at the minimum. In that case, $U(1)_{\text{em}}$ symmetry is guaranteed, since the electrically charged fields have no vacuum expectation value. We are then left with the potential

$$\begin{aligned} V(H_u, H_d) = &\left(|\mu|^2 + m_{H_u}^2\right)|H_u^0|^2 + \left(|\mu|^2 + m_{H_d}^2\right)|H_d^0|^2 \\ &+ \frac{1}{8}\left(g^2 + g'^2\right)\left(|H_u^0|^2 - |H_d^0|^2\right)^2 - \left(bH_u^0 H_d^0 + \text{c.c.}\right). \end{aligned} \tag{2.57}$$

It can be shown [22] that the two former conditions for electroweak symmetry breaking are fulfilled if

$$b > \left(|\mu|^2 + m_{H_u}^2\right)\left(|\mu|^2 + m_{H_d}^2\right), \tag{2.58}$$

and

$$2b < 2|\mu|^2 + m_{H_u}^2 + m_{H_d}^2, \tag{2.59}$$

where Eq. (2.58) ensures that the potential has a minimum for non-zero field values — or in other words: a negative mass term — and Eq. (2.59) ensures that the potential is bounded from below.

Like any other quantum field theory, the MSSM is subject to renormalization, which leads to RGE running of the coupling constants and masses of the model, as discussed in Sec. 1.5. If we assume that $m_{H_u}^2 = m_{H_d}^2$ at some high energy scale, e.g. $\Lambda_{\text{GUT}} \sim 10^{16}$ GeV, Eqs. (2.58) and (2.59) cannot simultaneously be satisfied *at that scale*. However, both these masses run down with energy, and the extent of the running is mostly determined by their Yukawa couplings. Since the top Yukawa coupling dominate the running of $m_{H_u}^2$, while the bottom Yukawa coupling does the same for $m_{H_d}^2$, the former runs down much faster than the latter, and can in fact become negative. In that case, both of the above equations can be fulfilled simultaneously, leading to the wanted symmetry breaking. This is called radiative electroweak symmetry breaking (REWSB), and gives an explanation for the Higgs mechanism. The term *radiative* comes from the fact that the symmetry breaking in this case is driven by quantum corrections from the running. This is in contrast to the Standard Model, where the Higgs mechanism is put in by hand.

One of the wanted results of the symmetry breaking is that the neutral components of both the Higgs doublets acquire a non-vanishing vacuum expectation value, $v_u = \langle H_u^0 \rangle$ and $v_d = \langle H_d^0 \rangle$, respectively. These must relate to the Standard Model vector boson masses through

$$v^2 = v_u^2 + v_d^2 = \frac{2m_Z^2}{g^2 + g'^2} \approx (174\,\text{GeV})^2. \tag{2.60}$$

This relation gives one free parameter, for the vevs, which conventionally is parametrized as

$$\tan\beta \equiv \frac{v_u}{v_d}, \tag{2.61}$$

Table 2.2: The particle spectrum of the MSSM. SM fermions and bosons are not included.

Name	Spin	P_R	Gauge eigenstates	Mass eigenstates
Higgs bosons	0	+1	$H_u^0\ H_d^0\ H_u^+\ H_d^-$	$h^0\ H^0\ A^0\ H^\pm$
squarks	0	−1	$\tilde{u}_L\ \tilde{u}_R\ \tilde{d}_L\ \tilde{d}_R$	(same)
			$\tilde{s}_L\ \tilde{s}_R\ \tilde{c}_L\ \tilde{c}_R$	(same)
			$\tilde{t}_L\ \tilde{t}_R\ \tilde{b}_L\ \tilde{b}_R$	$\tilde{t}_1\ \tilde{t}_2\ \tilde{b}_1\ \tilde{b}_2$
sleptons	0	−1	$\tilde{e}_L\ \tilde{e}_R\ \tilde{\nu}_e$	(same)
			$\tilde{\mu}_L\ \tilde{\mu}_R\ \tilde{\nu}_\mu$	(same)
			$\tilde{\tau}_L\ \tilde{\tau}_R\ \tilde{\nu}_\tau$	$\tilde{\tau}_1\ \tilde{\tau}_2\ \tilde{\nu}_\tau$
neutralinos	1/2	−1	$\tilde{B}^0\ \tilde{W}^0\ \tilde{H}_u^0\ \tilde{H}_d^0$	$\tilde{\chi}_1^0\ \tilde{\chi}_2^0\ \tilde{\chi}_3^0\ \tilde{\chi}_4^0$
charginos	1/2	−1	$\tilde{W}^\pm\ \tilde{H}_u^+\ \tilde{H}_d^-$	$\tilde{\chi}_1^\pm\ \tilde{\chi}_2^\pm$
gluino	1/2	−1	$\tilde{g}$	(same)

where $0 < \beta < \pi/2$.

Using the condition for the existence of an extremal point (minimum),

$$\frac{\partial V}{\partial H_u^0} = \frac{\partial V}{\partial H_d^0} = 0, \tag{2.62}$$

b and $|\mu|$ can be eliminated as free parameters from the model.[6] Alternatively, we can choose to eliminate $m_{H_u}^2$ and $m_{H_d}^2$.

2.8 Particle phenomenology of the MSSM

The field content of the MSSM was presented in Sec. 2.6, along with some information on what particles the different fields form. In this section, more detailed information on the physical particles will be given. To get an overview, all of the

[6] However, not the sign of μ.

supersymmetry particles (and Higgs) in the MSSM are listed in Table 2.2. The SM fermions and bosons are not included.

As previously noted, each Standard Model fermion get two superpartner scalar particles, with the same gauge charges. For instance, the superpartners of the up-quark u are labeled $\tilde{u}_R$ and $\tilde{u}_L$, where the indices R and L denote that they couple to the left- and right-handed parts of the up-quark, respectively. Due to effects from supersymmetry breaking and electroweak symmetry breaking, the sparticle mass eigenstates are in general mixtures of the gauge eigenstates. For the sfermions (sleptons and squarks), the amount of mixing can be shown to be proportional to the masses (or more precisely, the Yukawa couplings) of their corresponding SM fermions, and is therefore negligible for the two first generations. All mixed mass eigenstates are numbered according to increasing mass, e.g. $\tilde{t}_1$ is the lighter of the two stops.

The fermionic superpartners of the SM gauge bosons are collectively called gauginos. From Table 2.2, we see that the gauge and mass eigentstates are identical for the gluino, the superpartner of the Standard Model gluon. This is because the gluino is a color octet Majorana fermion, and thus has nothing to mix with in the MSSM. The superpartners of the B^0 and $W^{1,2,3}$ fields, which in the SM make up the photon, Z and $W^{\pm}$ bosons, $\tilde{B}^0, \tilde{W}^0$ and $\tilde{W}^{\pm}$, mix with the superpartner Higgs fields (the higgsinos) and form the so-called *neutralinos* and *charginos*. The neutralinos are four neutral Majorana fermions, labeled $\tilde{\chi}_i^0$, $i = 1, ..., 4$, while the charginos are two charged fermion–antifermion pairs, labeled $\tilde{\chi}_i^{\pm}$, $i = 1, 2$, as seen in the above table. The lightest neutralino $\tilde{\chi}_1^0$ is the lightest supersymmetric particle (LSP) in most of the MSSM parameter space.

The mixing of the MSSM Higgs sector was touched on already in Sec. 2.6. In addition to the Standard Model like Higgs h, there are four other scalar Higgs particles after mixing (the Higgs mechanism), labeled H, $H^{\pm}$ and A^0. H is also a neutral scalar such as h, except for its larger mass, and is therefore often called "heavy Higgs", in contrast to the "light Higgs" h which is similar to the one in the Standard Model.

2.8.1 Sparticle masses

The main contributions to the sparticle masses come from the soft supersymmetry breaking terms, which should not come as a surprise, since these terms were introduced to produce the mass differences between the SM and supersymmetry particles required by experiment. The mass parameters from these terms are the gaugino mass parameters $M_{1,2,3}$, the sfermion mass parameters m_{ij}^f, and the Higgs mass parameters m_{H_u} and m_{H_d}. Also the parameter μ, which couples the two Higgs doublets in the superpotential, contributes.

Expressions for the different sparticle masses are given below.

- At tree level, the different Higgs masses can be shown to be

$$m_A^2 = \frac{2b}{\sin 2\beta} = 2|\mu^2| + m_{H_u}^2 + m_{H_d}^2, \tag{2.63}$$

$$m_{h,H}^2 = \frac{1}{2}\left(m_A^2 + m_Z^2 \mp \sqrt{(m_A^2 - m_Z^2)^2 + 4m_Z^2 m_A^2 \sin^2 2\beta}\right), \tag{2.64}$$

$$m_{H^\pm} = m_A^2 + m_W^2. \tag{2.65}$$

- The gluino mass is given by

$$m_{\tilde{g}} = M_3\left[1 + \frac{\alpha_s}{4\pi}\left(15 + 6\ln\frac{\mu}{M_3} + \sum_{\text{all }\tilde{q}} A_{\tilde{q}}\right)\right], \tag{2.66}$$

  where α_s is the strong fine-structure constant, and $A_{\tilde{q}}$ are one-loop squark contributions given by

$$A_{\tilde{q}} = \int_0^1 dx\, x \ln\left(x\frac{m_{\tilde{q}}^2}{M_3^2} + (1-x)\frac{m_{\tilde{q}}^2}{M_3^2} - x(1-x) - i\epsilon\right). \tag{2.67}$$

- The neutralinos $\tilde{\chi}_i^0$ are the mass eigenstates of the neutral bino, wino and higgsino fields. In the gauge eigenstate basis

$$(\tilde{\psi}^0)^T = \left(\tilde{B}^0, \tilde{W}^0, \tilde{H}_d^0, \tilde{H}_u^0\right), \tag{2.68}$$

  the neutralino mass term can be written as

$$\mathcal{L}_{m_{\tilde{\chi}^0}} = -\frac{1}{2}(\tilde{\psi}^0)^T M_{\tilde{\chi}^0}\tilde{\psi}^0. \tag{2.69}$$

  At tree level, the mass matrix may be written as

$$M_{\tilde{\chi}^0} = \begin{bmatrix} M_1 & 0 & -c_\beta s_{\theta_W} m_Z & s_\beta s_{\theta_W} m_Z \\ 0 & M_2 & c_\beta c_{\theta_W} m_Z & -s_\beta c_{\theta_W} m_Z \\ -c_\beta s_{\theta_W} m_Z & c_\beta c_{\theta_W} m_Z & 0 & -\mu \\ s_\beta s_{\theta_W} m_Z & -s_\beta c_{\theta_W} m_Z & -\mu & 0 \end{bmatrix}, \tag{2.70}$$

  where $c_x = \cos x$ and $s_x = \sin x$, and θ_W is the weak mixing angle. The neutralino masses can be found by diagonalizing this matrix.

- Similarly, the charginos are the mass eigenstates of the charged wino and higgsino fields. In the gauge eigenstate basis

$$(\tilde{\psi}^\pm)^T = \left(\tilde{W}^+, \tilde{H}_u^+, \tilde{W}^-, \tilde{H}_d^-\right), \tag{2.71}$$

the chargino mass matrix may be written as

$$M_{\tilde{\chi}^\pm} = \begin{bmatrix} 0 & 0 & M_2 & \sqrt{2}c_\beta m_W \\ 0 & 0 & \sqrt{2}s_\beta m_W & \mu \\ M_2 & \sqrt{2}s_\beta m_W & 0 & 0 \\ \sqrt{2}c_\beta m_W & \mu & 0 & 0 \end{bmatrix}. \tag{2.72}$$

As for the neutralinos, the chargino masses can be found by diagonalizing this matrix.

- It was stated above that the first two generations of sfermions (to a good approximation) do not experience mixing. It can be shown that these sfermions therefore "only" get masses according to

$$m_F^2 = m_{F,\text{soft}}^2 + \Delta_F, \tag{2.73}$$

where $m_{F,\text{soft}}^2$ is the contribution from soft mass terms of the form $m_F^2 \tilde{F}^\dagger \tilde{F}$, and Δ_F is given by

$$\Delta_F = (T_{3F} - Q_F \sin^2\theta_W)\cos(2\beta) m_Z^2. \tag{2.74}$$

Here, T_{3F} and Q_F are the weak isospin and electric charge, respectively, of the left-handed supermultiplet F to which the sfermion belongs. For example, the masses of the left- and right-handed up squarks are

$$m_{\tilde{u}_L}^2 = m_{Q_1}^2 + \Delta_{\tilde{u}_L}, \tag{2.75}$$
$$m_{\tilde{u}_R}^2 = m_{u_1}^2 + \Delta_{\tilde{u}_R}, \tag{2.76}$$

respectively.

The mass splitting between same generation sleptons/squarks is then universal, and given by

$$m_{\tilde{e}_L}^2 - m_{\tilde{\nu}_L}^2 = m_{\tilde{d}_L}^2 - m_{\tilde{u}_L}^2 = -\cos(2\beta) m_W^2. \tag{2.77}$$

- Both the Yukawa and trilinear couplings are larger for third generation sfermions than for sfermions from the two first generations. Third generation sfermions thus have more complicated mass contributions. As an example, in the gauge eigenstate basis $(\tilde{t_L}, \tilde{t_R})$ for the stop quarks, the mass term is given by

$$\mathcal{L}_{m_{\tilde{t}}} = -(\tilde{t}_L, \tilde{t}_R) m_{\tilde{t}}^2 \begin{pmatrix} \tilde{t}_L \\ \tilde{t}_R \end{pmatrix}, \tag{2.78}$$

where the mass matrix is

$$m_{\tilde{t}}^2 = \begin{bmatrix} m_{Q_3}^2 + m_t^2 + \Delta_{\tilde{u}_L} & v(a_t^* \sin\beta - \mu y_t \cos\beta) \\ v(a_t \sin\beta - \mu^* y_t \cos\beta) & m_{u_3}^2 + m_t^2 + \Delta_{\tilde{u}_R} \end{bmatrix} \tag{2.79}$$

The mass eigenstates $\tilde{t}_1$ and $\tilde{t}_2$ can be found by diagonalizing this matrix. Similar expressions exists for sbottom squarks and staus.

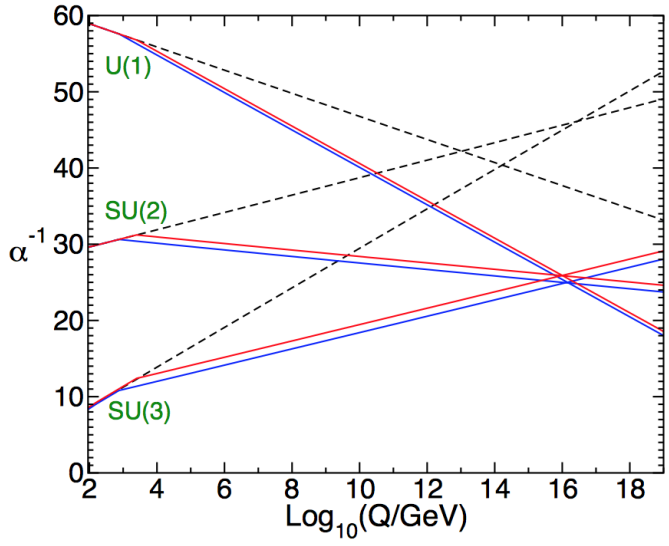

Figure 2.1: RGE evolution of the inverse couplings $\alpha_i^{-1} = 4\pi/g_i^2$ in the Standard Model (dashed lines) and the MSSM (solid lines) to two-loop order. Figure taken from [22].

2.9 Gauge coupling unification

As discussed in Sec. 1.6, one of the main motivations for extending the Standard Model is that it does not unite the three coupling constants g', g and g_s at some high energy scale. In supersymmetry, however, the evolution of the couplings is altered, and they can meet in a single point.

More specifically, with the MSSM field content, and the couplings

$$g_1 = \sqrt{\frac{5}{3}}g', \quad g_2 = g \quad \text{and} \quad g_3 = g_s, \tag{2.80}$$

the gauge couplings intersect at the GUT scale $\Lambda_{\text{GUT}} \approx 2\times 10^{16}$ GeV, see Fig. 2.1. The assumption is that a unified gauge group, e.g. SU(5) or SO(10), is broken down to the SM gauge group at that scale.[7]

An interesting feature can occur from this. If we assume, as explained above, that the coupling constants unify to a common coupling g_u at the GUT scale, and also that the gauginos have a common mass at the same scale: $m_{1/2} = M_1(\Lambda_{\text{GUT}}) = M_2(\Lambda_{\text{GUT}}) = M_3(\Lambda_{\text{GUT}})$, RGE evolution of the gaugino mass parameters M_i leads to the strikingly simple relation at one-loop level:

$$\frac{M_1}{g_1^2} = \frac{M_2}{g_2^2} = \frac{M_3}{g_3^2} = \frac{m_{1/2}}{g_u^2}, \tag{2.81}$$

[7]The somewhat odd normalization choice for g_1 is the correct numerical factor when breaking $SU(5)$ or $SO(10)$ down to the SM group. This factor might be different for a different unified group.

which is valid at all scales. In terms of the electromagnetic and strong fine-structure constants α and α_s, and the weak mixing angle θ_W, this leads to

$$M_3 = \frac{\alpha_s}{\alpha}\sin^2\theta_W M_2 = \frac{3}{5}\frac{\alpha_s}{\alpha}\cos^2\theta_W M_1, \tag{2.82}$$

which at a scale of 1 TeV numerically predicts

$$M_3 : M_2 : M_1 \approx 6 : 2 : 1. \tag{2.83}$$

If the lightest neutralino is mostly bino, and the second lightest neutralino and lightest charginos are mostly wino, which is true as long as $|mu| \gg M1, M2$, this gives the following relations between the sparticle masses:

$$m_{\tilde{g}} \approx 6m_{\tilde{\chi}_1^0} \quad \text{and} \quad m_{\tilde{\chi}_2^0} \approx m_{\tilde{\chi}_1^\pm} \approx 2m_{\tilde{\chi}_1^0}. \tag{2.84}$$

2.10 GUT scale motivated models

As briefly mentioned in Sec. 2.6.1, the MSSM introduces over 100 new parameters, where most of them come from the soft supersymmetry breaking terms. This means that further restricting assumptions on the supersymmetry breaking mechanism are needed to improve predictability.

2.10.1 The constrained CMSSM

A much studied theory is the *Constrained MSSM* (CMSSM), also known as *minimal supergravity* (mSUGRA). Planck-scale Mediated Supersymmetry Breaking, which was introduced in Sec. 2.5, is assumed in the CMSSM. Motivated by the wish for gauge unification, one also assumes a minimal form for the parameters at the GUT scale, resulting in a highly predictive theory parametrized by just four "and a half" free parameters:

$$m_{1/2},\ m_0,\ A_0,\ \tan\beta \text{ and } \mathrm{sign}(\mu). \tag{2.85}$$

The mass parameters m_0 and $m_{1/2}$ are the common scalar and gaugino masses, respectively, at the GUT scale. Further, A_0 is the common trilinear coupling, $\tan\beta$ was introduced in Sec. 2.7, while $\mathrm{sign}(\mu)$ is the sign of the by now well-known superpotential parameter μ.

The CMSSM is defined by choosing these input parameters at the GUT scale. By evolving the mass parameteres m_0 and $m_{1/2}$ down to a lower scale, the mass splitting between the individual sparticles appears. This is shown in Fig. 2.2 for a particular choice of the CMSSM parameters. This figure also shows that the quantity $(\mu^2 + m_{H_u}^2)^{1/2}$ (which appears in the Higgs potential) runs negative for low energies, providing for radiative electroweak symmetry breaking, as discussed in Sec. 2.7.

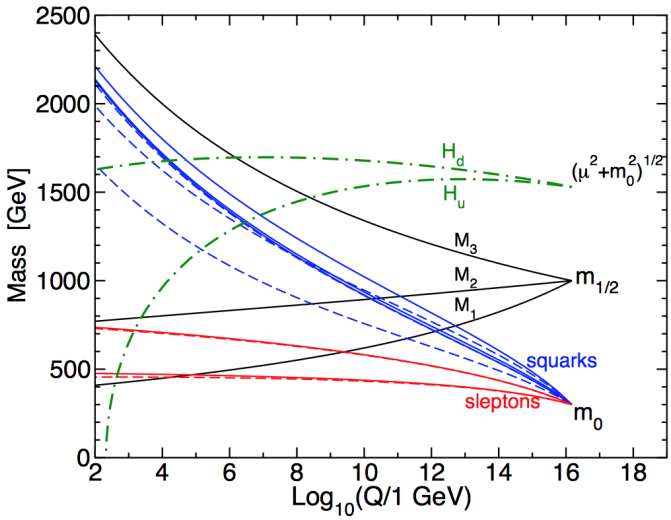

Figure 2.2: RGE evolution of the sfermion and gaugino masses in the MSSM, with CMSSM conditions $m_0 = 300$ GeV, $m_{1/2} = -A_0 = 1000$ GeV, $\tan\beta = 15$, and $\text{sign}(\mu) = +$. Figure taken from [22].

2.10.2 Non-Universal Higgs Mass models

While the universality of the sfermion masses is motivated by GUT theories, universality in the Higgs sector is less theoretically motivated. It can thus be tempting to generalise the CMSSM by letting the soft Higgs masses, $m^2_{H_u}$ and $m^2_{H_d}$, be non-universal.

The first Non-Universal Higgs Mass (NUHM1) model is a such a generalisation, which includes a common (but non-universal) soft Higgs mass at the GUT scale different from the common scalar mass m_0. It has only one single additional parameter, namely m_H:

$$m^2_{H_u} = m^2_{H_d} \equiv m^2_H, \tag{2.86}$$

which is the common mass for the two soft Higgs masses at the GUT scale.

A further generalisation can be done by allowing the two soft Higgs masses to take different values at the GUT scale, which is done in the second Non-Universal Higgs Mass (NUHM2) model.

The non-universality of the model may then either be parametrized by $m^2_{H_u}$ and $m^2_{H_d}$, or, by using Eq. (2.62), these may be eliminated for b and $|\mu|$, where b in turn can be traded for the pole mass m_A of the pseudo-scalar Higgs A^0, using Eq. (2.63).

Chapter 3

The hierarchy problem and naturalness

The concept of *naturalness*, concerning how comfortable we are with large numbers cancelling seemingly by chance, has been an important topic in particle physics over the last 30 years. However, with the discovery of the Higgs boson in 2012, the question of naturalness has come to the forefront. It turns out that the Higgs mass predicted by the Standard Model is off by $\sim$ 14–16 orders of magnitude compared to the measured mass. Whereas the Standard Model offers no explanation for this, and is thus regarded as a highly unnatural theory, supersymmetry provides an elegant solution. This is regarded as one of the main motivations for supersymmetry. However, since supersymmetry must be broken in order to produce the mass differences between the Standard Model and supersymmetric particles required by experiment, the problem is partially reintroduced, and needs to be taken into account also when considering supersymmetric theories.

3.1 The hierarchy problem

The physical Higgs boson mass squared can be expressed as

$$m_h^2 = (m_h^0)^2 + \Delta m_h^2, \tag{3.1}$$

where m_h^0 denotes the "bare" (non-renormalized) Higgs mass, closely related to the Higgs parameter μ in the SM Lagrangian[1], see Eq. (1.39), and Δm_h represents the radiative corrections to this mass due to self-energy loop diagrams like the ones in Fig. 3.1. Here, f is some fermion and s is some scalar, while λ_f and λ_s are their couplings to the Higgs boson. There exists diagrams like these for all the massive fermions and bosons in the SM, including the Higgs itself.

[1]Not to be confused with μ in the MSSM superpotential.

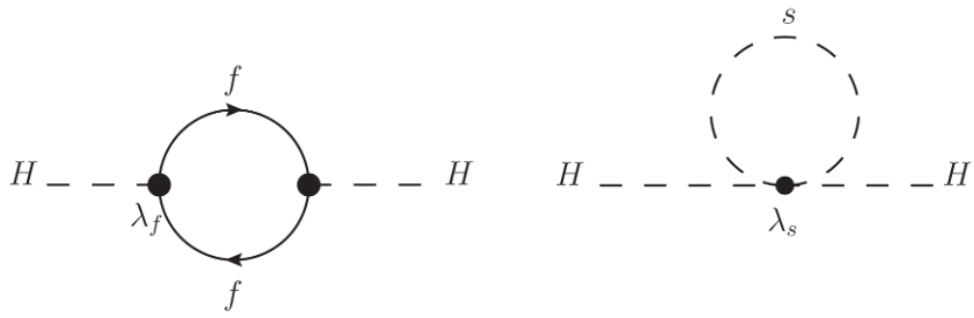

(a) Fermion loop. (b) Scalar loop.

Figure 3.1: One-loop contributions to the Higgs mass from fermions (a) and scalars (b). The largest contribution in the SM is from the top quark, for which $\lambda_f = \lambda_t \sim 1$. Figures taken from [23].

When evaluated in quantum field theory, these loop contributions diverge — meaning that they are infinite. This is clearly a problem, since the Higgs boson mass has been found to be ~ 125 GeV [24]. However, regularization, introduced in Sec. 1.5, comes to the rescue. By arguing that the SM is not valid at very high energies, where we know we need a yet to be discovered quantum theory of gravitation, a cut-off scale Λ (regulator) can be introduced to limit the integrals in the loop corrections to energies below this scale. The loop corrections to the Higgs mass, at leading order in Λ, is then

$$\Delta m_h^2 = -\frac{|\lambda_f|^2}{8\pi^2}\Lambda^2 + \frac{\lambda_s}{16\pi^2}\Lambda^2 + ..., \tag{3.2}$$

where the first term comes from fermion loops and the second term comes from scalar loops. The terms left out are at most logarithmically dependent on Λ. This high energy cut-off scale Λ is often taken to be the GUT scale, $\Lambda = \Lambda_{\text{GUT}} \sim 10^{16}$ GeV, or the Planck scale, $\Lambda = \Lambda_P \sim 10^{18}$ GeV, which gives very large corrections.

Since there is no apparent symmetry between the fermion and boson masses of the SM that could lead to an internal cancellation of the contributions to Δm_h^2, it is difficult to keep the Higgs mass at the electroweak scale of 10^2 GeV. This is known as the *hierarchy problem*.[2] In order to cancel the radiative corrections and end up with a physical Higgs mass of ~ 125 GeV, the contributions with different sign would have to be extremely fine-tuned. The hierarchy problem is therefore also referred to as a *fine-tuning problem*.

[2]In cosmology, the cosmological constant, observed as dark energy, is constrained by observations to be very tiny, i.e. around 10^{-3} eV. This is a hierarchy problem similar to that of the Higgs boson mass, but worse, since the cosmological constant interpreted as vacuum energy is also very sensitive to quantum corrections.

3.1.1 Supersymmetry solution

Introducing supersymmetry into the problem will increase the number of correction terms to the Higgs mass because of all the new supersymmetric particles. However, as supersymmetry is a fermion-boson symmetry, the correction terms from SM fermions turn out to cancel the correction terms from the new SUSY bosons, and vice versa. This is because there are exactly twice as many bosons as fermions in supersymmetry, and their couplings can be shown to satisfy the relation

$$|\lambda_f|^2 = \lambda_s. \tag{3.3}$$

For unbroken supersymmetry, the cancellation is exact for all orders of Λ, because the particles and their corresponding sparticles are mass degenerate. This is one of the main motivations for SUSY in the first place. In this case, the physical Higgs mass would simply correspond to the bare Higgs mass m_h^0.

However, since no sparticles have yet been observed, we know that SUSY is a broken symmetry. This makes the non-leading order terms in the expression for the correction, Eq. (3.2), important, as they are mass dependent. For *softly* broken supersymmetry, we end up with contributions to the Higgs mass of at most

$$\Delta m_h^2 = -\frac{\lambda_s}{16\pi^2} m_s^2 \ln\left(\frac{\Lambda^2}{m_s^2}\right) + ... \tag{3.4}$$

at leading order in Λ, where m_s is the mass scale of the soft breaking terms, which can be seen as the "extra" mass of the SUSY particles compared to their corresponding SM particles.[3] This is regarded as the main motivation for SUSY to be manifest at a relatively low energy scale, because m_s can not be too large if the above corrections ought to be small. In fact, $m_s \sim \mathcal{O}(1 \text{ TeV})$ is needed in order to keep the corrections of the same size as the tree level terms. This is often called the *little hierarchy problem*.

3.2 Naturalness

As explained in the previous section, the introduction of superpartners provides a solution to the "big" hierarchy problem in the Standard Model. But we are still left with the little hierarchy problem, due to the fact that SUSY is broken. It appears that a minimum of parameter fine-tuning is required in order to obtain predictions in agreement with observations.

Theories that require fine-tuned cancellations of large numbers in order to explain results are often thought to be theoretically unsatisfactory, or rather *unnatural*. It has been argued that fundamental parameters should be independent and uncorrelated. This has led to the concept of *naturalness* in theoretical

[3] In fact, the name "soft term" is given to those possible SUSY breaking terms that at worst give mass corrections logarithmic in Λ.

physics, which can be interpreted as the *heuristic rule* that parameters in a fundamental physical theory should not be too fine-tuned.[4,5]

Historically, the concept of naturalness has been formulated in several different ways. 't Hooft was the first to formulate a naturalness criterion in relation to particle physics, concerning small parameters and symmetries: in the late 1970s [26], he stated that a dimensionless parameter

> *is allowed to be much smaller than unity only if setting it to zero increases the symmetry of the theory. It this does not happen, the theory is unnatural.*

Around the same time, Susskind stated [27] that naturalness means that

> *the observable properties of a theory should be stable against minute variations of the fundamental parameters.*

This latter formulation is closer to the understanding of naturalness that we take on in this thesis, which will become clear shortly.

Obviously, the concept of naturalness does not only apply to the SM — which is an extreme case — and supersymmetric models. However, since one of the main reasons for investigating supersymmetry in the first place is that it provides a solution to the hierarchy problem, naturalness arguments have increased relevance to studies of supersymmetry. As we investigate in this thesis, experimental searches push the lower bounds on SUSY masses upwards. This causes the minimum fine-tuning that SUSY can have to increase, lowering our confidence in that the universe is supersymmetric at low energies.[6]

The question then becomes *how much* fine-tuning we are comfortable with. In order to answer that, we first need to introduce a measure for naturalness. A quantitative analogue of Susskind's formulation is introduced below.

3.2.1 Quantifying naturalness

As we have seen above, to keep the little hierarchy problem at bay, the soft masses of the sparticles can not be too far above the weak scale. However, these are free parameters of the theory, parametrizing our ignorance of the true (spontaneous) SUSY breaking at a possibly very high energy scale. A popular measure for naturalness is defined in terms of this tension between the electroweak scale,

[4] It is important to stress that this is an aesthetic criterion, not a physical one, but it has shown to be a powerful guiding principle in physics.

[5] Almost every branch of science has its own version of the naturalness concept. For example, in agriculture it refers to the acceptable level of product manipulation, while it in environmental sciences refers to the degree to which an area is pristine, i.e. free from human influence [25].

[6] However, high fine-tuning in itself should not be regarded as an argument to completely rule out a theory. That would immediately rule out the Standard Model.

represented by the Z boson mass m_Z, and the model parameters. In the 1980s, Barbieri and Giudice quantified naturalness — in the following denoted c — by relating it to the *sensitivity* of m_Z with respect to the model parameters θ_i [28]:

$$c \equiv \max_i\{|c_{\theta_i}|\}, \tag{3.5}$$

where

$$c_{\theta_i} = \frac{\partial \ln m_Z^2}{\partial \ln \theta_i} = \frac{\theta_i}{m_Z^2}\frac{\partial m_Z^2}{\partial \theta_i}. \tag{3.6}$$

A model with $c = 10$ suffers from a parameter tuning of no more than 10%, a model with $c = 100$ of no more than 1%, and so on. This means that the higher the naturalness score, the more fine-tuned are the parameters, and the more *unnatural* is the theory. In the original paper, Barbieri and Giudice chose the number 10 as a *natural* upper bound on c. However, as the experimental constraints became stronger, this limit has been pushed upwards. In this work, we will be rather agnostic about what exact amount of fine-tuning we will consider as natural, and rather quantify what we can learn about naturalness in supersymmetry from collider experiments.

3.3 Natural supersymmetry

In Eqs. (3.5) and (3.6), i runs over all the parameters in the model, in principle including the Standard Model parameters. However, by requiring that the Z boson mass corresponds to a minimum of the scalar potential in the radiative electroweak symmetry breaking of the MSSM, m_Z can be expressed in terms of MSSM scalar potential parameters only.[7] For large $\tan\beta$, i.e. large values for the ratio of the vevs of the two Higgs fields in the MSSM, we get the relation

$$m_Z^2 = -2(m_{H_u}^2 + |\mu|^2), \tag{3.7}$$

where $m_{H_u}^2$ is the soft mass for the up-type Higgs doublet, including radiative corrections, and μ is the superpotential Higgs mixing parameter. The terms on the right-hand side of Eq. (3.7) must combine into the correct value for m_Z of ~ 91 GeV.

Instead of worrying about the naturalness score of already existing SUSY models, so-called Natural SUSY models [29] have emerged as the result of an attempt at starting in the other end. They are based on the criterion that the amount of fine-tuning from Eq. (3.7) should be kept as low as possible, which in general is fulfilled if $m_{H_u}^2$ and μ do not become too large. This is easily seen

[7] Standard Model parameters enter again from loop corrections to the potential, the most important being the top Yukawa coupling.

by calculating the sensitivity of the Z boson mass with respect to these two parameters:

$$c_\mu = \frac{\mu}{m_Z^2}\frac{\partial m_Z^2}{\partial \mu} = \frac{-4\mu^2}{m_Z^2}, \tag{3.8}$$

$$c_{m_{H_u}} = \frac{m_{H_u}}{m_Z^2}\frac{\partial m_Z^2}{\partial m_{H_u}} = \frac{-4m_{H_u}^2}{m_Z^2}. \tag{3.9}$$

This requirement of small $m_{H_u}^2$ and μ leads to a standard set of phenomenological predictions for Natural SUSY models, which is summarized below.

First, as μ directly controls the higgsino masses, Natural SUSY predicts light higgsinos. In terms of mass eigenstates, this implies, unless either M_1 or M_2 is also very small, that the two lightest neutralinos and the lightest chargino are mostly higgsino and have similar masses, see Eqs. (2.70) and (2.72). Second, it can be shown that the most important one-loop contribution to $m_{H_u}^2$ is from top squarks, which means that also stops are expected to be light in Natural SUSY scenarios. The left-handed sbottom also contributes at one-loop and is expected to be rather light. Finally, at two-loop, the most important contribution is from gluinos. Thus, gluinos are not expected to be too heavy in Natural SUSY scenarios either. This is especially interesting, since gluinos are among the sparticles with the most stringent constraints from the previous LHC searches. The other sparticles not mentioned are less constrained by naturalness arguments.

In this thesis, Natural SUSY, represented by the second Non-Universal Higgs Mass (NUHM2) model introduced in Sec. 2.10, will be investigated as a contrast to its "parent model" CMSSM, which in general is not very natural given current LHC constraints. The goal is to quantify the reach of future colliders for different scenarios of these two models in terms of the range of naturalness covered, quantified by the Barbieri–Giudice measure. We will also quantify the reach in terms of the *information gained* about naturalness — a procedure that will be explained in detail in the next chapter.

From Sec. 2.10.2, it is clear that the NUHM2 model can be parametrized by the parameters m_0, $m_{1/2}$, A_0, $\tan\beta$, μ and m_A. What regions of this parameter space that are considered natural are discussed in Ref. [30], and the correponding framework is referred to as *Radiatively-driven Natural SUSY* (RNS). The sparticle mass spectrum of RNS differs from the spectrum listed above for "standard" Natural SUSY models in that it has quite heavy stop and bottom squarks, no lighter than 1 TeV.

A few comments should be made about the above discussion on naturalness and Natural SUSY. It is important to stress that the Barbieri–Giudice measure presented in Sec. 3.2.1 is only one out of several naturalness measures suggested in the literatue. For instance, a similar measure is *electroweak naturalness*, which is also based on the Z boson mass. Whereas the Barbieri–Giudice measure quantifies the *sensitivity* of m_Z with respect to changes in the model's (possibly very high scale) input parameters, electroweak naturalness determines the degree to

which the parameters that enter into the expression for m_Z are at the electroweak scale themselves (low fine-tuning), or much larger (high fine-tuning).

However, when actually using the Barbieri–Giudice measure, it is not given exactly what set of parameters that should be included in the analysis. In particular, should Standard Model parameters such as the top Yukawa coupling be included? In principle should all the model's parameters be included, but this is not always feasible in practice. What parameters we include in our naturalness analyses will be given in Chapter 5.

Finally, the basis for Natural SUSY was the fine-tuning from Eq. (3.7), i.e. the expression for the Z boson mass. However, the introduction of naturalness was given in context of the hierarchy problem and fine-tuning of the Higgs boson mass. It can be argued that the fine-tuning of these two parameters are closely related, since both are manifestations of the tension between the electroweak scale and the soft masses at a possibly very high scale.

Chapter 4

Statistics and inference

The main goal of physics is to construct mathematical models that describe nature. When observing some phenomenon, physicists seek to construct a mathematical model that predicts it. For instance, the most succesful theory of gravity (phenomenon) to date is *general relativity* (mathematical model), which was published by Einstein in 1915. How successful a model is depends on how well it actually agrees with the observed phenomenon. But how is such a model tested? The process of drawing conclusions about scientific models from observed data is called *statistical inference*, which has two main concepts: *parameter estimation* and *hypothesis testing*.

4.1 Parameter estimation and hypothesis testing

In parameter estimation, we assume that the overall model is correct, but we do not make any assumptions on the free parameters of the model a priori. We then try to determine what values for the free parameters that are preferred by the data. For instance, if we assume that the overall model for some quantity y is $y(x) = ax+b$, where x is some other quantity and a and b are the free parameters of the model, we want to find the values for a and b that makes the model fit the data best. See Fig. 4.1(a).

In hypothesis testing, on the other hand, we assume that a *particular* model is correct — we make a hypothesis — and ask whether this hypothesis is consistent with the data. If not, the hypothesis can be excluded. For instance, if we assume the same overall model as above, $y(x) = ax + b$, but with say $a = 1.8$ and $b = 5$, we want to check whether this hypothesis is consistent with the data.[1] See

[1]Hypothesis testing can also be used to test models without fixing the parameters. The hypothesis under study is then the overall model in itself. This is often called model comparison. We will not perform model comparison in this thesis, but both parameter estimation and hypothesis testing with fixed parameters are used.

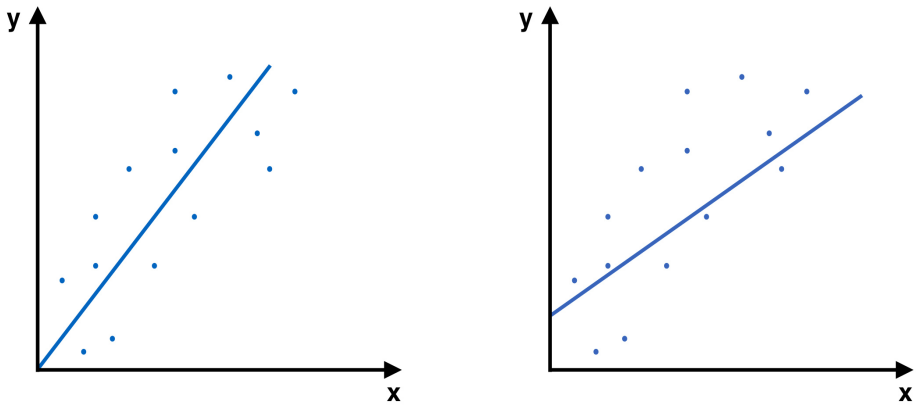

(a) Parameter estimation. (b) Hypothesis testing.

Figure 4.1: Two of the main concepts in statistical inference. In parameter estimation (a), the parameters are chosen so that the model fits the data. In hypothesis testing (b), we check how well a particular model fits the data, and determine whether this model (hypothesis) should be excluded or not.

Fig. 4.1(b). In this context, *p-values* are commonly used. The p-value is defined as the probability, under the assumption of a hypothesis, of obtaining a result equal to or "more extreme" (worse) than the observed data. If the p-value is low, the hypothesis can be excluded. A p-value of 0.05 is often used as the limit for exclusion, more about this in Sec. 4.8.

Simply put, statistical inference is all about trying to find the right model based on a set of known outcomes. This is in many ways the opposite of standard probability theory, which is mainly concerned with predicting outcomes for random variables given a known model. However, both concepts are dependent on how probability is interpreted. There are actually two different approaches to statistics, based on different interpretations of probability: *frequentist* and *Bayesian* statistics. The difference between the two will be discussed in the next section.

4.2 Frequentist and Bayesian statistics

In the frequentist interpretation of probability, probabilities can only be discussed when dealing with a *random* and *repeatable* experiment. The relative frequency of an outcome, observed in a number of repetitions of the experiment, is a measure of the probability of that outcome. Thus, if N is the total number of trials, and n_A is the number of trials with the outcome A, the probability $P(A)$ of outcome

A occuring is approximated by the relative frequency

$$P(A) \approx \frac{n_A}{N}. \tag{4.1}$$

As the number of trials is increased, the relative frequency becomes a better approximation to the "true" probability. In fact, in the frequentist approach, the relative frequency will converge exactly to the true probability when the number of trials approaches infinity:

$$P(A) = \lim_{N\to\infty} \frac{n_A}{N}. \tag{4.2}$$

The above interpretation of probability is useful when dealing with standard probability theory, for instance outcomes of games of chance. If we are told that a fair coin is flipped ten times, we can calculate the probability of yielding for example seven heads and three tails. This is often referred to as *deductive logic*. However, we may also want to know something about the reverse situation: if ten flips of a coin yields seven heads, can we say anything about whether the coin is fair or biased? This is related to statistical inference: it is similar to the challenges we face in physics when we try to pin down mathematical models based on observed phenomena, rather than the other way around. It has to do with *inductive logic*, or *plausible reasoning*, which in general is much more complex than deductive logic. The most we can hope to do is to make the best inference based on the experimental data and any prior knowledge we have available. The latter — prior knowledge — is the key feature of Bayesian statistics.

In the Bayesian interpretation, the probability $P(A)$ is defined as the *degree of belief* in proposition A or the *state of knowledge* about proposition A. This greatly extends the range of use of probability, since it is no longer only applicable to random and repeatable experiments. The foundation is that the rules of probability theory also applies for this interpretation of probability, not only the frequentist interpretation. In the Bayesian interpretation, every proposition is associated with a real number; the larger the numerical value associated with a proposition, the more we believe in it. These numbers obey the usual rules of probability theory:

$$P(A|I) + P(\bar{A}|I) = 1 \qquad \text{(sum rule)}, \tag{4.3}$$

$$P(A, B|I) = P(A|B, I) \times P(B|I) \qquad \text{(product rule)}, \tag{4.4}$$

where $P(\text{false}) = 0$ and $P(\text{true}) = 1$. Here, $\bar{A}$ denotes the proposition that A is false, the vertical bar is read as "given", and the comma is read as "and".

The sum rule states that the probability that A is true plus the probability that A is false is equal to one. The product rule states that the probability that both A and B are true is equal to the probability that A is true given that B is true times the probability that B is true (regardless of A). The probabilities

above are all conditional on I, which denotes the relevant background information at hand. It is important to stress that there is no such thing as an absolute probability in the Bayesian interpretation. For instance, the probability assigned to the proposition "it will rain tomorrow" depends on whether there are dark clouds or a clear blue sky the evening before.

For a general introduction to Bayesian methods, see Refs. [31, 32].

4.2.1 Bayes' theorem

The sum and product rules in Eqs. (4.3) and (4.4) form the basic algebra of probability theory, which many other results can be derived from. For instance, *Bayes' theorem* [33],

$$P(A|B,I) = \frac{P(B|A,I) \times P(A|I)}{P(B|I)}, \tag{4.5}$$

follows directly from the product rule.[2] This theorem is useful because it relates the probabilities $P(A|B,I)$ and $P(B|A,I)$. The importance of this property for the present discussion becomes apparent if we replace A by "hypothesis" and B by "data":

$$P(\text{hypothesis}|\text{data},I) = \frac{P(\text{data}|\text{hypothesis},I) \times P(\text{hypothesis}|I)}{P(\text{data}|I)}. \tag{4.6}$$

We see that Bayes' theorem relates the quantity of interest, namely the probability that the hypothesis is true given the data, to a quantity it is easier to find, namely the probability of the observed data if the hypothesis is true.

The various factors in Bayes' theorem have formal names. The left-hand side of Eq. (4.6) is called the *posterior probability*, often just referred to as the *posterior*. It represents our state of knowledge about the truth of the hypothesis in light of the data. Oppositely, the first factor in the nominator on the right hand side represents the probability for obtaining the observed data under the assumption that the hypothesis is true. When interpreted as a function of the hypothesis, it is referred to as the *likelihood*, and is often denoted $\mathcal{L}$. The second factor in the nominatior is called the *prior probability*, or simply *prior*, and is often denoted π. It represents our state of knowledge about the truth of the hypothesis before the data has been taken into account. The very concept of this factor is hard to accept for frequentists. They argue that this opens for *subjectivity*, which should not be part of probability theory. Bayesians, on the other hand, argue that objectivity is ensured as long as two people with identical

[2] As Bayes' theorem follows directly from the product rule of probability theory, it is equally valid in both frequentist and Bayesian statistics. But in the frequentist case, it has no dependency on any prior knowledge, here denoted I.

information assign identical priors. We will return the concept of objective priors in Sec. 4.4.

Finally, the denominator on the right hand side of Eq. (4.6) is often called the Bayesian *evidence*. It corresponds to the expression in the nominator *marginalized* over all possible hypotheses. For a discrete set of hypotheses H_i, which is both exhaustive, $\sum_i P(H_i|I) = 1$, and mutually exclusive, this means

$$P(D|I) = \sum_i P(D|H_i, I)P(H_i|I), \tag{4.7}$$

where D from now on stands for "data".

One of the key features of Bayesian statistics is that we are always allowed to update our belief in a hypothesis as new data becomes available. The posterior resulting from previous data then becomes the new prior.

Up until now, we have only discussed discrete probabilites. In the continuum limit, the above sum becomes an integral, and the probabilites become *probability distribution functions* (pdfs).

4.3 Exploring parameter spaces

In this thesis, Bayesian parameter estimation will be used to study the parameter spaces of the CMSSM and NUHM2 models introduced in Sec. 2.10. A hypothesis will in this case correspond to a particular choice of parameter values, assuming that the underlying model is correct. Such analyses thus tell us what parameter regions the data prefer relative to the rest of the model's parameter space.

In Sec. 2.10, we learned that the CMSSM and NUHM2 models are parameterised by four and six continuous parameters, respectively, in addition to the sign of the superpotential parameter μ for the CMSSM. However, in order for the analyses performed in this thesis to be computationally feasible, only two of the parameters are varied in each model scenario, while the rest are kept constant, leaving a simple two-dimensional parameter space to scan over.[3] The choice of parameters is discussed in Chapter 5, while the general analysis method is given below.

Starting from a model M with a set of parameters $\boldsymbol{\Theta}$, the goal of the Bayesian parameter estimation is to use a set of data $\mathbf{D}$ to determine the posterior pdf for the parameters, $P(\boldsymbol{\Theta}|\mathbf{D}, M)$. Bayes' theorem now reads

$$P(\boldsymbol{\Theta}|\mathbf{D}, M) = \frac{P(\mathbf{D}|\boldsymbol{\Theta}, M)P(\boldsymbol{\Theta}|M)}{P(\mathbf{D}|M)} \equiv \frac{\mathcal{L}(\boldsymbol{\Theta})\pi(\boldsymbol{\Theta})}{\mathcal{Z}}, \tag{4.8}$$

[3] If the number of free parameters is increased, we quickly fall victim to the so-called "curse of dimensionality": if d is number of parameters studied, and n is the number of evaluation points per parameter, the total number of evaluation points in a grid scan is n^d, which quickly becomes computationally intractable.

where the latter expression is written in a more compact notation, which will be used in the following. However, we emphasize that all quantites are conditioned on the overall model being true, and also on any available background information.

In this compact notation, it is evident that the likelihood $\mathcal{L}(\boldsymbol{\Theta}) = P(\mathbf{D}|\boldsymbol{\Theta}, M)$ can be interpreted as a function of the model parameters, given the data. The likelihood is actually not a pdf itself, but it is constructed from one. For every parameter point $\boldsymbol{\Theta}$ in the model, a pdf for an observable can be constructed. As an example, consider the Higgs mass m_h. It is common to assume a Gaussian pdf for mass measurements like this, where we often only have a central value with an error estimate, i.e. a width. So for every parameter point $\boldsymbol{\Theta}$, we construct a Gaussian centered at the Higgs mass $m_h(\boldsymbol{\Theta})$ predicted by the given parameter point, with standard deviation σ. By inserting the actual observed Higgs mass m_h^{obs} as data, this pdf can be evaluated at each point, and the resulting expression can be interpreted as a function of the model parameters:

$$\mathcal{L}^{\text{Higgs}}(\boldsymbol{\Theta}) \propto \exp\left[-\frac{(m_h(\boldsymbol{\Theta}) - m_h^{\text{obs}})^2}{2\sigma^2}\right]. \tag{4.9}$$

The likelihood function thus quantifies the level of agreement between the model and the data across the parameter space. It will become clear below that the normalizing factor is not important in Bayesian parameter estimation, since the denominator in Eq. (4.8) properly normalizes the posterior pdf. For independent observables, the total likelihood can be constructed as

$$\mathcal{L}(\boldsymbol{\Theta}) = \prod_i \mathcal{L}_i(\boldsymbol{\Theta}), \tag{4.10}$$

where $\mathcal{L}_i(\boldsymbol{\Theta})$ are the likelihoods for the individual observables.

The prior $\pi(\boldsymbol{\Theta}) = P(\boldsymbol{\Theta}|M)$ is in this case a pdf describing our degree of belief in a given parameter point, or, in the context of the example above, a given value of the Higgs mass, before the data has been introduced. Results from previous experiments or theoretical arguments may influence this belief. Finally, the Bayesian evidence $\mathcal{Z} = P(\mathbf{D}|M)$ is given by

$$\mathcal{Z} = \int \mathcal{L}(\boldsymbol{\Theta})\pi(\boldsymbol{\Theta})d\boldsymbol{\Theta}, \tag{4.11}$$

where we see that the dependence on the model parameters is integrated out. Thus, the evidence does not affect the shape of the posterior pdf across the parameter space, and is therefore nothing else than a normalizing factor in Bayesian parameter estimation.[4]

[4]This is in contrast to Bayesian hypothesis testing in the form of model comparison, where the evidence is a key quantity.

Equation (4.8) gives a recipe for finding the posterior pdf for the parameters starting from a prior pdf and a likelihood function based on the data. In addition to the Higgs likelihood function introduced above, with the observed Higgs mass as data, we will in this work use accelerator simulations to obtain likelihood functions for future supersymmetry searches, which takes the rôle of data. A detailed explanation of this procedure will be given in Sec. 4.7. But first, the basic prior pdfs used for the parameters in this thesis is introduced in the next section.

4.4 Objective priors

As briefly mentioned in the previous section, the prior is a pdf describing our degree of belief in a given parameter point before the data has been introduced. The prior $\pi(\boldsymbol{\Theta})$ is constructed from the priors $\pi_i(\theta_i)$ for each individual, independent parameter:

$$\pi(\boldsymbol{\Theta}) = \prod_i \pi_i(\theta_i). \tag{4.12}$$

But what priors should we assign the individual parameters of the supersymmetry models we are studying? The *objective* Bayesian approach is to assign priors according to a set of common principles for how information, or the lack thereof, should be translated into a probability distribution. We will not go into much detail on the various principles proposed in this thesis, as this is a extensive topic, but rather just briefly introduce the simplest one and present two of the resulting priors that are widely used.

The principle of *transformation group invariance* states that the prior should be invariant under any transformation that is considered irrelevant to the problem. It is applicable when the only available information about a parameter is what rôle it plays in the model. For a *location parameter* x, this means that the prior $\pi(x)$ should be invariant under a constant coordinate translation $x' = x + a$:

$$\pi(x)dx = \pi(x')dx' = \pi(x+a)d(x+a) \Rightarrow \pi(x) = \pi(x+a), \tag{4.13}$$

where the latter expression holds because $d(x+a) = dx$. From this it follows that the prior $\pi(x)$ must be *uniform*, often referred to as *flat*, i.e. $\pi(x) \propto 1$. Flat priors have a long history in Bayesian statistics.

A *scale parameter* is a parameter that brings a definite scale into the problem, for instance some mass parameter m. In this case, the prior $\pi(m)$ should be invariant under a scaling $m' = cm$, where c is a constant:

$$\pi(m)dm = \pi(m')dm' = \pi(cm)d(cm) = \pi(cm)cdm. \tag{4.14}$$

This is satisfied if the prior $\pi(m)$ has the form $\pi(m) \propto 1/m$, which is called a *log prior*. The somewhat misleading name "log" is used because it corresponds to the prior $\pi(\log(m))$ being uniform.

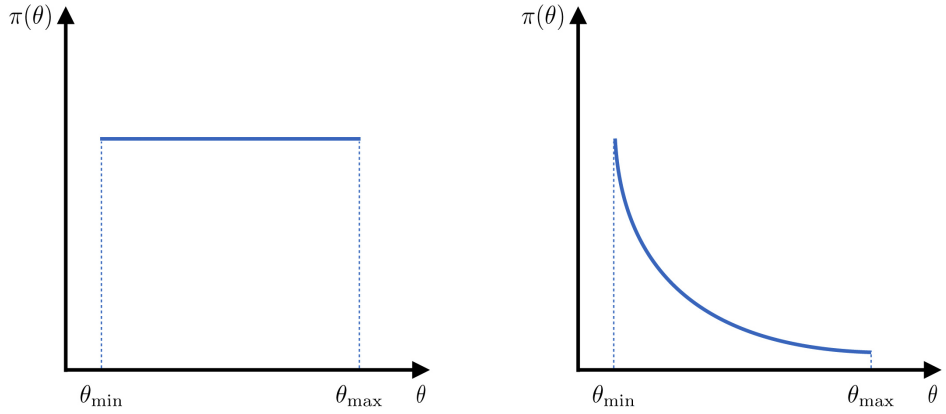

(a) Flat prior. (b) Log prior.

Figure 4.2: Priors $\pi(\theta)$ used for the individual parameters in this thesis. Hard cuts $(\theta_{\min}, \theta_{\max})$ on the allowed parameter ranges are imposed, avoiding the problem of improper priors not integrating to unity.

Technically, both flat and log priors on the real numbers do not integrate to unity — a property that is required for pdfs — and are thus so-called *improper priors*. But if the likelihood falls off quickly enough, such priors can indeed produce properly normalized posteriors, and are still used. In this thesis, however, hard cuts $(\theta_{\min}, \theta_{\max})$ on the allowed parameter ranges are imposed, avoiding this problem, see Fig. 4.2. The price we pay for this is excluding parts of the a priori allowed parameter range. We discuss this more in Sec. 5.1.

Since the flat and log priors introduced above originate from a common principle for how prior information (or the lack thereof) should be handled in Bayesian statistics, they are so-called *objective priors*. But even so, the choice of prior will indeed affect the resulting posterior, depending on the strength of the data. For very strong data, the posterior will be dominated by the likelihood function, and so the choice of prior will be largely irrelevant. On the other hand, if the posteriors resulting from different priors vary significantly, the data is not strong enough to dominate the prior. In this thesis, we will investigate the strength of different data by comparing the resulting posteriors from both flat and log priors. See Fig. 4.3 for an illustration of this, where the posteriors resulting from a flat and a log prior are very similar, i.e. the data is strong enough to dominate the posterior.

4.5 The Kullback–Leibler divergence

Bayes' theorem in Eq. (4.8) tells us how we should upgrade our belief in a given parameter point $\mathbf{\Theta}$ in light of new data, i.e. how to go from $\pi(\mathbf{\Theta})$ (prior) to $P(\mathbf{\Theta}|\mathbf{D})$ (posterior). The posterior is interesting in itself, as it tells us what regions of parameter space that are preferred by the data. However, it does not tell us anything about how much *information* we have gained from the data. In this thesis, we want to ask questions of the form "what data are most informative, i.e. what type of particle accelerator should we spend money on". In order to answer this, we need to introduce a measure for the information gain.

The Kullback–Leibler divergence [34] can be used as a measure of the information gained in moving from a prior distribution to a posterior distribution, or reversely: the amount of information lost when the prior is used to approximate the posterior. In the notation of Bayesian parameter estimation introduced above, it is defined as

$$D_{\mathrm{KL}} \equiv \int P(\mathbf{\Theta}|\mathbf{D}) \ln \left[\frac{P(\mathbf{\Theta}|\mathbf{D})}{\pi(\mathbf{\Theta})} \right] d\mathbf{\Theta}. \tag{4.15}$$

It can be shown that the Kullback–Leibler divergence is always positive, $D_{\mathrm{KL}} \geq 0$, with equality only if the two distributions are identical. Thus, the greater the value of D_{KL}, the more we have learned from the data. It is also easy to show that the Kullback–Leibler divergence is invariant under a parameter transformation $\Phi(\mathbf{\Theta})$.

A simple example illustrating priors, posteriors and the Kullback–Leibler divergence is given below.

4.5.1 Example

To illustrate the Kullback–Leibler divergence introduced above, we will consider a simple toy model with a single parameter θ. Both flat and log priors are used for this parameter,

$$\pi_{\mathrm{flat}}(\theta) \propto 1, \tag{4.16}$$

$$\pi_{\log}(\theta) \propto \frac{1}{\theta}, \tag{4.17}$$

so that their corresponding D_{KL} values can be compared. We will use a Gaussian likelihood function with mean θ_0 and standard deviation σ,

$$\mathcal{L}(\theta) \propto \exp\left[-\frac{(\theta - \theta_0)^2}{2\sigma^2} \right], \tag{4.18}$$

obtained from some data D. From the two priors and this likelihood, the two correponding posteriors can easily be found through Bayes' theorem:

$$P_{\mathrm{flat/log}}(\theta|D) \propto \mathcal{L}(\theta)\pi_{\mathrm{flat/log}}(\theta). \tag{4.19}$$

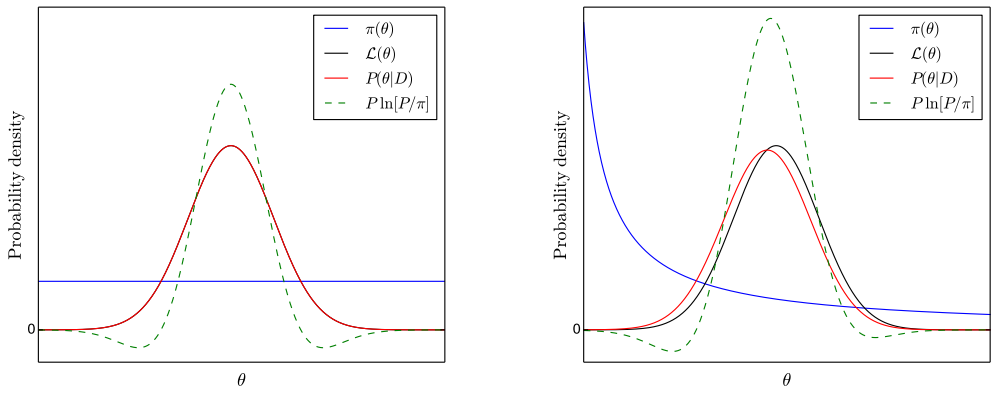

(a) Flat prior. (b) Log prior.

Figure 4.3: Qualitative illustrations of the prior (blue), likelihood (black), posterior (red) and D_{KL} integrand (dashed green) for two different priors. The assumed likelihood $\mathcal{L}(\theta)$ is the same in the two plots, and for the flat prior in (a), it coincides with the posterior.

When evaluating this numerically, hard cuts are set on the parameter range, avoiding the problem of the priors not integrating to unity. Both the priors and posteriors are then easily normalized, and it is straightforward to calculate the Kullback–Leibler divergence given by Eq. (4.15). Figure 4.3 shows qualitative illustrations of the prior, likelihood, posterior and D_{KL} integrand for the two different priors. The likelihood $\mathcal{L}(\theta)$ is the same in the two subplots, and for the flat prior in (a), it coincides with the posterior. Note that the D_{KL} integrand is partially negative.

As a quantitative example, consider the simple case $(\theta_{\mathrm{min}}, \theta_{\mathrm{max}}) = (0.05, 1)$, $\theta_0 = 0.5$ and $\sigma = 0.1$. For a flat prior, the Kullback–Leibler divergence is then $D_{\mathrm{KL}}^{\mathrm{flat}} = 0.83$, while it for a log prior is $D_{\mathrm{KL}}^{\mathrm{log}} = 1.19$. The exact values are not important here, but we see that $D_{\mathrm{KL}}^{\mathrm{log}} > D_{\mathrm{KL}}^{\mathrm{flat}}$, meaning that the information gain for a symmetric likelihood is greatest when starting from a logarithmic prior, compared to starting from a flat prior. By comparing the visual difference between the prior and the posterior in the two illustrative subplots of Fig. 4.3, it is easy to argue that this makes sense — the difference between the two is indeed largest for the log prior.

If we consider the exact same example, but with $\sigma = 0.15$, i.e. a little wider Gaussian, the numbers are $D_{\mathrm{KL}}^{\mathrm{log}} = 0.64$ and $D_{\mathrm{KL}}^{\mathrm{flat}} = 0.44$. As expected, $D_{\mathrm{KL}}^{\mathrm{log}}$ is still greater that $D_{\mathrm{KL}}^{\mathrm{flat}}$. However, in this case, the data is not as strong as in the previous example, and the Kullback–Leibler divergence is thus lower, for both priors.

4.6 Marginalization

The previous section explains how the gain in information about a model's parameter space, when moving from prior to posterior, can be quantized through the Kullback–Leibler divergence. However, we are also interested in the Kullback–Leibler divergence for other properties of the model, such as the Baribieri–Giudice naturalness measure introduced in Chapter 3. In fact, one of the main goals of this thesis is to quantify how much we can learn about naturalness from different data. In order to calculate this quantity, we first need to determine the prior and posterior for naturalness in the parameter space studied, which are also interesting distributions in themselves. This is done by *marginalization*, which is explained below. For simplicity we will only refer to the posterior, but the same approach also applies to the prior.

From Eqs. (3.5) and (3.6), it is clear that the Barbieri–Giudice measure is a function of the model parameters, i.e. $c(\boldsymbol{\Theta})$. The posterior for such a function can relatively easily be obtained from the posterior for the parameters themselves, we simply need to perform a change of variable from $\boldsymbol{\Theta}$ to c. The starting point for this change of variable is the joint posterior for both c and $\boldsymbol{\Theta}$, which is related to the posterior $P(\boldsymbol{\Theta}|\mathbf{D})$ for the parameters through

$$P(c, \boldsymbol{\Theta}|\mathbf{D}) = P(c|\boldsymbol{\Theta}, \mathbf{D})P(\boldsymbol{\Theta}|\mathbf{D}). \tag{4.20}$$

The first factor on the right hand side of this expression is a pdf relating c and $\boldsymbol{\Theta}$. Since the value of c is completely determined by the parameters $\boldsymbol{\Theta}$, i.e. independent of any data, this factor takes the simple form of a delta function:[5]

$$P(c|\boldsymbol{\Theta}, \mathbf{D}) = \delta(c(\boldsymbol{\Theta}) - c). \tag{4.21}$$

The posterior for c is related to the joint posterior through *marginalization* over the model parameters:

$$P(c|\mathbf{D}) = \int P(c, \boldsymbol{\Theta}|\mathbf{D}) d\boldsymbol{\Theta} = \int \delta(c(\boldsymbol{\Theta}) - c) P(\boldsymbol{\Theta}|\mathbf{D}) d\boldsymbol{\Theta}, \tag{4.22}$$

which corresponds to weighting all values of c by the posterior probability for the corresponding parameter point(s).

In this thesis, all of this is done numerically, and the posterior $P(\boldsymbol{\Theta}|\mathbf{D})$ is approximated by Monte Carlo methods. The result is a set of sampled parameter points $\boldsymbol{\Theta}_i$ distributed according to $P(\boldsymbol{\Theta}|\mathbf{D})$. Due to the delta function in the joint posterior $P(c, \boldsymbol{\Theta}|\mathbf{D})$, we can obtain a set of samples $(c, \boldsymbol{\Theta})_i$ distributed according to this posterior by simply calculating $c_i = c(\boldsymbol{\Theta}_i)$ for each sampled $\boldsymbol{\Theta}_i$. Finally, the marginalization in Eq. (4.22) then corresponds to histogramming these samples in terms of c only.

[5] Note that multiple parameter points $\boldsymbol{\Theta}_i$ may map to the same value of c.

When both the naturalness prior $\pi(c)$ and posterior $P(c|\mathbf{D})$ have been found following the above recipe, it is straightforward to calculate the Kullback–Leibler divergence for naturalness.

4.7 Likelihoods from accelerator simulations

Our prior state of knowledge, or ignorance, about parameter space is modified by data through the likelihood function. In Sec. 4.3 we introduced the Higgs likelihood function with the observed Higgs mass as data. In this section, we will explain how likelihood functions for future supersymmetry searches are obtained from accelerator simulations, which for the work presented in this thesis correspond to data.

4.7.1 Monte Carlo event generation

Monte Carlo event generators are software libraries that simulate high-energy particle physics events. In this thesis, Monte Carlo event generation is used to investigate future collider searches for supersymmetry. We will consider several search analyses for two different future colliders: the planned International Linear Collider (ILC), with centre-of-mass energy options of 500 GeV and 1 TeV, and the already approved High-Luminosity Large Hadron Collider (HL-LHC), operating at a centre-of-mass energy of 14 TeV and collecting up to 3000 fb^{-1} of data. The focus of this thesis wil be the ILC results

The different search analyses are presented in detail in the next chapter. However, the general statistical procedure is the same for all analyses, and is presented in the following. For each parameter point, a total of N_{tot} SUSY events are generated. These events are then propagated through our implementation of the given analysis, which consists of a set of *cuts* designed to isolate a specific SUSY production signature. One cut can for example be a lower limit on the number of final leptons in the event. Some analyses have multiple *signal regions*, corresponding to different sets of cuts on the same events. The number of accepted events, i.e. the number of events that pass the cuts for a particular signal region at a given parameter point, is in the following denoted N_{acc}.

The above discussion is only concerned with SUSY *signal* events. However, there are Standard Model processes that produce signatures similar to supersymmetry signatures. The number of SM events that pass the cuts for a particular signal region is referred to as the Standard Model *background*, and is in the following denoted b. The background is of course independent of the considered SUSY parameter point, and is thus a fixed value for each signal region. We will not perform background simulations in this work, but rather use the background estimates supplied by the experimental analyses we use.

4.7.2 Number of signal events

For a given parameter point, the ratio between the number of accepted events N_{acc} (for a given signal region) and the total number of SUSY events N_{tot} in a Monte Carlo event generator should be the same as the physical ratio if this parameter point is realised in nature. This gives us the relation

$$\frac{N_{\text{acc}}^{\text{MC}}}{N_{\text{tot}}^{\text{MC}}} = \frac{N_{\text{acc}}}{N_{\text{tot}}}, \tag{4.23}$$

where MC stand for Monte Carlo. The number of accepted events N_{acc} is the number of events in which the requirements for a given signal region are met, and is therefore often referred to as the *number of signal events*, s. The (physical) expected number of signal events can be estimated through

$$s \simeq \left(\frac{N_{\text{acc}}^{\text{MC}}}{N_{\text{tot}}^{\text{MC}}}\right) N_{\text{tot}} = \mathcal{E}_{\text{MC}} \mathcal{L} \sigma_{\text{tot}}, \tag{4.24}$$

where $\mathcal{E}_{\text{MC}} \equiv N_{\text{acc}}^{\text{MC}}/N_{\text{tot}}^{\text{MC}}$ is called the *selection efficiency* or *Monte Carlo factor*, and $N_{\text{tot}} = \mathcal{L}\sigma_{\text{tot}}$ is the standard event rate expression from the integrated luminosity and total cross section. The integrated luminosity $\mathcal{L} = \int L dt$ depends on how much data that has been collected, and thus varies from collider to collider, while σ_{tot} is the total cross section for all supersymmetry processes, which depends on the considered parameter point.

When finding s following the above recipe, it is important that the selection efficiency is as accurate as possible, to avoid Monte Carlo fluctutations influencing the result. The total number of generated events $N_{\text{tot}}^{\text{MC}}$ should therefore be large, forcing the selection efficiency to converge to its "true" value. In this work, Monte Carlo event generators are used to determine both $\mathcal{E}_{\text{MC}}$ and σ_{tot} at leading order, except for when more sophisticated alternatives (with loop corrections) are available for the cross section. The details of the different software used will be given in the next chapter.

4.7.3 Likelihood

The previous sections introduced the concept of Monte Carlo event generators and explained how these allow for finding the number of SUSY signal events for different signal regions at each parameter point. But how is this related to the likelihood function we set out to find?

In counting experiments like this (either we keep an event or we discard it), where the number of events is very large ($N_{\text{tot}} \to \infty$), the probability of keeping an event is low ($p \to 0$), and the expected number of kept events is constant ($N_{\text{tot}} p \to \nu$), the actual number of kept events n is said to follow a *Poisson distribution*, given by

$$P(n;\nu) = \frac{\nu^n e^{-\nu}}{n!}. \tag{4.25}$$

The distribution $P(n;\nu)$ gives the probability of getting n events when the expected number of events is ν. In our case, the expected number of events is $s+b$, where s is the expected number of signal events given by Eq. (4.24), and b is the expected number of SM background events. Equation (4.25) can thus be written as

$$P(n; s+b) = \frac{(s+b)^n e^{-(s+b)}}{n!}. \tag{4.26}$$

In this work, the likelihood function is constructed from the *cumulative* Poisson distribution,

$$P(n \leq n_{\text{obs}}; s+b) = \sum_{n=0}^{n_{\text{obs}}} \frac{(s+b)^n e^{-(s+b)}}{n!}, \tag{4.27}$$

which gives the probability of getting the *observed* number of events or less when the expected number of events is $s+b$. This probability is often called the p-value, which was briefly mentioned in Sec. 4.1.

Note that Eq. (4.27) requires that there exists an observed number of events for each signal region. However, there exists no such numbers for the colliders we are studying in this thesis, since they either do not exist or operate at the considered energy yet. In this case, the variable n_{obs} is replaced by the expected background b:

$$P(n \leq b; s+b) = \sum_{n=0}^{b} \frac{(s+b)^n e^{-(s+b)}}{n!}. \tag{4.28}$$

By inserting the background b and the signal yield s for each point in parameter space into this expression, the likelihood function in obtained for the individual signal regions.

For simplicity, we will join the likelihoods for the individual signal regions when there are more than one. This is done by *minimizing* the likelihood over parameter space, i.e. choosing the lowest p-value obtained for the given analysis for each parameter point. This is equivalent to choosing the most unlikely signal region for each parameter point.

4.8 The 95% CL exclusion limit

Up until now, the focus of this chapter has been Bayesian parameter estimation. Such analyses tell us what regions of parameter space, *relative* to the rest of the model's parameter space, that are preferred by the data. In this case, the cumulative Poisson distribution, or p-value, given by Eq. (4.28) is interpreted as likelihood. However, it is also interesting to know whether any given *single* parameter point should be excluded or not in light of the data, independent of the rest of the parameter space. Such analyses are also performed in this work.

In this context, a lower limit on the p-value is imposed. Parameter points with p-value less than or equal to this limit are excluded. When there are multiple signal regions that are joined together as explained above, this corresponds to excluding a point if it should be excluded for at least one of the signal regions. We will use an exclusion limit of 0.05 for the p-value, which is often expressed as a 95% *Confidence Level* (CL) exclusion.

Even though the exclusion limit is set on the p-value directly, it can be illustrative to see what it means for the expected number of signal events s at each point. This *lower* limit on p-value can in fact be translated into an *upper* limit on s, which corresponds to parameter points with large s being excluded. Such points would easily show an excess of events compared to the expected SM background. But exactly how large can s be before we exclude the corresponding point? This upper limit can be found by doing a hypothesis test for all possible values of s. Each value of s correspond to a hypothesis, which we check if should be excluded or not from the lower limit in p-value.

To find the 95% CL upper limit on s, denoted s_{95}, we need to solve the following equation for s:

$$P(n \leq b; s+b) = \sum_{n=0}^{b} \frac{(s+b)^n e^{-(s+b)}}{n!} \stackrel{!}{=} 0.05. \tag{4.29}$$

If s for a given point is below or equal to this limit ($s \leq s_{95}$), this point should *not* be excluded at 95% CL.

As an example, consider a signal region with an expected SM background of 4 ± 1.2 events. Solving Eq. (4.29) numerically for $b = 4$, in steps of 0.001 for s, gives $s_{95} = 5.154 \approx 5.2$ events. This means that points in parameter space which yield more than 5.2 expected signal events are excluded.[6] Note that this was calculated for $b = 4$. If the uncertainty in b is taken into account, things get more complicated. It can ultimately lead to a *weaker* limit on s, i.e. a *higher* value for s_{95}, so that less parameter points are excluded. However, considering background uncertainties are outside the scope of this thesis.

[6]Since the selection efficiency $\mathcal{E}_{\text{MC}}$ is estimated using a Monte Carlo event generator, we can get fractional events.

Chapter 5

Simulations of future supersymmetry searches

As discussed in the previous chapter, one of the goals of this work is to obtain the p-value across parameter space for different searches at the future ILC and HL-LHC, as this forms the basis for both our Bayesian parameter estimation, where the p-value is interpreted as a likelihood, and the 95% CL exclusion limit, where a lower limit on the p-value is imposed. In this way, we can compare the advantages of the two colliders in different supersymmetry scenarios.

We begin this chapter by introducing the specific supersymmetry models considered, and proceed by going through the parameter scan setup, including information on all of the software used. Finally, the different search analyses used are presented in detail, including the validation of our implementations using benchmark points.

5.1 Considered model scenarios

In this thesis, we consider two different sets of parameter choices (scenarios) for the CMSSM, and one for the NUHM2 model. In Sec. 4.3, we argued that only two of the parameters can be varied in each model, in order to keep the simulations performed in this work computationally feasible. For both CMSSM scenarios, we perform a grid scan in m_0 and $m_{1/2}$, while the rest of the parameters are held fixed. In the first scenario, in the following referred to as CMSSM10, the fixed parameters are $\tan\beta = 10$, $A_0 = 0$, and $\text{sign}(\mu) > 0$.[1] This is a standard scenario that allows for comparison with other work. In the other scenario, in the following referred to as CMSSM30, the fixed parameters are $\tan\beta = 30$,

[1]The sign of μ is usually taken to be positive, as a negative sign will give a contribution to the $(g-2)$ anomalous magnetic moment of the muon that corrects the SM value away from measurements, where a discrepancy of $\sim 3\sigma$ already exists [35].

Table 5.1: Fixed parameters for the three supersymmetry scenarios considered, in addition to the prior ranges used for the parameters that are varied.

Scenario	Parameter	Prior range [GeV]	Fixed parameters
CMSSM10	m_0	[50, 5000]	$\tan\beta = 10$, $A_0 = 0$,
	$m_{1/2}$	[72, 1854]	$\text{sign}(\mu) > 0$
CMSSM30	m_0	[50, 5000]	$\tan\beta = 30$, $A_0 = -2m_0$,
	$m_{1/2}$	[36, 1818]	$\text{sign}(\mu) > 0$
NUHM2	$m_{1/2}$	[40, 2000]	$\tan\beta = 15$, $m_0 = 5$ TeV,
	μ	[30, 2010]	$A_0 = -1.6m_0$, $m_A = 1$ TeV

$A_0 = -2m_0$, and $\text{sign}(\mu) > 0$. This scenario predicts a Higgs mass that is in agreement with the measured value, unlike the CMSSM10 scenario.

In contrast, in the NUHM2 scenario, we perform a grid scan in $m_{1/2}$ and μ, while the rest of the parameters are held fixed at $m_0 = 4$ TeV, $\tan\beta = 15$, $A_0 = -1.6m_0 = 6.4$ TeV, and $m_A = 1$ TeV. This is in accordance with the discussion in Ref. [30] on what regions of the NUHM2 parameter space that are considered natural, and also predicts a Higgs mass in agreement with measurements. The prior ranges used for the parameters that are varied in each of the three scenarios are listed in Table 5.1. They are chosen to enable comparison with previous work. We evaluate 99 uniformly distributed points within each of these ranges, giving 9801 evaluation points in total for each scenario.[2]

The different lower limits on the $m_{1/2}$ prior for the two CMSSM scenarios is due to the chargino mass. Results from the Large Electron–Positron Collider (LEP), operating at CERN from 1989 to 2000, showed that chargino masses below ~ 45 GeV are ruled out. If the chargino mass is less than this, the Z boson with mass ~ 90 GeV should in principle be able to decay into two charginos. However, LEP measured the decays of the Z boson to extreme precision, and the results showed that there is no room for such a decay [21]. There is thus no point in allowing chargino masses below 45 GeV in our priors. This requirement has different consequences for $m_{1/2}$ in the CMSSM10 and CMSSM30 scenarios, giving different minimum values for $m_{1/2}$. In order to get the same number of evaluation points with the same step size for the two scenarios, the upper limits on $m_{1/2}$

[2]Approximately 4000, 6800 and 8300 CPU hours was used to obtain the results for the CMSSM10, CMSSM30 and NUHM2 scenarios, respectively.

have been scaled correspondingly.

The same argument also applies to the lower limit on μ in the NUHM2 scenario. The lightest chargino would be dominantly higgsino for small μ, since μ is the higgsino mass parameter. For μ less that ~ 45 GeV, this would again mean that the Z could boson in principle decay into two charginos, which LEP has ruled out. Similar restrictions from slepton searches at LEP bound m_0.

Different parameters are included in the naturalness analyses of the two models. There are four and six free parameters, respectively, in the CMSSM and NUHM2 models, in addition to the Standard Model ones, and in principle should all of these be included. However, the relatively large top Yukawa coupling is the only SM parameter with a significant naturalness contribution [36]. Further, in Sec. 3.3, we explained why it is not feasible to actually include all of the parameters. Since it can be argued that a model does not depend on fixed parameters, we choose to only include the two parameters that are varied in each of the models when calculating the naturalness score. This means that the naturalness score is calculated from m_0 and $m_{1/2}$ in the two CMSSM scenarios, while it is calculated from $m_{1/2}$ and μ in the NUHM2 scenario.

The scan setup is the same for all of the three scenarios studied in this thesis, and is explained in the next section.

5.2 Scan setup

The main part of this work has been to build up a framework that takes care of the complete parameter scan of the considered supersymmetry model scenarios. The basis for this framework is a `Python` code.[3] Every external tool is associated with a separate `Python` module, which the main code handles. Each module is an independent executable that runs the given external tool and manages all input and output. This makes it straightforward to add, remove or rearrange tools.

The main code takes care of creating the parameter space grid itself. The scan is perfomed using parallell processing, meaning that the main code distributes the parameter points among a set of n processes, each handling one parameter point at a time. Once a specific parameter point has been selected, the model is fully specified.

The first ingredient needed is the mass spectrum, as it forms the basis for most other model predictions. The RGE code `SOFTSUSY 3.7.0` [38] is used to evolve the model parameters down to the weak scale and calculate the mass and coupling spectrum, and also the Barbieri–Giudice naturalness measure given by Eqs. (3.5) and (3.6). The sparticle branching ratios are then calculated with `SUSY-HIT 1.5` [39]. Further, a more detailed calculation of the masses and decays in the Higgs sector is performed with `FeynHiggs 2.12.0` [40–45]. The spectrum

[3]This has been developed based on the script `point_sampler.py` by Anders Kvellestad [37].

and decay information is communicated via the SUSY Les Houches Accord (SLHA) [46], and the interface PySLHA [47] is used to ease communication between the different modules, as well as processing the final results.

For colored sparticle production at the HL-LHC, the cross sections are calculated at next-to-leading order in the strong coupling constant, including the resummation of soft gluon emission at next-to-leading-logarithmic accuracy (NLO+NLL), with NLL-fast 4.01 [48–51]. As this version of NLL-fast for $\sqrt{s} = 14$ TeV only covers pair production of stop squarks ($\tilde{t}\tilde{t}^*$), first and second generation squarks ($\tilde{q}\tilde{q}^*$) and gluinos ($\tilde{g}\tilde{g}$) in the decoupling limits, only these indvidual processes can be used for colored production in the parameter scan. For the electroweak production of other sparticles, we use the leading order (LO) cross sections calculated by the Monte Carlo event generator itself, as discussed in Sec. 4.7.2.

Finally, the last step is to generate Monte Carlo events as decribed in Sec. 4.7.1. We run two different versions of the same event generator at each parameter point: PYTHIA 8.2.15 [52] for the HL-LHC searches and PYTHIA 6.4.28 [53] for the ILC searches. This is because PYTHIA 8 does not have the processes for producing supersymmetric particles from leptons implemented. In PYTHIA 8, jets are reconstructed with the embedded FastJet jet reconstruction program [54], with the anti-k_t clustering algorithm [55].[4] In PYTHIA 6, we use a modified version of the embedded jet clustering routine PYCELL, which clusters on energy rather than transverse energy. There are also some other minor modifications to PYCELL, which will be explained in Sec. 5.3. The modified PYCELL routine can be found in Appendix B. For each of the search analyses we consider, both for the ILC and the HL-LHC, 100 000 events are generated and propagated through our implementation of them.[5]

If one of the tools in the chain above expresses that the given parameter point is unphysical, or for some reason encounters an unrecoverable error, the main code discards the parameter point right away, so that we don't waste any computing power. The non-default settings used for all of these tools are summarized in Table 5.2, while Fig. 5.1 shows a flowchart of the scan setup.

All of the information obtained for a given parameter point is stored in the correponding SLHA-file. SOFTSUSY, SUSY-HIT and FeynHiggs does this automatically, while the cross sections and Monte Carlo efficiencies from NLL-fast and the two PYTHIA versions are manually added and managed using extra SLHA BLOCKS that PySLHA handles.

We have now introduced everything needed for the parameter scan, and are ready to present the future supersymmetry searches used in this work.

[4] Because of the nature of QCD, quarks are never observed as free particles — they are always found confined within hadrons. Quarks and gluons thus form showers of hadrons called *jets*, which is what we observe in a detector.

[5] With one exception, where the number of generated events are doubled. Which analysis this concerns will be clarified below.

Table 5.2: Summary of non-default settings and comments on the operation of the different tools used in this work.

Tool	Non-default settings / comment	Reference
`SOFTSUSY 3.7.0`	SM parameters: $m_t^{\text{pole}} = 173.4$ GeV $m_b(m_b) = 4.18$ GeV $\alpha_s(m_Z) = 127.944$ $\alpha_{\text{em}}^{-1}(m_Z) = 0.1184$	[38]
`SUSY-HIT 1.5`	—	[39]
`FeynHiggs 2.12.0`	Log level: 2.	[40–45]
`NLL-fast 4.01`	Parton distribution function: CTEQ6.	[48–51]
`PYTHIA 8.2.15`	Parton distribution function: CTEQ6.	[52]
`PYTHIA 6.4.28`	Modified `PYCELL` jet clustering routine.	[53]
`PySLHA`	—	[47]

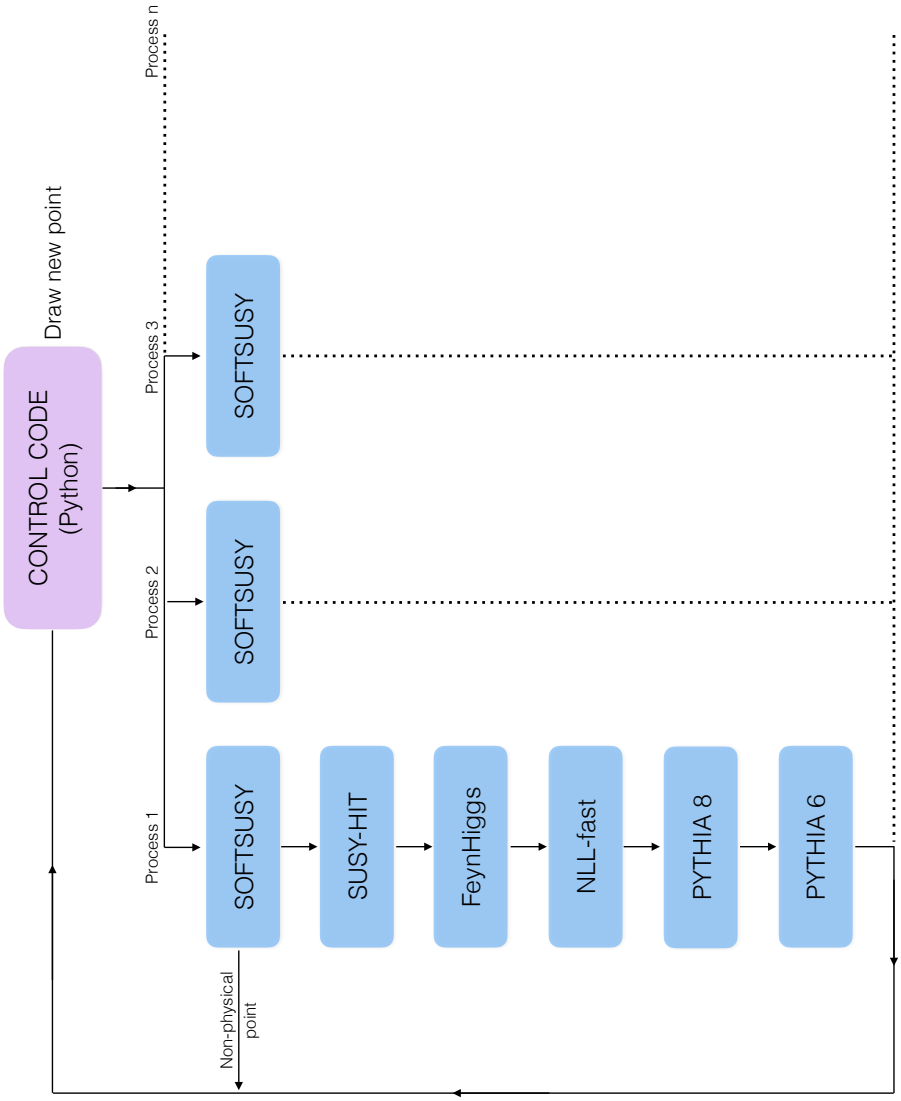

Figure 5.1: Flowchart of scan setup. The blue boxes correspond to the modules managing the external tools.

5.3 Supersymmetry at the ILC

The sum of the charges of the incoming particles in an electron-positron collider is zero, so these collisions can only produce electrically neutral final states. Particle-antiparticle pairs are typically produced. All sparticles, except gluinos, can be produced at tree-level:

$$e^+e^- \to Z^0/\gamma \to \tilde{\chi}_i^+\tilde{\chi}_j^-,\ \tilde{\chi}_i^0\tilde{\chi}_j^0,\ \tilde{\ell}^+\tilde{\ell}^-,\ \tilde{\nu}\tilde{\nu}^*,\ \tilde{q}\tilde{q}^*. \tag{5.1}$$

In Ref. [56], the linear collider capabilities for supersymmetry at centre-of-mass energies $\sqrt{s} = 500$ GeV and 1 TeV are investigated. Three different regions of the CMSSM parameter space with different phenomenology are studied, and results are shown for an integrated luminosty of 100 fb^{-1}. At low m_0, and $m_{1/2} \sim 300 - 500$ GeV, slepton pair production is very efficient due to light sleptons. At low $m_{1/2}$ values, the charginos are light, and chargino pair production thus occurs at a large rate. Chargino pair production is also efficient in the hyperbolic branch/focus point (HB/FP) region of the CMSSM parameter space, at large values of m_0 and small μ, near the region of no EWSB.

Here, we investigate the search for sleptons and charginos based on the selection cuts for these three regions given in [56]. To validate our implementation, we compare our results to a benchmark point in the HB/FP region, given in Table 2 of that paper.

5.3.1 ILC detector simulation

When simulating the ILC detector, jets are identified using the cone jet finding algorithm `PYCELL` in `PYTHIA 6`, modified to cluster on energy rather than transverse energy. As `PYCELL` was originally intended for proton-proton collisions, where the composite nature of protons does not allow for full energy conservation, only transverse energy is used. Leptons, on the other hand, are elementary particles, which means that full energy conservation can be used at lepton colliders. In addition to this energy modification, we do not allow any leptons in the jets, in order to avoid double counting when final state leptons are expected.[6]

A fixed cone size of

$$\Delta R \equiv \sqrt{(\Delta\phi)^2 + (\Delta\eta)^2} = 0.6, \tag{5.2}$$

is used in `PYCELL`, where ϕ is the azimuthal angle around the beam axis, and η is the pseudorapidity. The latter is defined as

$$\eta \equiv -\ln\left[\tan\frac{\theta}{2}\right], \tag{5.3}$$

[6]Only electrons and muons are regarded as leptons in this context. The heavier tau lepton has a very short lifetime and thus decays before it can be detected, while the neutrinos are invisible to all detectors.

where θ is the polar angle with respect to the beam axis. The hadronic calorimeter is assumed to cover the region $0 < \phi < 2\pi$, $-4 < \eta < 4$, with cell size $\Delta\phi \times \Delta\eta = 0.05 \times 0.05$. Due to calorimetric resolution effects, the hadronic energy E_h is smeared, cell by cell. This is done according to a Gaussian distribution, with standard deviation ΔE_h given by

$$\frac{\Delta E_h}{E_h} = \frac{0.5}{\sqrt{E_h}} \oplus 0.02, \tag{5.4}$$

where $\oplus$ denotes addition in quadrature. This agrees with Ref. [56]. The latter, constant term, is significant for large E_h. The final modification of the original `PYCELL` algorithm was to add this term to the smearing routine, as it is not implemented by default. All of the above settings are given as input to `PYCELL`. Thereafter, clusters with $E_h > 5$ GeV and $|\eta| < 2.5$ are labeled as jets.

Also the electromagnetic energy E_{em} is subject to calorimetric resolution effects. In Ref. [56], the electromagnetic resolution is given as

$$\frac{\Delta E_{\text{em}}}{E_{\text{em}}} = \frac{0.15}{\sqrt{E_{\text{em}}}} \oplus 0.01, \tag{5.5}$$

where ΔE_{em}, as for the hadronic case, is the standard deviation of a Gaussian distribution. As `PYTHIA 6` does not have smearing of electromagnetic energy implemented, this is added. The energy of electrons and photons is smeared according to

$$E_{\text{em}}^{\text{smeared}} = E_{\text{em}} + \Delta E_{\text{em}} \times N(0,1), \tag{5.6}$$

where E_{em} is the energy of the particle before smearing, and $N(0,1)$ is the Gaussian distribution around 0 with standard deviation 1. After smearing, leptons with energy $E > 5$ GeV and $|\eta| < 2.5$ are selected. They are required to be isolated by imposing that the visible activity within a cone of $\Delta R = 0.5$ around the lepton is less than $\max[E/10, 1]$ GeV.

5.3.2 Search for slepton pair production

If both of the sleptons decay into a lepton and the LSP, $\tilde{\ell}^{\pm} \to \ell^{\pm}\tilde{\chi}_1^0$, the signal is a pair of Same-Flavour Opposite-Sign (SFOS) leptons and missing energy.[7] In Ref. [56], each of the two leptons are required to have an energy $E_{\ell^{\pm}}$ between 5 and 200 GeV, and at least 25 GeV of missing transverse energy $E_{\text{T}}^{\text{miss}}$ is required in the event. Further, a cut on the invariant mass m_{SFOS} of the SFOS lepton pair is introduced to make sure that the leptons do not come from an on-shell Z boson directly: $|m_{\text{SFOS}} - m_Z| > 10$ GeV.[8]

[7] Missing energy refers to energy which is not detected in a particle detector, but is expected due to the laws of conservation of energy and momentum. It is used to infer the presence of non-detectable particles such as the Standard Model neutrino and the LSP.

[8] From the energy–momentum relation

$$E^2 = m^2 + |\mathbf{p}|^2, \tag{5.7}$$

Table 5.3: Summary of the selection cuts for slepton pair production. The signal is a pair of Same-Flavour Opposite-Sign (SFOS) leptons and missing energy. In addition to these cuts, events with any jet activity are vetoed.

Selection cuts for slepton production	
$E_{\ell^\pm}$ [GeV] >	5
$E_{\ell^\pm}$ [GeV] <	200
$E_{\mathrm{T}}^{\mathrm{miss}}$ [GeV] >	25
$\lvert m_{\mathrm{SFOS}} - m_Z \rvert$ [GeV] >	10
E_{visible} [GeV] >	20
E_{visible} [GeV] <	$\sqrt{s} - 100$
$\lvert \cos\theta_{\ell^\pm} \rvert$ [rad] <	0.9
$-q_{\ell^\pm} \cos\theta_{\ell^\pm}$ [rad] <	0.75
$\theta_{\mathrm{acop}}(\ell^+\ell^-)$ [°] >	30

Some less intuitive cuts are also introduced. Between 20 GeV and $\sqrt{s} - 100$ GeV of visible energy E_{visible} is required in the event. In addition, the cosine of the polar angles of the leptons with respect to the beam axis, $|\cos\theta_{\ell^\pm}|$, are required to be less than 0.9. This cut is introduced to make sure that the leptons are sufficiently far away from the beam, since their energy can be badly reconstructed if not. A similar and stronger requirement is that $-q_{\ell^\pm}\cos\theta_{\ell^\pm}$ should be less than 0.75, where $q_{\ell^\pm}$ is the lepton charge. Finally, a cut on the acoplanarity angle of the two leptons,

$$\theta_{\mathrm{acop}}(\ell^+\ell^-) \equiv \pi - \cos^{-1}(\hat{p}_x^+\hat{p}_x^- + \hat{p}_y^+\hat{p}_y^-) > 30^\circ, \quad \hat{p}_i = \frac{p_i}{|\mathbf{p}|}, \tag{5.9}$$

is introduced to avoid Standard Model background, since a pair of leptons produced directly from a (virtual) photon or Z boson would be more or less acoplanar.

The selection cuts introduced for slepton pair production are summarized in Table 5.3. In addition to these cuts, events with any jet activity are vetoed. To

where m is the mass, E is the energy and $\mathbf{p}$ is the momentum, we can define the invariant mass of a two-particle decay as

$$m_0^2 = (E_1 + E_2)^2 - |\mathbf{p}_1 + \mathbf{p}_2|^2, \tag{5.8}$$

where the indices 1 and 2 refers to the two daugther particles. This is not to be confused with the CMSSM common scalar mass.

maximize the slepton pair production cross section and minimize the Standard Model background from W boson pair production, $W^{\pm} \to \ell^{\pm}\nu$, the electron beams are assumed to be right-polarized, $P_L(e^-) = -0.9$. The expected Standard Model background is in Ref. [56] given as 1.79 (0.045) fb^{-1} for a centre-of-mass energy $\sqrt{s} = 0.5$ (1) TeV.

5.3.3 Search for chargino pair production

Chargino pair production can lead to events with one lepton, two jets and missing energy ($1\ell + 2j + E_{\mathrm{T}}^{\mathrm{miss}}$). This signature is obtained if each of the charginos decay into a (virtual) W boson and the LSP, $\tilde{\chi}_1^{\pm} \to W^{\pm}\tilde{\chi}_1^0$, and in turn, one of the W bosons decay hadronically, $W^{\pm} \to qq'$, and the other one decays leptonically, $W^{\pm} \to \ell^{\pm}\nu$. The same signature can also be obtained for other chargino decays, for instance $\tilde{\chi}_1^{\pm} \to \tilde{\ell}^{\pm}\nu \to \ell^{\pm}\nu\tilde{\chi}_1^0$ and $\tilde{\chi}_1^{\pm} \to \tilde{q}q' \to qq'\tilde{\chi}_1^0$. The selection cuts introduced in Ref. [56] to target chargino production at low $m_{1/2}$ values are presented in the following.

As for slepton pair production, events with at least 25 GeV of missing transverse energy and between 20 GeV and $\sqrt{s}-100$ GeV of visible energy are selected. In order to avoid Standard Model background from direct production of W^+W^-, the invariant mass $m_{\ell\nu}$ of the lepton and the neutrino (missing energy) is required to be at least 10 GeV away from the W boson mass at ~ 80 GeV. Also, if the summed energy E_{jj} of the two jets is larger than 200 GeV, as it would be if they came from a pair produced W boson at $\sqrt{s} \geq 500$ GeV, their invariant mass m_{jj} has to be less than 68 GeV, in order to be sufficiently far away from the W boson mass.

Further, the cosine of the polar angles of both the lepton and the two jets are required to be less than 0.9 in order to avoid the beam, and the similar and stronger requirements $-q_\ell \cos\theta_\ell < 0.75$ and $q_\ell \cos\theta_{jj} < 0.75$ are also introduced. Finally, also a cut on acoplanarity is introduced in order to avoid Standard Model background from direct production of W^+W^-, $\theta_{\mathrm{acop}}(W^+W^-) > 30^\circ$, where one of the W's is reconstructed from the four-vector sum of the two jets, and the other one from the four-vector sum of the lepton and the neutrino.

The selection cuts for chargino pair production are summarized in Table 5.4. In this case, the electron beams are assumed to be unpolarized. The expected Standard Model background is in Ref. [56] given as 15.5 (2.1) fb^{-1} for a centre-of-mass energy $\sqrt{s} = 0.5$ (1) TeV.

Other selection cuts are needed to target chargino pair production in the HB/FB region of the CMSSM parameter space, which we in the following will refer to as the "chargino extended" cuts. We still expect the same signature, i.e. $1\ell+2j+E_{\mathrm{T}}^{\mathrm{miss}}$, however, since the lightest neutralinos and the lightest chargino have a large higgsino component in this region where μ is small, the $\tilde{\chi}_1^{\pm} - \tilde{\chi}_1^0$ mass gap is small, leading to very little visible energy release from chargino

Table 5.4: Summary of the selection cuts for chargino pair production. The signal is an isolated lepton, two jets, and missing energy ($1\ell + 2j + E_{\mathrm{T}}^{\mathrm{miss}}$).

Selection cuts for chargino production	
$E_{\mathrm{T}}^{\mathrm{miss}}$ [GeV] >	25
$\lvert m_{\ell\nu} - m_W \rvert$ [GeV] >	10
If $E_{jj} > 200$ GeV, then $m_{jj} < 68$ GeV	
E_{visible} [GeV] >	20
E_{visible} [GeV] <	$\sqrt{s} - 100$
$\lvert \cos\theta_\ell \rvert$ [rad] <	0.9
$\lvert \cos\theta_j \rvert$ [rad] <	0.9
$-q_\ell \cos\theta_\ell$ [rad] <	0.75
$q_\ell \cos\theta_{jj}$ [rad] <	0.75
$\theta_{\mathrm{acop}}(W^+W^-)$ [°] >	30

decays. This makes detection of chargino pair production using the standard cuts introduced above difficult. In order to find some more suitable selection cuts for this region, a particular benchmark point in the HB/FB region is studied in Ref. [56]: $m_0 = 4625$ GeV, $m_{1/2} = 885$ GeV, $A_0 = 0$, $\tan\beta = 30$ and $\mathrm{sign}(\mu) > 0$. For this point, only the lighter charginos and neutralinos are accessible to a linear collder.

The bulk of the Standard Model background for this benchmark point can be eliminated by requiring quite little visible energy in the event. The analysis thus requires between 20 GeV and 100 GeV visible energy in this case, where the upper limit is chosen to also accommodate points with larger $\tilde{\chi}_1^\pm - \tilde{\chi}_1^0$ mass gaps than the benchmark point.[9] To get rid of the background that survives this cut, a cut on the transverse dijet opening angle ϕ_{jj} is introduced. For instance, in the Standard Model process $\gamma\gamma \to b\bar{b}$, a lepton can arise from semi-leptonic decay of one of the b's, $b \to c\ell\nu$, and two jets can arise from the remaining b-quark and the c-quark. In this case, the two b's will typically emerge back-to-back in the transverse plane, meaning that the transverse dijet opening angle will peak at $\cos\phi_{jj} \sim -1$. We thus require $\cos\phi_{jj} > -0.6$ for signal events. Finally, it was found that any background from $\gamma\gamma \to b\bar{b}$ surviving the previous cut can

[9] In the next chapter, we find that this cut has a significant negative impact on the reach in parts of our parameter space, in particular at $\sqrt{s} = 1$ TeV.

Table 5.5: Summary of the selection cuts for chargino production in the "chargino extended" anaysis. The signal is an isolated lepton, two jets and missing energy ($1\ell + 2j + E_{\mathrm{T}}^{\mathrm{miss}}$), as for chargino pair production at low $m_{1/2}$ values.

Selection cuts for chargino extended	
E_{visible} [GeV] >	20
E_{visible} [GeV] <	100
$\cos\phi_{jj}$ [rad] >	-0.6
$m_{\ell j_{\mathrm{near}}}$ [GeV] >	5

Table 5.6: Cut-flow in terms of effective cross sections $\mathcal{E}\sigma$ for the cuts in Table 5.5. The results are only given for a centre-of-mass energy of $\sqrt{s} = 500$ GeV. The uncertainties in our numbers are statistical only.

Cuts	Our result [fb]	From [56] [fb]	Ratio [–]
$2\ell + 1j$	15.8 ± 0.3	16.2	0.98 ± 0.02
20 GeV $< E_{\mathrm{visible}} <$ 100 GeV	15.5 ± 0.3	14.4	1.08 ± 0.02
$\cos\phi_{jj} > -0.6$ rad	14.2 ± 0.3	13.5	1.04 ± 0.02
$m_{\ell j_{\mathrm{near}}} > 5$ GeV	14.0 ± 0.3	12.9	1.08 ± 0.02

be eliminated by requiring that the invariant mass $m_{\ell j_{\mathrm{near}}}$ of the lepton and its nearest jet (in space angle) is greater than 5 GeV, since the bottom quark has a mass of 4.18 GeV.

The selection cuts for chargino extended are summarized in Table 5.5. The electron beams are assumed to be unpolarized also for this search. The expected Standard Model background is in Ref. [56] given as 1.01 (0.92) fb^{-1} for a centre-of-mass energy $\sqrt{s} = 0.5$ (1) TeV.

Benchmark validation

For the ILC searches presented in this section, the benchmark point in the HB/FP region introduced above is the only case for which we can test our implementation. In Table 2 of Ref. [56], they give the cut-flow in terms of effective cross sections $\mathcal{E}\sigma$ for this point after introducing the different cuts in Table 5.5 one by one. It is only given for a centre-of-mass energy of $\sqrt{s} = 500$ GeV.

As in [56], we calculate the mass spectrum of this benchmark point with `ISAJET 7.69` [57]. Both the total leading order cross section and the branching ratios are taken directly from `PYTHIA 6`. A comparison of our results and the effective cross sections from the paper is given in Table 5.6, where 100 000 events have been generated to obtain our results. The first line, $2\ell + 1j$, refers to that selected events must include exactly two leptons and one jet, based on the selection requirements for leptons and jets given in Sec. 5.3.1. We see that our effective cross sections are in quite good agreement with Ref. [56].

Note that the uncertainties in our numbers are statistical only, i.e. in the selection efficiencies $\mathcal{E} = N_{\text{acc}}/N_{\text{tot}}$. Since the number of accepted events follow a Poisson distribution, this uncertainty is given by

$$\Delta\mathcal{E} = \frac{\Delta N_{\text{acc}}}{N_{\text{tot}}} \simeq \frac{\sqrt{N_{\text{acc}}}}{N_{\text{tot}}} \tag{5.10}$$

for large N_{acc}. Further, the uncertainty in the ratio is given by one of the standard formulas for propagation of uncertainties. The uncertainty in a ratio $f = A/B$ is

$$\Delta f = f\sqrt{\left(\frac{\Delta A}{A}\right)^2 + \left(\frac{\Delta B}{B}\right)^2}. \tag{5.11}$$

5.4 Supersymmetry at the HL-LHC

An ATLAS note from 2014 presents benchmark studies for pair production of gluinos ($\tilde{g}\tilde{g}$), first and second generation squarks ($\tilde{q}\tilde{q}^*$) and bottom squarks ($\tilde{b}\tilde{b}^*$), as well as production of charginos and neutralinos ($\tilde{\chi}_2^0\tilde{\chi}_1^\pm$), at a centre-of-mass energy $\sqrt{s} = 14$ TeV [58]. The results are shown for integrated luminosities of 300 and 3000 fb^{-1}.

Reference [1] investigates chargino–neutralino production and pair production of gluinos and squarks based on the selection cuts given in the ATLAS note. To make sure that the implementations of these searches are reasonable, it is checked how well they, within the relevant uncertainties, reproduce the expected number of signal events for the benchmark points given in Tables 2, 8 and 9 in the ATLAS note. The searches used to obtain the results in Ref. [1] are summarised in the following.

5.4.1 Search for charginos and neutralinos

In scenarios with heavy squarks and gluinos, production of neutralinos and charginos can dominate the supersymmetry production at the LHC. In that case, final states with exactly three leptons and missing energy can be expected, for instance if the $\tilde{\chi}_1^\pm$ and $\tilde{\chi}_2^0$ decay into the LSP and $W^{(*)}$ and $Z^{(*)}$ bosons, respectively, and the (possibly) virtual W and Z bosons then decay into a lepton–neutrino

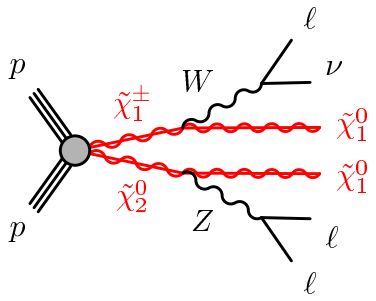

Figure 5.2: Feynman diagram for production and decay of $\tilde{\chi}_2^0\tilde{\chi}_1^{\pm}$. The $\tilde{\chi}_1^{\pm}$ is assumed to decay as $\tilde{\chi}_1^{\pm} \to W^{\pm(*)}\tilde{\chi}_1^0$, and the $\tilde{\chi}_2^0$ as $\tilde{\chi}_2^0 \to Z^{(*)}\tilde{\chi}_1^0$. The (possibly) virtual W and Z bosons then decay into a lepton–neutrino pair and a Same-Flavour Opposite-Sign (SFOS) lepton pair, respectively, giving a total of three final state leptons. Figure taken from [58].

pair and a Same-Flavour Opposite-Sign (SFOS) lepton pair, respectively, see Fig. 5.2. The selection cuts for chargino–neutralino production used in Ref. [1] are introduced below.

Jets are selected with the anti-k_t algorithm [55] with a radius parameter of $\Delta R \equiv \sqrt{(\Delta\phi)^2 + (\Delta\eta)^2} = 0.4$, and their energy is smeared by 3% to better simulate a realistic detector response in ATLAS. Thereafter, the selection requirements on transverse momentum p_{T} and pseudorapidity η as they appear in the ATLAS note are imposed: $p_{\mathrm{T}} > 20$ GeV and $|\eta| < 2.5$. Jets containing one or more b-quarks, i.e. with ΔR between a b-quark and the jet less than 0.4, are tagged as originating from b-decays with an average efficiency of 70%. Jets not containing any b-quarks are tagged as originating from b-decays with a misidentification probability of 1%.

Leptons are selected with $p_{\mathrm{T}} > 10$ GeV and $|\eta| < 2.47$ (2.4) for electrons (muons) in the ATLAS note, however, for simplicity, $|\eta| < 2.4$ is used for both electrons and muons in the implementation in [1]. They are required to be isolated by imposing that the scalar sum of the transverse momenta of charged particles with $p_{\mathrm{T}} > 1$ GeV and within a cone of $\Delta R = 0.3$ around the lepton cone (excluding the lepton track itself) is less that 15 % of the lepton p_{T}. In addition, they are required to be separated from each other through $\Delta R(\ell, \ell') \geq 0.1$. Leptons not fulfilling these two requirements are discarded.

Events with exactly three final state leptons, all with $p_{\mathrm{T}} > 50$ GeV, are selected. They are required to include at least one Z boson candidate, defined as a SFOS lepton pair with invariant mass m_{SFOS} satisfying $|m_{\mathrm{SFOS}} - m_Z| < 10$ GeV. The remaining lepton, which in the process we are searching for should come from a $W^{(*)}$ boson, is combined with the missing transverse energy $E_{\mathrm{T}}^{\mathrm{miss}}$ in the

event, and their *transverse mass* m_{T} is calculated.[10] Both large $E_{\mathrm{T}}^{\mathrm{miss}}$ and m_{T} is required, since both the neutrino and the two neutralinos are expected to carry a significant amount of momentum. If there are two SFOS lepton pairs in the event, the transverse mass m_{T} is constructed from the lepton not forming the SFOS pair with invariant mass closest to the Z boson. Events with b-tagged jets are vetoed to suppress $t\bar{t}$ Standard Model background, since this process can produce a similar signature.

Four signal regions are defined by different cuts on $E_{\mathrm{T}}^{\mathrm{miss}}$ and m_{T}. They are shown in Table 5.7, together with the rest of the selection cuts introduced above. The signal regions B, C and D are optimised for exclusion, where the latter only applies to the $\mathcal{L} = 3000$ fb^{-1} scenario. Signal region A, on the other hand, is optimised for discovery, and is not included in our parameter scan. At each parameter point, 200 000 events are generated for this search analysis, i.e. this is the exception mentioned in Sec. 5.2. All of the SUSY proton–proton processes implemented in `PYTHIA 8` is turned on for this search.[11]. The expected Standard Model backgrounds from [58] for the different signal regions / luminosities are listed in Table 5.9.

Benchmark validation

In order to check that the implementation of this search in Ref. [1] is reasonable, the expected number of signal events for four benchmark points

$$m(\tilde{\chi}_2^0\tilde{\chi}_1^0)\,[\mathrm{GeV}] = (400, 0),\ (600, 0),\ (800, 0),\ (1000, 0), \tag{5.14}$$

given in Table 2 in the ATLAS note, is attempted reproduced.

As in the parameter scan, the mass spectra for these benchmark points are calculated with `SOFTSUSY`, and the sparticle branching ratios are found using `SUSY-HIT`.[12] Both the $\tilde{\chi}_1^{\pm}$ and the $\tilde{\chi}_2^0$ are assumed to be wino-like with equal masses, while the LSP is bino-like. In addition, all sleptons and sneutrinos are assumed to be heavy, and the only allowed decays are $\tilde{\chi}_2^0 \to Z^0\tilde{\chi}_1^0$ and $\tilde{\chi}_1^{\pm} \to W^{\pm}\tilde{\chi}_1^0$. The production cross sections are calculated at next-to-leading order (NLO) with

[10] In hadron collider physics, transverse mass is defined in terms of $1 \to 2$ decays where one of the particles can not be detected directly and is only indicated by missing transverse energy. It is given by

$$m_{\mathrm{T}}^2 = (E_{\mathrm{T},1} + E_{\mathrm{T},2})^2 - |\mathbf{p}_{\mathrm{T},1} - \mathbf{p}_{\mathrm{T},2}|^2, \tag{5.12}$$

where E_{T} and $\mathbf{p}_{\mathrm{T}}$ are energy and momentum in the transverse plane, with energy–momentum relation

$$E_{\mathrm{T}}^2 = m^2 + |\mathbf{p}_{\mathrm{T}}|^2. \tag{5.13}$$

[11] This is not the case for the search for squark and gluino pair production, which will become clear in Sec. 5.4.2

[12] As `PYTHIA 8` for technical reasons can not handle a $\tilde{\chi}_1^0$ mass of exactly 0 GeV, a mass of 1 GeV is used in this benchmark validation.

Table 5.7: Summary of the selection cuts for chargino–neutralino production at the HL-LHC. The expected signal is final states with exactly three leptons, with at least one Same-Flavour Opposite-Sign (SFOS) lepton pair among them, and missing transverse energy.

	Signal regions			
Selection cuts	SRA	SRB	SRC	SRD
# b-tagged jets [–]	0			
# leptons [–]	3			
Lepton p_{T}(1,2,3) [GeV] >	50			
m_{SFOS} [GeV]	81.2 – 101.2			
m_{T} [GeV] >	150	200	200	200
$E_{\mathrm{T}}^{\mathrm{miss}}$[GeV] >	250	300	400	500

`Prospino 2.1` [59], since NLO cross sections have been used in Ref. [58]. The obtained cross sections are given in Table 5.8. Finally, 200 000 events are generated with `PYTHIA 8` for each of the four benchmark points, with only production of $\tilde{\chi}_2^0\tilde{\chi}_1^\pm$ turned on.

The expected number of signal events obtained for the different signal regions and luminosities are given in Table 5.9, where we for reference also list the numbers from the ATLAS note, as well as the ratio between the two. Signal region A has also been included for the purpose of benchmark validation. The uncertainties given in this table are statistical only, i.e. they are due to the uncertainty in the selection efficiency, given by Eq. (5.10). The uncertainty in the ratio is given

Table 5.8: Next-to-leading order (NLO) cross sections for $\tilde{\chi}_2^0\tilde{\chi}_1^\pm$ production used to calculate the number of signal events for the four benchmark points given in Table 5.9.

$m(\tilde{\chi}_2^0, \tilde{\chi}_1^0)$ [GeV]	σ [fb]
(400, 0)	130.4
(600, 0)	23.09
(800, 0)	5.53
(1000, 0)	1.646

Table 5.9: Expected number of signal events for $\tilde{\chi}_2^0\tilde{\chi}_1^\pm$ production for the four benchmark points given in Ref. [58]. 200 000 events were generated for each point to obtain the results in [1]. The uncertainties are statistical only.

	$\mathcal{L} = 300$ fb^{-1}			$\mathcal{L} = 3000$ fb^{-1}				
$m(\tilde{\chi}_2^0, \tilde{\chi}_1^0)$ [GeV]	SRA	SRB	SRC	SRA	SRB	SRC	SRD	
(400,0)	42.4 ± 2.9	27.6 ± 2.3	10.8 ± 1.5	424.5 ± 28.8	275.8 ± 23.2	107.6 ± 14.5	52.8 ± 10.2	[1]
	38.5 ± 0.6	20.1 ± 0.5	5.47 ± 0.23	407 ± 6	224 ± 5	67.9 ± 2.6	19.7 ± 1.4	[58]
	1.1 ± 0.1	1.4 ± 0.1	2.0 ± 0.3	1.0 ± 0.1	1.2 ± 0.1	1.6 ± 0.2	2.7 ± 0.5	[1]/ [58]
(600,0)	20.2 ± 0.8	16.1 ± 0.7	8.7 ± 0.5	201.9 ± 8.4	161.4 ± 7.5	86.9 ± 5.5	40.9 ± 3.8	[1]
	19.40 ± 0.20	14.69 ± 0.17	7.76 ± 0.12	194.8 ± 2.0	148.9 ± 1.7	81.6 ± 1.3	33.5 ± 0.8	[58]
	1.04 ± 0.04	1.1 ± 0.1	1.1 ± 0.1	1.04 ± 0.04	1.1 ± 0.1	1.1 ± 0.1	1.2 ± 0.1	[1] / [58]
(800,0)	6.6 ± 0.2	5.7 ± 0.2	4.1 ± 0.2	66.1 ± 2.3	56.7 ± 2.2	41.1 ± 1.8	24.5 ± 1.4	[1]
	6.97 ± 0.06	5.90 ± 0.06	4.21 ± 0.05	69.6 ± 0.6	59.1 ± 0.6	42.4 ± 0.5	25.2 ± 0.4	[58]
	0.94 ± 0.03	0.96 ± 0.04	0.98 ± 0.05	0.95 ± 0.03	0.96 ± 0.04	0.97 ± 0.05	0.97 ± 0.06	[1] / [58]
(1000,0)	2.1 ± 0.1	1.8 ± 0.1	1.4 ± 0.1	20.9 ± 0.7	18.3 ± 0.7	13.6 ± 0.6	9.8 ± 0.5	[1]
	2.31 ± 0.02	2.05 ± 0.02	1.64 ± 0.02	22.94 ± 0.19	20.42 ± 0.18	16.36 ± 0.16	11.55 ± 0.14	[58]
	0.90 ± 0.03	0.89 ± 0.03	0.83 ± 0.04	0.91 ± 0.03	0.90 ± 0.03	0.83 ± 0.04	0.85 ± 0.04	[1] / [58]
SM background	12.4 ± 0.4	5.89 ± 0.28	2.35 ± 0.16	239 ± 6	75.6 ± 3.3	27.7 ± 1.8	10.3 ± 1.1	[58]

by Eq. (5.11).

We see that the result in [1], within the uncertainties, are in relatively good overall agreement with the ATLAS results, with only a few exceptions at the lowest masses.

5.4.2 Search for squark and gluino pair production

Given that they are light enough to be produced at the LHC, strongly produced supersymmetric particles are expected to have the highest production cross section of all supersymmetric processes. With strongly produced supersymmetry, events with many jets, large $E_{\mathrm{T}}^{\mathrm{miss}}$ and no leptons are expected. The gluinos can decay directly into two quarks and the LSP, while the squarks can decay into a quark and the LSP, see Fig. 5.3. The selection cuts for strongly produced supersymmetry used in Ref. [1] are introduced below.

The selection requirements for jets and leptons in Sec. 5.4.1 are imposed also in this search, with one exception: here, jets are selected with pseudorapidity $|\eta| < 4.5$, in contrast to $|\eta| < 2.5$ in Sec. 5.4.1. Events with no leptons and at least 160 GeV of missing transverse energy are selected. Between a minimum of two and a minimum of six jets with $p_{\mathrm{T}} > 20$ GeV are required for different signal regions, where the hardest one has an additional requirement of $p_{\mathrm{T}} > 160$ GeV. In order to make sure that the missing energy does not come from bad jet reconstruction, requirements on the difference in azimuthal angle ϕ between the missing transverse energy (vector) and the centre of the jets are imposed. For the three hardest jets, the requirement is $\Delta\phi(\mathrm{jet}_{1,2,3}, E_{\mathrm{T}}^{\mathrm{miss}})_{\mathrm{min}} > 0.4$ radians, while for all other jets with $p_{\mathrm{T}} > 40$ GeV it is $\Delta\phi(\mathrm{jet}_{p_{\mathrm{T}}>40\ \mathrm{GeV}}, E_{\mathrm{T}}^{\mathrm{miss}})_{\mathrm{min}} > 0.2$ radians.

Three more cuts are introduced in terms of the missing transverse energy $E_{\mathrm{T}}^{\mathrm{miss}}$, H_{T} and the *effective mass* m_{eff}, where the two latter quantities are defined as

$$H_{\mathrm{T}} = \sum_{\mathrm{jets}} p_{\mathrm{T}}^{\mathrm{jet}}, \tag{5.15}$$

and

$$m_{\mathrm{eff}} = E_{\mathrm{T}}^{\mathrm{miss}} + H_{\mathrm{T}}. \tag{5.16}$$

A lower limit on m_{eff} is introduced to make sure that the total energy from the LSPs and the jets is large, which is expected due to large squark and gluino masses. Further, a lower limit on the ratio $E_{\mathrm{T}}^{\mathrm{miss}}/m_{\mathrm{eff}}$ is introduced to make sure that a substantial part of the outgoing energy comes from missing energy, not only jets, which would be the case for QCD backgrounds. A cut on the ratio $E_{\mathrm{T}}^{\mathrm{miss}}/\sqrt{H_{\mathrm{T}}}$ is imposed for the same reason.

Altogether ten different signal regions are defined in terms of different cuts on these three quantities, see Table 5.10. The 2j, 3j and 4jl signal regions, targetting squark pair production, have two different cuts on m_{eff}. The first is designed for scenarios where the gluino is completely decoupled, the other for the case in

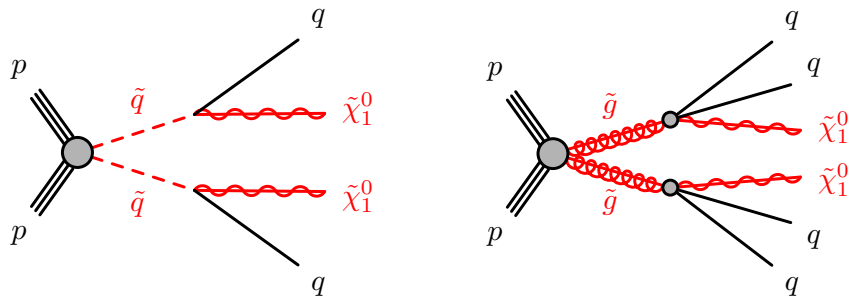

(a) Squark production and decay. (b) Gluino production and decay.

Figure 5.3: Feynman diagrams for production and decay of $\tilde{g}\tilde{g}$ and $\tilde{q}\tilde{q}$. Each quark is assumed to the decay into a quark and the LSP, while each gluino is assumed to decay into to quarks and the LSP directly. Figures taken from [58].

which the gluino mass is large. Since there only exists background estimates for the latter case (given in Tables 8 and 9 of the ATLAS note), only the last m_{eff}-cut for these three signal regions are included in the analysis used in Ref. [1].

As briefly discussed in Sec. 5.2, only pair production of $\tilde{t}\tilde{t}^*$, $\tilde{q}\tilde{q}^*$ and $\tilde{g}\tilde{g}$ can be used, due to the limitations `NLL-fast 4.01`. These three processes are turned on in turn, meaning that both `NLL-fast` and `PYTHIA 8` is run three times for each parameter point. The results can be joined according to

$$s \simeq \mathcal{L}(\mathcal{E}_{\tilde{t}\tilde{t}^*}\sigma_{\tilde{t}\tilde{t}^*} + \mathcal{E}_{\tilde{q}\tilde{q}^*}\sigma_{\tilde{q}\tilde{q}^*} + \mathcal{E}_{\tilde{g}\tilde{g}}\sigma_{\tilde{g}\tilde{g}}). \tag{5.17}$$

Note that the expected number of signal events is underestimated and conservative when only specific processes are turned on.

The expected Standard Model backgrounds from [58] for the different signal regions / luminosities are listed in Tables 5.12, 5.13, 5.14 and 5.15.

Benchmark validation

The implementation of this search can be validated by reproducing the expected number of signal events for four benchmark points,

$$m(\tilde{g}, \tilde{\chi}_1^0)\,[\text{GeV}] = (1950, 1),\ (1425, 1400) \tag{5.18}$$

and

$$m(\tilde{q}, \tilde{\chi}_1^0)\,[\text{GeV}] = (2250, 1),\ (1050, 900), \tag{5.19}$$

given in Tables 8 and 9 in the ATLAS note [58].

Again, the mass spectra for these benchmark points are calculated with `SOFTSUSY`, while the sparticle branching ratios are calculated with `SUSY-HIT`. Only the decays depicted in Fig. 5.3 are allowed. For the gluino points, all sparticles except the gluino and the LSP are decoupled. For the squark points, all

Table 5.10: Summary of the selection cuts for squark and gluino pair production. The 2j, 3j and 4jl signal regions, targetting squark pair production, have two different cuts on m_{eff}. The first is designed for scenarios where the gluino is completely decoupled, the other for the case in which the gluino mass is large. There are background estimates only for the latter.

	Signal regions									
Selection cuts	2jl	2jm	3j	4jl	4jm	4jt	5j	6jl	6jm	6jt
# leptons [–]	0									
$E_{\text{T}}^{\text{miss}}$ [GeV] >	160									
$N_{\text{jets}}(p_{\text{T}} > 60$ GeV) [–] $\geq$	2	2	3	4	4	4	5	6	6	6
$p_{\text{T}}(j_1)$ [GeV] >	160									
$\Delta\phi(\text{jet}, E_{\text{T}}^{\text{miss}})_{\text{min}}$ [rad] >	$0.4\,(j_1, j_2, j_3)$, $0.2\,(\text{all}\, p_{\text{T}} > 40\,\text{GeV}\,\text{jets})$									
	$\mathcal{L} = 300$ fb^{-1}									
$E_{\text{T}}^{\text{miss}}/m_{\text{eff}}$ [–] >	—	—	0.3	0.40	0.25	—	0.20	0.30	0.15	0.20
$E_{\text{T}}^{\text{miss}}/\sqrt{H_{\text{T}}}$ [GeV$^{1/2}$] >	8	15	—	—	—	10	—	—	—	—
m_{eff} [GeV] >	3600	3100, 4300	3600, 3000	3000, 2200	3200	3400	3000	2800	3400	3400
	$\mathcal{L} = 3000$ fb^{-1}									
$E_{\text{T}}^{\text{miss}}/m_{\text{eff}}$ [–] >	—	—	0.3	0.35	0.25	—	0.25	0.25	0.35	0.15
$E_{\text{T}}^{\text{miss}}/\sqrt{H_{\text{T}}}$ [GeV$^{1/2}$] >	8	15	—	—	—	10	—	—	—	—
m_{eff} [GeV] >	4500, 5000	4500, 4900	4000	4000, 3800	4000	4500	4000	3400	3500	5000

Table 5.11: Cross sections for gluino and squark–antisquark pair production used for calculating the number of signal events in Tables 5.12, 5.13, 5.14 and 5.15. Please see the text for details.

$m(\tilde{g}, \tilde{\chi}_1^0)$ [GeV]	σ [fb]	Source	$m(\tilde{q}, \tilde{\chi}_1^0)$ [GeV]	Process	σ [fb]	Source
(1425, 1400)	32.4	`NLL-fast`	(1050, 900)	sb	85.4	`Prospino`
				ss	66.5	`Prospino`
(1950,1)	2.14	`NLL-fast`	(2250, 1)	sb	0.245	`Prospino`
				ss	1.29	`Prospino`

sparticles except the squarks, the LSP and the gluinos are decoupled, where the gluino mass is set to 4.5 TeV, as in [58].

For gluino pair production, the cross sections are calculated at NLO+NLL accuracy with `NLL-fast 4.01` for decoupled squarks. For squark pair production, the gluino is not completely decoupled, so `NLL-fast 4.01` can not be used. Instead, `Prospino 2.1` is used to calculate the cross sections to NLO accuracy for the squark points. For the purpose of benchmark validation, both squark–antisquark (sb) and squark–squark (ss) production are included.[13] The cross sections obtained for the benchmark points are given in Table 5.11.

Finally, 1 000 000 and 100 000 events are generated with `PYTHIA 8` for the mass degenerate and non-degenerate benchmark points, respectively. The expected number of signal events for gluino pair production are given in Tables 5.12 ($\mathcal{L} = 300$ fb^{-1}) and 5.13 ($\mathcal{L} = 3000$ fb^{-1}), where we have for reference also listed the numbers from the article, as well as the ratio between them. The uncertainties given in these tables are statistical only. To obtain the expected number of signal events for squark production, the results from ss and sb are joined according to

$$s \simeq \mathcal{L}(\mathcal{E}_{ss}\sigma_{ss} + \mathcal{E}_{sb}\sigma_{sb}). \tag{5.20}$$

These are given in Tables 5.14 ($\mathcal{L} = 300$ fb^{-1}) and 5.15 ($\mathcal{L} = 3000$ fb^{-1}).

We see that the result in [1], within the uncertainties, are in relatively good overall agreement with the ATLAS results, however, with a few exceptions for the benchmark points with mass degeneration.

[13] Only squark–antisquark production is included in the parameter scan, again due to limits in `NLL-fast 4.01`.

Table 5.12: Expected number of signal events for gluino pair production with decoupled squarks for two benchmark points. 100 000 and 1 000 000 events have been generated for the mass degenerate and non-degenerate points, respectively, and the results have been normalized to a luminosity of 300 fb^{-1}. The uncertainties are statistical only.

	$\mathcal{L} = 300$ fb^{-1}										
$m(\tilde{g}, \tilde{\chi}_1^0)$ [GeV]	2jl	2jm	3j	4jl	4jm	4jt	5j	6jl	6jm	6jt	
(1425,1400)	6.5 ± 0.3	1.5 ± 0.1	13.1 ± 0.4	15.9 ± 0.4	4.7 ± 0.2	3.6 ± 0.2	3.0 ± 0.2	1.4 ± 0.1	0.6 ± 0.1	0.6 ± 0.1	[1]
	12.6 ± 1.2	3.7 ± 0.6	8.5 ± 1.0	7.5 ± 0.9	8.1 ± 0.9	6.2 ± 0.8	4.7 ± 0.7	1.6 ± 0.4	1.05 ± 0.33	1.05 ± 0.33	[58]
	0.5 ± 0.1	0.4 ± 0.1	1.5 ± 0.2	2.1 ± 0.3	0.6 ± 0.1	0.6 ± 0.1	0.6 ± 0.1	0.9 ± 0.2	0.6 ± 0.2	0.6 ± 0.2	[1] / [58]
(1950,1)	85.2 ± 0.7	14.9 ± 0.3	61.4 ± 0.6	17.9 ± 0.3	72.7 ± 0.7	99.8 ± 0.8	90.6 ± 0.8	24.6 ± 0.4	48.3 ± 0.6	37.4 ± 0.5	[1]
	68.8 ± 0.6	12.48 ± 0.27	35.4 ± 0.5	18.41 ± 0.33	70.6 ± 0.7	102.4 ± 0.8	83.4 ± 0.7	25.6 ± 0.4	44.6 ± 0.5	35.4 ± 0.5	[58]
	1.24 ± 0.02	1.20 ± 0.04	1.74 ± 0.03	0.97 ± 0.03	1.03 ± 0.01	0.97 ± 0.01	1.09 ± 0.01	0.96 ± 0.02	1.08 ± 0.02	1.06 ± 0.02	[1] / [58]
SM background	183 ± 5	23.6 ± 1.7	64.9 ± 2.9	72.6 ± 3.1	125 ± 4	300 ± 8	138 ± 5	38.3 ± 2.5	28.1 ± 2.2	18.8 ± 1.7	[58]

Table 5.13: See caption of Table 5.12. In this table, the results have been normalized to a luminosity of 3000 fb^{-1}.

$m(\tilde{g},\tilde{\chi}_1^0)$ [GeV]	$\mathcal{L} = 3000$ fb^{-1}										
	2jl	2jm	3j	4jl	4jm	4jt	5j	6jl	6jm	6jt	
(1425,1400)	4.9 ± 0.7	4.1 ± 0.6	21.4 ± 1.4	15.3 ± 1.2	12.2 ± 1.1	4.5 ± 0.7	5.1 ± 0.7	5.8 ± 0.8	4.3 ± 0.6	0.6 ± 0.2	[1]
	10.5 ± 3.3	15 ± 4	48 ± 7	19 ± 4	23 ± 5	8.4 ± 3.0	14 ± 4	7.4 ± 2.8	5.3 ± 2.4	0.00 ± 0.00	[58]
	0.5 ± 0.2	0.3 ± 0.1	0.4 ± 0.1	0.8 ± 0.2	0.5 ± 0.1	0.5 ± 0.2	0.4 ± 0.1	0.8 ± 0.3	0.8 ± 0.4	–	[1] / [58]
(1950,1)	48.4 ± 1.8	72.3 ± 2.2	126.5 ± 2.9	99.3 ± 2.5	188.7 ± 3.5	130.2 ± 3.0	157.0 ± 3.2	257.1 ± 4.1	66.8 ± 2.1	24.1 ± 1.2	[1]
	55.8 ± 1.8	43.4 ± 1.6	163.9 ± 3.1	75.2 ± 2.1	191.0 ± 3.4	159.1 ± 3.1	152.7 ± 3.0	257 ± 4	73.4 ± 2.1	36.0 ± 1.5	[58]
	0.87 ± 0.04	1.7 ± 0.1	0.77 ± 0.02	1.32 ± 0.05	0.99 ± 0.03	0.82 ± 0.02	1.03 ± 0.03	1.00 ± 0.02	0.91 ± 0.04	0.67 ± 0.04	[1] / [58]
SM background	76 ± 10	72 ± 9	269 ± 18	104 ± 11	176 ± 14	292 ± 23	99 ± 11	141 ± 14	48 ± 8	5.6 ± 2.4	[58]

Table 5.14: Expected number of signal events for squark pair production with $m_{\tilde{g}} = 4.5$ TeV for two benchmark points. 100 000 and 1 000 000 events have been generated for the mass degenerate and non-degenerate points, respectively, and the results have been normalized to a luminosity of 300 fb^{-1}. The uncertainties are statistical only.

	$\mathcal{L} = 300$ fb^{-1}										
$m(\tilde{q}, \tilde{\chi}_1^0)$ [GeV]	2jl	2jm	3j	4jl	4jm	4jt	5j	6jl	6jm	6jt	
(1050, 900) GeV	8.1 ± 0.4	2.0 ± 0.2	23.9 ± 0.8	37.0 ± 0.9	13.5 ± 0.6	9.4 ± 0.5	13.0 ± 0.6	7.9 ± 0.4	3.0 ± 0.3	3.0 ± 0.3	[1]
	2.5 ± 1.1	1.5 ± 0.9	2.0 ± 1.0	3.5 ± 1.3	6.4 ± 1.8	4.0 ± 1.4	7.4 ± 1.9	3.5 ± 1.3	1.5 ± 0.9	1.5 ± 0.9	[58]
	3.2 ± 1.4	1.4 ± 0.8	11.9 ± 6.0	10.6 ± 3.9	2.1 ± 0.6	2.3 ± 0.8	1.8 ± 0.5	2.3 ± 0.8	2.0 ± 1.2	2.0 ± 1.2	[1] / [58]
(2250, 1) GeV	151.3 ± 0.7	65.9 ± 0.5	112.8 ± 0.6	37.0 ± 0.4	51.5 ± 0.4	51.6 ± 0.4	22.2 ± 0.3	5.6 ± 0.1	5.9 ± 0.1	5.6 ± 0.1	[1]
	141.7 ± 0.9	60.1 ± 0.6	82.1 ± 0.7	39.2 ± 0.5	59.3 ± 0.6	58.9 ± 0.6	28.4 ± 0.4	7.84 ± 0.21	8.00 ± 0.21	7.57 ± 0.20	[58]
	1.07 ± 0.01	1.10 ± 0.01	1.37 ± 0.01	0.94 ± 0.01	0.87 ± 0.01	0.88 ± 0.01	0.78 ± 0.01	0.72 ± 0.03	0.73 ± 0.03	0.74 ± 0.03	[1] / [58]
SM background	183 ± 5	23.6 ± 1.7	64.9 ± 2.9	72.6 ± 3.1	125 ± 4	300 ± 8	138 ± 5	38.3 ± 2.5	28.1 ± 2.2	18.8 ± 1.7	[58]

Table 5.15: See caption of Table 5.14. In this table, the results have been normalized to a luminosity of 3000 fb^{-1}.

	$\mathcal{L} = 3000$ fb^{-1}										
$m(\tilde{q}, \tilde{\chi}_1^0)$ [GeV]	2jl	2jm	3j	4jl	4jm	4jt	5j	6jl	6jm	6jt	
(1050, 900) GeV	5.2 ± 1.1	5.4 ± 1.1	31.5 ± 2.8	28.2 ± 2.6	26.5 ± 2.5	8.9 ± 1.5	16.6 ± 2.0	28.0 ± 2.6	12.4 ± 1.7	1.5 ± 0.6	[1]
	5 ± 5	10 ± 7	15 ± 9	10 ± 7	15 ± 9	15 ± 9	10 ± 7	25 ± 11	5 ± 5	5 ± 5	[58]
	1.0 ± 1.1	0.5 ± 0.4	2.1 ± 1.3	2.8 ± 2.0	1.8 ± 1.1	0.6 ± 0.4	1.7 ± 1.2	1.1 ± 0.5	2.5 ± 2.5	0.3 ± 0.3	[1] / [58]
(2250, 1) GeV	200.1 ± 2.6	167.3 ± 2.4	540.0 ± 4.3	258.0 ± 2.9	278.0 ± 3.0	162.2 ± 2.3	103.8 ± 1.8	51.5 ± 1.3	33.6 ± 1.0	9.8 ± 0.5	[1]
	186 ± 3	208.2 ± 3.4	558 ± 6	254 ± 4	320 ± 4	182.6 ± 3.2	136.4 ± 2.7	75.2 ± 2.0	50.9 ± 1.7	13.6 ± 0.9	[58]
	1.08 ± 0.02	0.80 ± 0.02	0.97 ± 0.01	1.02 ± 0.02	0.87 ± 0.01	0.89 ± 0.02	0.76 ± 0.02	0.69 ± 0.02	0.66 ± 0.03	0.72 ± 0.06	[1] / [58]
SM background	76 ± 10	72 ± 9	269 ± 18	104 ± 11	176 ± 14	292 ± 23	99 ± 11	141 ± 14	48 ± 8	5.6 ± 2.4	[58]

Chapter 6

Results and discussion

In this chapter, the results obtained in this work will be presented and discussed. As the focus of this thesis is the ILC, these results will be discussed in more detail than the HL-LHC results, which are thoroughly reviewed in Ref. [1].

Since the ILC is an electron–positron collider, it offers a well-defined initial state. The collision energy is known and tuneable, allowing the choice of the best suited center-of-mass energy, e.g. thresholds for particle pair production. With energy options of 0.5 and 1 TeV, the ILC allows for detection of pair produced particles up to 250 and 500 GeV, respectively.

6.1 The CMSSM10 scenario

In the CMSSM10 scenario, defined in Sec. 5.1, the predicted Higgs mass is too low compared to the measured value of ~ 125 GeV. However, this is a standard scenario that allows for comparison with other work. For instance, Ref. [36] from 2000, i.e. before the LHC started operating, investigates the naturalness reach of the LHC in this scenario. Below, we will compare our results to Fig. 3 of that paper, included here as Fig. 6.1 for ease of reference.

6.1.1 95% CL exclusion limits

Figure 6.2 shows the 95% CL exclusion limits obtained in this work for the CMSSM10 scenario. The green and blue lines show the limits for the ILC at centre-of-mass energies 0.5 and 1 TeV, respectively. There are three lines in each color, representing the three different searches presented in Sec. 5.3, for sleptons ($\tilde{\ell}\tilde{\ell}^*$), charginos ($\tilde{\chi}_1^+\tilde{\chi}_1^-$) and "charginos extended" ($\tilde{\chi}_1^+\tilde{\chi}_1^-$E). The red lines show the HL-LHC exclusion limits based on the searches presented in Sec. 5.4, for squarks and gluinos ($\tilde{g}\tilde{g}/\tilde{q}\tilde{q}^*$) and charginos and neutralinos ($\tilde{\chi}_2^0\tilde{\chi}_1^\pm$), for two different integrated luminosities: 300 and 3000 fb^{-1}.

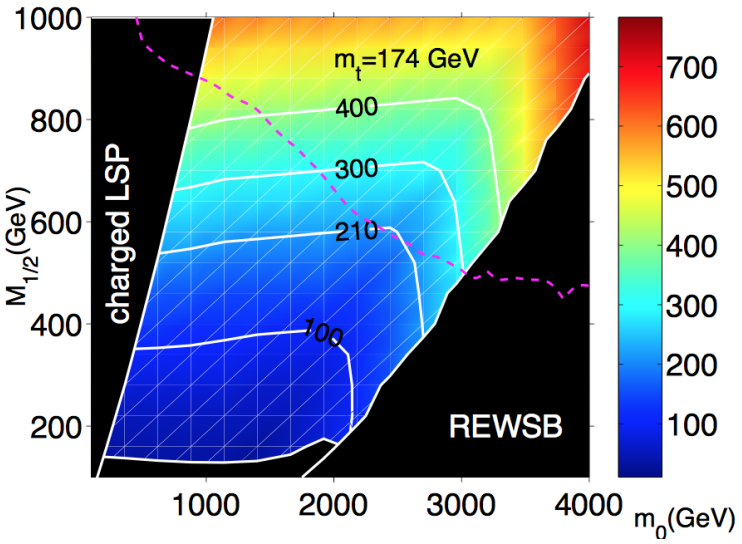

Figure 6.1: Expected naturalness reach of the LHC in the m_0–$m_{1/2}$ mass plane for $\tan\beta = 10$, $A_0 = 0$ and $\text{sign}(\mu) > 0$, from Ref. [36]. Included for ease of reference.

Also shown are mass contours for sleptons (dark blue), squarks (purple), gluinos (dark green), Higgs (black), charginos (turquoise) and neutralinos (yellow).[1,2] The background density represents the naturalness score given by Eqs. (3.5) and (3.6), as indicated by the bar on the right-hand side of the figure. White contours for the naturalness score are also shown. The two black areas in the plot are unphysical. In the left-most black area, the lightest sparticle (LSP) would be electrically charged, which we know can not be the case. In the black area on the right, there is no radiative electroweak symmetry breaking (REWSB).

We see that all of the three green (blue) lines more or less follow the 250 (500) GeV chargino mass contour, as expected.[3] However, there are two areas where this is not the case. In the lower left corner of the plot, the slepton line follows the 250 (500) GeV slepton mass contour instead, meaning that this analysis actually finds slepton pair production here. Further, in the HB/FP region of the CMSSM parameter space, close to the area with no REWSB, the lines fall off compared to the chargino mass contour(s). This effect is most pronounced in the 1 TeV case. As indicated by the mass contours, the charginos

[1]The squark mass contour is the average mass of the first and second generation squarks, both left- and right-handed, while the slepton mass contour is the average mass of the left- and right-handed selectrons.

[2]The 250 and 500 GeV mass contours for $\tilde{\chi}_1^\pm$ and $\tilde{\chi}_1^0$ overlap for large values of m_0, leading to an unfortunate color mixing. We ran out of colors.

[3]Chargino production can produce the same signature as slepton production if both of the charginos decay leptonically, $\tilde{\chi}_1^\pm \to W^\pm \tilde{\chi}_1^0 \to \ell^\pm \nu \tilde{\chi}_1^0$.

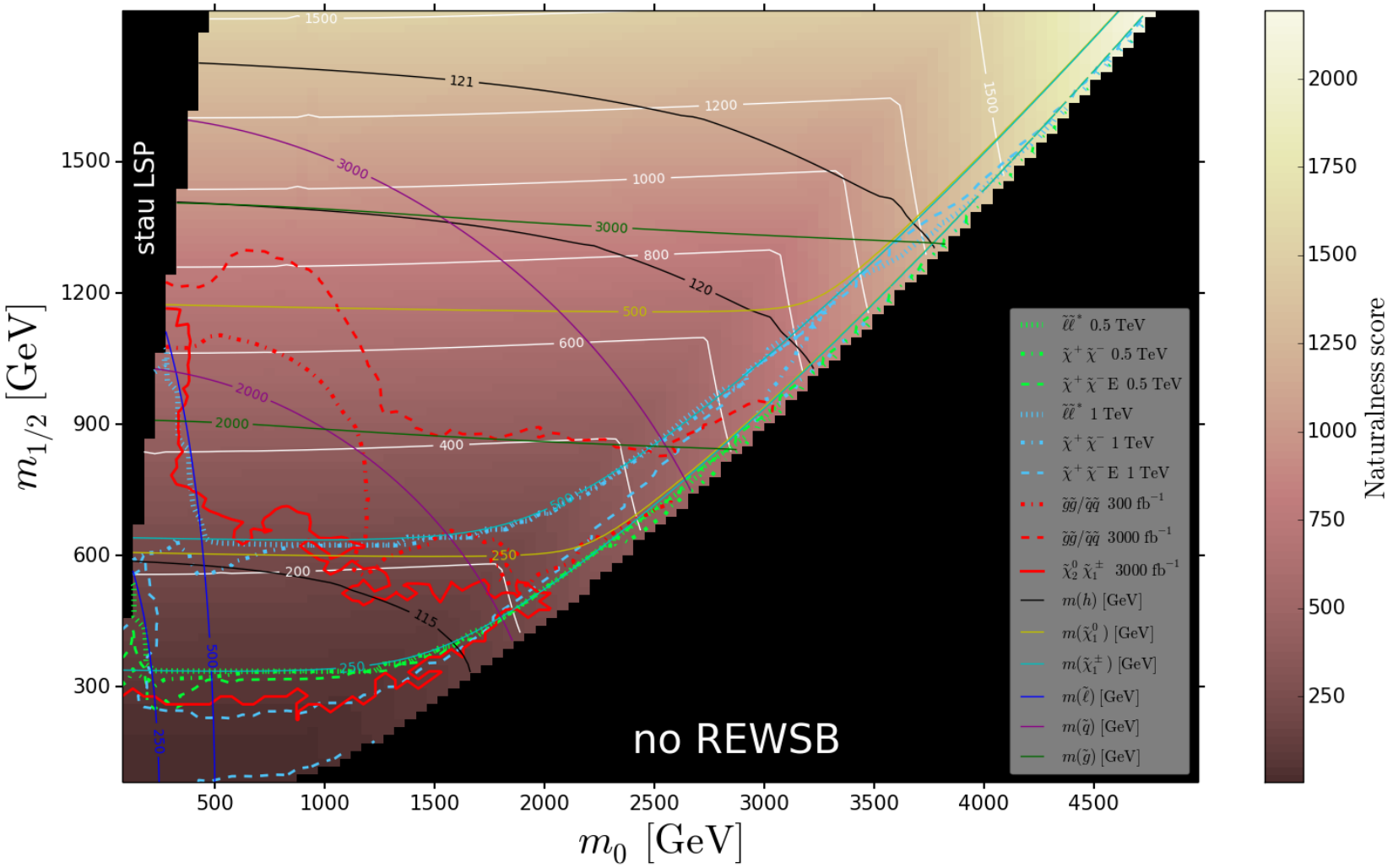

Figure 6.2: 95% CL exclusion limits for the CMSSM10 scenario, with $\tan\beta = 10$, $A_0 = 0$ and $\mathrm{sign}(\mu) > 0$. The white lines are contours for the naturalness score, represented by the background density and the bar on the right. Also shown are mass contours for sleptons (dark blue), squarks (purple), gluinos (dark green), Higgs (black), neutralinos (yellow) and charginos (turquoise).

and neutralinos become mass degenerate in this area, meaning that the energy release in the chargino decays falls drastically, leading to soft final state particles not passing the selection cuts for the different search analyses.[4]

When taking a closer look at the 1 TeV exclusion limits, there are two surprising things worth noticing. First, the slepton analysis appears to be very efficient in the HB/FP region. The chargino extended analysis, designed for this region, is just marginally better. Investigating this further, we found that the slepton analysis picks up production of $\tilde{\chi}_2^0\tilde{\chi}_1^0$ in this area, where $m_{\tilde{\chi}_2^0} \approx m_{\tilde{\chi}_1^0} \approx m_{\tilde{\chi}_1^\pm}$. If the $\tilde{\chi}_2^0$ decays into a virtual Z boson and the LSP, and the Z boson in turn decays into two leptons, this gives the signature the slepton analysis is searching for.

Second, the chargino extended analysis is very inefficicent for low values of m_0, more so than the standard chargino analysis. In principle, this line should follow the 500 GeV chargino mass contour. The inefficiency is due to too much visible energy. If two charginos with $m_{\tilde{\chi}_1^\pm} \approx 500$ GeV are produced, and each of them decay into the LSP with $m_{\tilde{\chi}_1^0} \approx 250$ GeV (predicted by Eq. (2.84)), there is approximately 2×250 GeV $= 500$ GeV of energy left for leptons and jets, i.e. visible energy. However, the chargino extended analysis only allows between 20 and 100 GeV of visible energy, see Table 5.5.[5] Although this analysis is no good in this area, it has the best reach in the HB/FB region, which it was designed for. We also observe that the 1 TeV chargino extended analysis does not exclude the lowest values of $m_{1/2}$. This is probably due to the same reason as discussed above: there is too much visible energy below the lower exclusion line.

The exclusion limit for the HL-LHC analysis searching for squark and gluino pair production is shown for both integrated luminosities considered, while only the 3000 fb^{-1} result has been included for the chargino–neutralino search. As seen in the plot, the latter analysis suffers from statistical fluctuations, although 200 000 events were generated for each parameter point, i.e. twice as many as for the other analyses.[6,7]

We see that the dashed red line, corresponding to the 3000 fb^{-1} $\tilde{g}\tilde{g}/\tilde{q}\tilde{q}^*$ exclusion limit, excludes all $m_{1/2}$ values below ~ 900 GeV, in addition to all squark and virtually all gluino masses below ~ 2000 GeV. The shape of this line is similar to the exclusion limit in Fig. 3 of Ref. [36], here given in Fig. 6.1. However, since

[4]Equation (2.84), predicted by GUT relations, is mostly valid in the CMSSM. The only exception is the HB/FB region, where μ is small and $\tilde{\chi}_2^0$, $\tilde{\chi}_1^0$ and $\tilde{\chi}_1^\pm$ all are dominantly higgsino, with masses $\sim \mu$.

[5]The effect discussed here is not so evident for the 0.5 TeV chargino extended line, since the decay products are not that hard at this energy.

[6]The statistical fluctuations are due to the uncertainty in the very low selection efficiency, given by Eq. (5.10).

[7]The HL-LHC results discussed in Ref. [1] are obtained from eight times the statistics used here, i.e. 800 000 (1 600 000) generated events for each parameter point for the gluino/squark (chargino–neutralino) search.

the integrated luminosity used here is much higher, 3000 fb^{-1} vs. 10 fb^{-1}, it lies above the limit in that figure. Another prominent difference between Figs. 6.1 and 6.2 is the clear shift of the "no REWSB" area, due to the improvement of RGE codes since 2000.

An important result in Fig. 6.2 is that the ILC has a better reach than the HL-LHC in the HB/FP region of the CMSSM parameter space. Two of the 1 TeV ILC analyses reach past gluino masses of 3000 GeV.

6.1.2 Naturalness reach

In Ref. [36], the naturalness reach of the LHC is quantified in terms of the largest naturalness score for which the contour is completely within the exclusion limit. The resulting naturalness reach in that paper is 210, which can be seen in Fig. 6.1. Following the same approach, we find a naturalness reach of 400 for the HL-LHC, given by the 3000 fb^{-1} $\tilde{g}\tilde{g}/\tilde{q}\tilde{q}^*$ exclusion limit. By comparing Figs. 6.1 and 6.2, it is evident that the naturalness contours are more or less located at the same place in the parameter space. The difference in the naturalness reach is thus mostly due to the luminosity difference discussed above. Following the same prescription for the ILC exclusion limits, the naturalness reach of the ILC can be quantified to be ~ 250, given by the 1 TeV slepton exclusion limit.

The definition of naturalness reach described above is rather limited. For instance, it does not reflect that the HL-LHC excludes regions of parameter space with naturalness scores up to $c \sim 800$, while the ILC excludes regions of parameter space with naturalness scores up to $c \sim 2000$. In this work, we have therefore also used Bayesian parameter estimation to investigate the naturalness reach of these colliders. In this context, the reach is quantified by the Kullback–Leibler divergence in Eq. (4.15), and reflects the amount of information that can be gained about naturalness from the different searches at the ILC and the HL-LHC.

Figure 6.3 shows the naturalness prior and posteriors for the different analyses in the case of flat priors in m_0 and $m_{1/2}$. These distributions have been obtained following the prescription in Sec. 4.6. The sudden drop at $c \sim 1500$ is due to the shape of the naturalness contour lines in Fig. 6.2 and the chosen prior ranges. The ILC 1 TeV and HL-LHC 3000 fb^{-1} posteriors are based on the product of the likelihoods for the different searches at the given energy/luminosity. For clarity, the ILC 0.5 TeV and HL-LHC 300 fb^{-1} posteriors have not been included in the figure. However, the total posterior is based on the product of all of the likelihoods obtained in this work, in addition to the Higgs likelihood given by Eq. (4.9), with standard deviation $\sigma = 2$ GeV, and the observed Higgs mass

$m_h^{\text{obs}} = 125$ GeV as data.[8]

From this figure, we see that the ILC's effect on the naturalness distribution is not very significant in this scenario. The distribution is more limited by the HL-LHC searches. This corresponds to what we found above, following the prescription in Ref. [36]. However, the total posterior is dominated by the Higgs likelihood. Since the standard deviation of 2 GeV is small compared to the measured Higgs mass of ~ 125 GeV, this likelihood represents very strong data. As the correct Higgs mass does not occur in this scenario, the Higgs likelihood favours the highest naturalness scores shown in Fig. 6.2. The total posterior peaks at $c \sim 1500$, meaning that after introducing all of the data, this is the most probable naturalness score in the CMSSM10 scenario for the given prior ranges.

Note that the HL-LHC posterior has a small peak for the lowest values of c. This is because the $\tilde{\chi}_2^0\tilde{\chi}_1^\pm$ exclusion limit in Fig. 6.2 does not exclude $m_{1/2}$ values below ~ 300 GeV, i.e. the area with the lowest naturalness scores. As the HL-LHC searches are designed to target heavy sparticle production, they are inefficient for low sparticle masses, for which the decay products are not hard enough to pass the selection cuts. However, due to the poor statistics, it is not clear exactly where the return line should be. Thus, although this is a physical effect, it may be exaggerated due to the bad statistics for this particular analysis. The $\tilde{g}\tilde{g}/\tilde{q}\tilde{q}^*$ exclusion limit also contributes to this effect, although this is not directly visible in Fig. 6.2. In any case, this particular area has already been excluded by previous searches, meaning that the effect can be ignored.

Figure 6.4 shows the corresponding results as Fig. 6.3, but for log priors in m_0 and $m_{1/2}$. We have used a logarithmic y-axis in this figure, to emphasize the differences between the distributions. The features discussed above can be seen also in this figure. The effect for the HL-LHC posterior at low values of c is more pronounced in this case, since the log priors favour low values of c, giving a larger contribution to the posterior in this area than flat priors. It is again evident that it is the Higgs likelihood that dominates the total posterior. In fact, we see that the probability density is virtually the same at large values of c for the two different prior choices, meaning that the total data in this case is so strong that the posterior is prior independent.

The Kullback–Leibler divergence (D_{KL}) values correponding to the naturalness priors and posteriors shown in Figs. 6.3 and 6.4 are given in Table 6.1. Note that the D_{KL} value for the total posterior is not the sum of the D_{KL} values for the individual posteriors, although it appears to be close. There is no linear relation between the D_{KL} values calculated from the individual likelihoods and the D_{KL} value calculated from the total likelihood.

[8] The experimental uncertainty in the measured Higgs mass is small. However, the theoretical uncertainty in the predicted Higgs mass at a given SUSY parameter point, calculated by `FeynHiggs`, is rather large (~ 2 GeV).

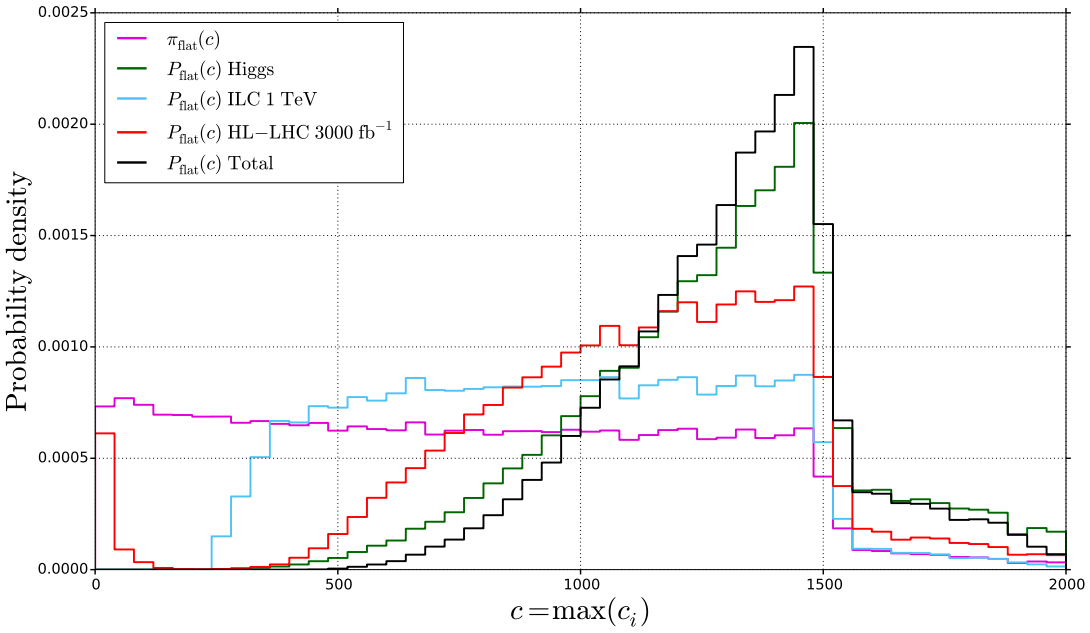

Figure 6.3: Naturalness prior and posterior distributions in the CMSSM10 scenario for flat priors in m_0 and $m_{1/2}$.

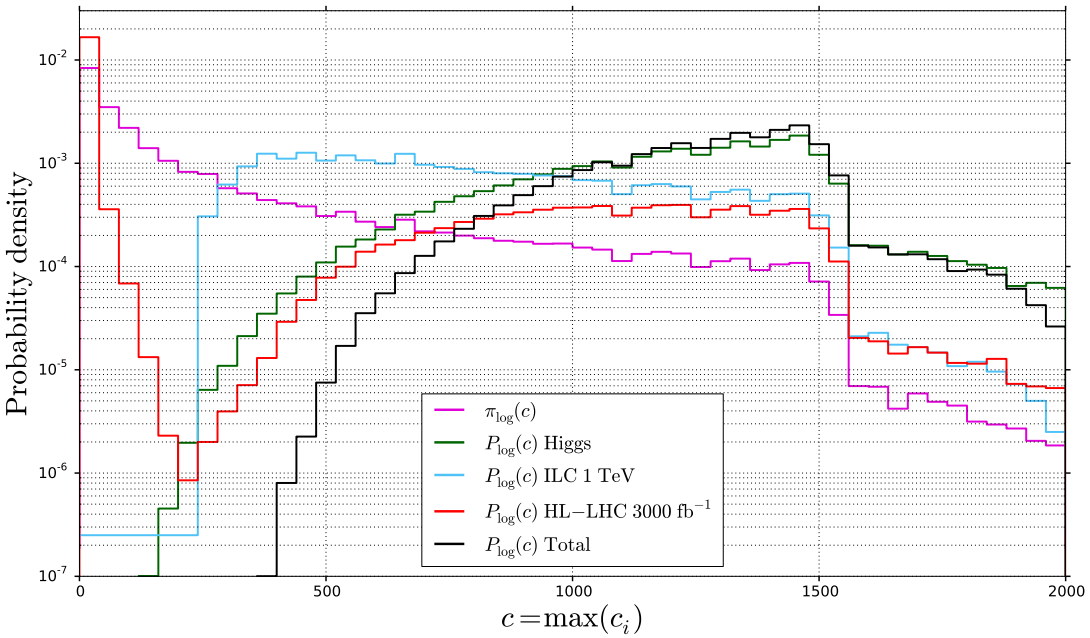

Figure 6.4: Naturalness prior and posterior distributions in the CMSSM10 scenario for log priors in m_0 and $m_{1/2}$.

Table 6.1: D_{KL} values in the CMSSM10 scenario, correponding to the priors and posteriors given in Figs. 6.3 and 6.4, for flat and log priors in m_0 and $m_{1/2}$, respectively. The ILC 0.5 TeV and HL-LHC 300 fb^{-1} likelihoods have been included in the total.

Posterior	Flat priors	Log priors
ILC 1 TeV	0.221	1.313
HL-LHC 3000 fb^{-1}	0.400	0.639
Higgs	0.708	2.141
Total	0.845	2.436

It is difficult to say anything about the absolute values of these numbers, as they depend on the prior ranges used for m_0 and $m_{1/2}$, especially for flat priors.[9] However, the Kullback–Leibler divergence is a well-behaved measure of information [60], and the different values can be compared to each other as long as they are based on the same ranges.

We see that we in general learn more when starting from log priors compared to starting from flat priors, as we also saw in the toy example in Sec. 4.5.1. This is no surprise, since log priors favour low sparticle masses, while the different likelihoods obtained in this work (mostly) favour large masses. The numbers in Table 6.1 again emphasize that the Higgs likelihood is completely dominant in this scenario — the information gain is by far largest for this data.

Note that the information gain for flat priors is larger for the HL-LHC than for the ILC. This corresponds to that the HL-LHC searches exclude a larger area of Fig. 6.2 than the ILC searches. In this case, we learn almost twice as much about naturalness from the HL-LHC than from the ILC. However, for log priors, it is the other way around, as log priors emphasize low sparticle masses. Since the HL-LHC searches used here allow small masses, the resulting information gain is small.

6.2 The CMSSM30 scenario

The goal of this work is to study the effect of future supersymmetry searches at the ILC and the HL-LHC on naturalness. The fact that the Higgs likelihood

[9] The likelihood becomes constant for large values of m_0 and $m_{1/2}$. By extending the prior ranges for flat priors in these parameters, a constant contribution is added to the Kullback–Leibler divergence, since the naturalness distribution then contains a bigger range of naturalness scores. For log priors, this contribution goes to zero, since these priors fade for large values of m_0 and $m_{1/2}$.

completely dominates the total posterior in the CMSSM10 scenario makes the above first encounter with Bayesian parameter estimation and Kullback–Leibler divergence in relation to naturalness a little silly. In this section, we will see how this changes for the more realistic CMSSM30 scenario, which contains the measured Higgs mass. The price we pay for this is that the naturalness score in this scenario in general is a little higher than in the CMSSM10 scenario.

6.2.1 95% CL exclusion limits

Figure 6.5 shows the 95% CL exclusion limits obtained in this work for the CMSSM30 scenario. The components of this plot are the same as in Fig. 6.2 for the CMSSM10 scenario. The only exception is that there is no unphysical area without radiative electroweak symmetry breaking in this scenario. Instead, there is an unphysical area due to tachyons, i.e. particles with negative (squared) masses. The 1 TeV chargino extended line has been removed for clarity, since the HB/FP region with mass degenerate charginos and neutralinos that this analysis was designed for does not appear in this figure. This region is located at larger values of m_0 in the CMSSM30 scenario. The excluded line ran along $m_{1/2} \sim 200$ GeV, not contributing much to the plot.

As expected, we see that the 0.5 and 1 TeV ILC exclusion limits follow the 250 and 500 GeV chargino mass contours, respectively.[10] The only exception is for small values of m_0, where the slepton analysis surprisingly exclude both slepton and chargino masses above these contours. This is most evident for the 1 TeV line. The analysis probably picks up production of $\tilde{\chi}_2^0\tilde{\chi}_1^0$ in this area, as we also saw in the HB/FP region of the CMSSM10 scenario.[11]

Only the $\tilde{g}\tilde{g}/\tilde{q}\tilde{q}^*$ results have been included for the HL-LHC in Fig. 6.5, since the $\tilde{\chi}_2^0\tilde{\chi}_1^\pm$ analysis suffers from massive statistical fluctuations in this scenario (much worse than in the CMSSM10 scenario), and its exclusion limits are located below the $\tilde{g}\tilde{g}/\tilde{q}\tilde{q}^*$ limits. These fluctuations are also evident for the lower $\tilde{g}\tilde{g}/\tilde{q}\tilde{q}^*$ lines, at low values of $m_{1/2}$. As stated in Sec. 6.1.2, the reason for these lower lines is that the HL-LHC analyses are inefficient for small sparticle masses.

The (upper) $\tilde{g}\tilde{g}/\tilde{q}\tilde{q}^*$ lines are close to being gluino mass isocurves, meaning that gluino pair production is very efficient in this scenario. At low m_0 values, where the squark and gluino mass contours meet, squark pair production takes over. Both squark and gluino masses below ~ 2300 GeV are excluded by the 3000 fb^{-1} line. Again, the HL-LHC results will be discussed in more detail in Ref. [1].

[10] The slepton analysis picks up chargino production also here.

[11] However, in this case, there is no chargino–neutralino mass degeneration. The relation $m_{\tilde{\chi}_2^0} \approx 2m_{\tilde{\chi}_1^0}$ from Eq. (2.84) is valid in the entire m_0–$m_{1/2}$ plane we are studying in this scenario.

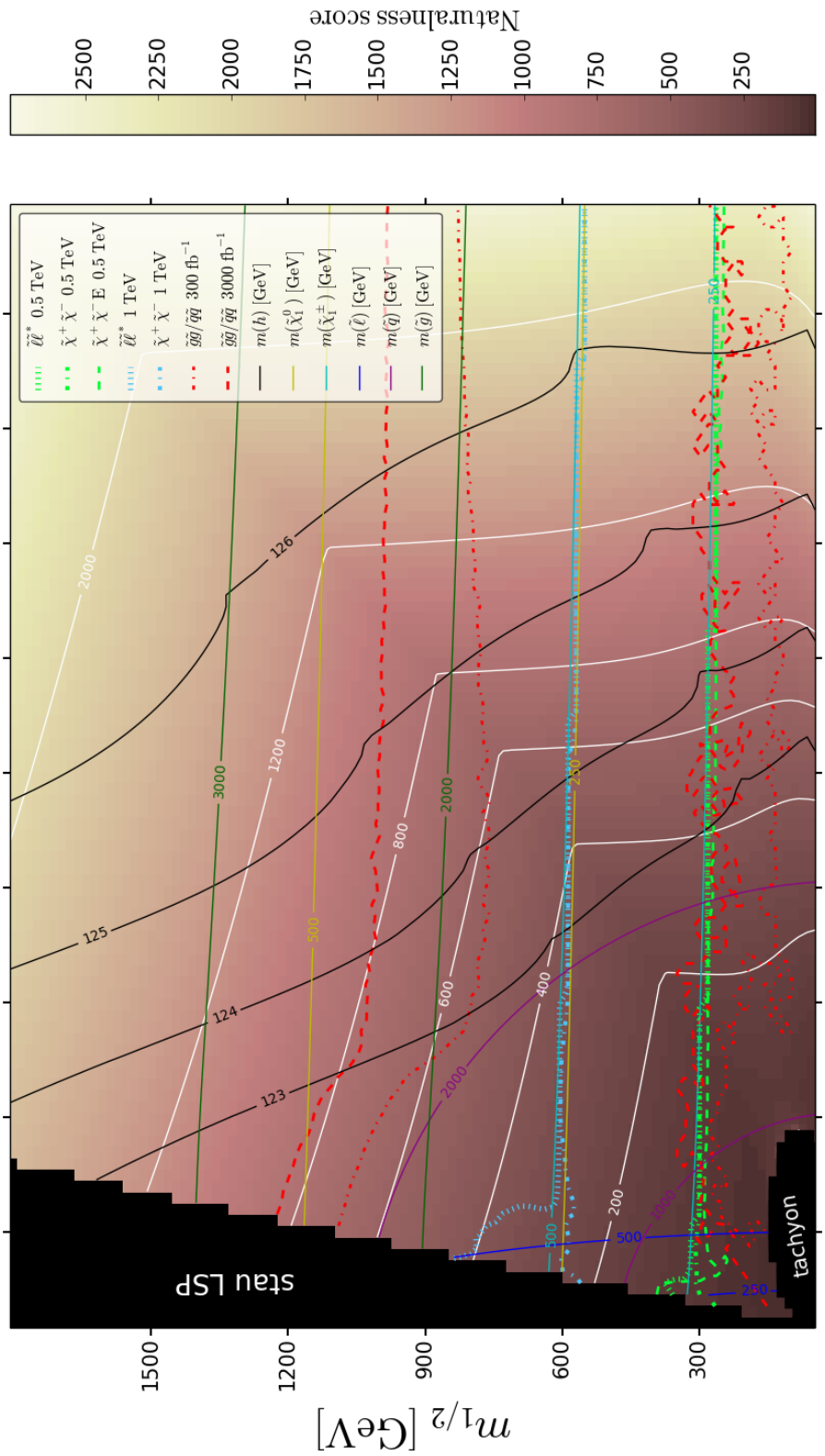

Figure 6.5: 95% CL exclusion limits for the CMSSM30 scenario, with $\tan\beta = 30$, $A_0 = -2m_0$ and $\text{sign}(\mu) > 0$. The white lines are contour lines for the naturalness score. Also shown are mass contours for sleptons (dark blue), squarks (purple), gluinos (dark green), Higgs (black), neutralinos (yellow) and charginos (turquoise).

6.2.2 Naturalness reach

By following the prescription in Ref. [36], the naturalness reach of the HL-LHC can be quantified to be 800 in this scenario, given by the 3000 fb^{-1} $\tilde{g}\tilde{g}/\tilde{q}\tilde{q}^*$ line. This is twice as much as in the CMSSM10 scenario. However, as mentioned in the introduction to this section, a higher naturalness reach was expected for this scenario. Similarly, the naturalness reach of the ILC can be quantified to be ~ 300, also in this scenario given by the 1 TeV slepton exclusion limit.

Figure 6.6 shows the naturalness prior and posteriors for the different analyses in the case of flat priors in m_0 and $m_{1/2}$, while Fig. 6.7 shows the same for log priors. Here, the HL-LHC 3000 fb^{-1} posterior is obtained from the $\tilde{g}\tilde{g}/\tilde{q}\tilde{q}^*$ likelihood alone, while the ILC 1 TeV posterior is obtained from the product of the likelihoods of all three ILC analyses, even though the 1 TeV chargino extended line has been removed from figure Fig. 6.5. As for the CMSSM10 scenario, the ILC 0.5 TeV and HL-LHC 300 fb^{-1} posteriors are not shown, but their likelihoods are included for the total posterior.

Most features seen in these distributions are the same as in Figs. 6.3 and 6.4 for the CMSSM10 scenario. The main difference is that the Higgs likelihood is less dominating, as expected, since the CMSSM30 scenario actually contains the measured Higgs mass. For flat priors in Fig. 6.6, it is the HL-LHC likelihood that dominates the total posterior. This is in good agreement with Fig. 6.5, where we see that the 3000 fb^{-1} HL-LHC exclusion limit excludes a larger area than the 1 TeV ILC exclusion limits. However, for log priors in Fig. 6.7, the HL-LHC posterior has a significant peak for the lowest naturalness scores. The rest of the distribution then needs to be rather low, as all posteriors must integrate to unity. It is thus the ILC likelihood (together with the Higgs likelihood) that dominates the total posterior in this case.

Despite the differences between Figs. 6.6 and 6.7, the total posterior has a peak at roughly the same naturalness score in the two figures, i.e. $c \sim 1600$, and with roughly the same magnitude. After introducing all of the data, this is thus the most probable naturalness score in the CMSSM30 scenario for the given prior ranges, independent of the prior choice. However, as the total posterior is much more flat in Fig. 6.7, naturalness scores below this value are also very probable in the case of log priors in m_0 and $m_{1/2}$.

The D_{KL} values correponding to the naturalness priors and posteriors shown in Figs. 6.6 and 6.7 are given in Table 6.2. By comparing these numbers to Table 6.1, we see that we in general learn less about naturalness in this scenario than in the CMSSM10 scenario. This is due to how the naturalness is distributed in Fig. 6.5, together with the shape of the exclusion limits. Thus, even though higher naturalness scores are excluded in this scenario than in the CMSSM10 scenario, we actually learn less about naturalness.

For the HL-LHC posterior, the information gain is largest when starting from flat priors in this scenario, in contrast to the trend in Table 6.1. This reflects

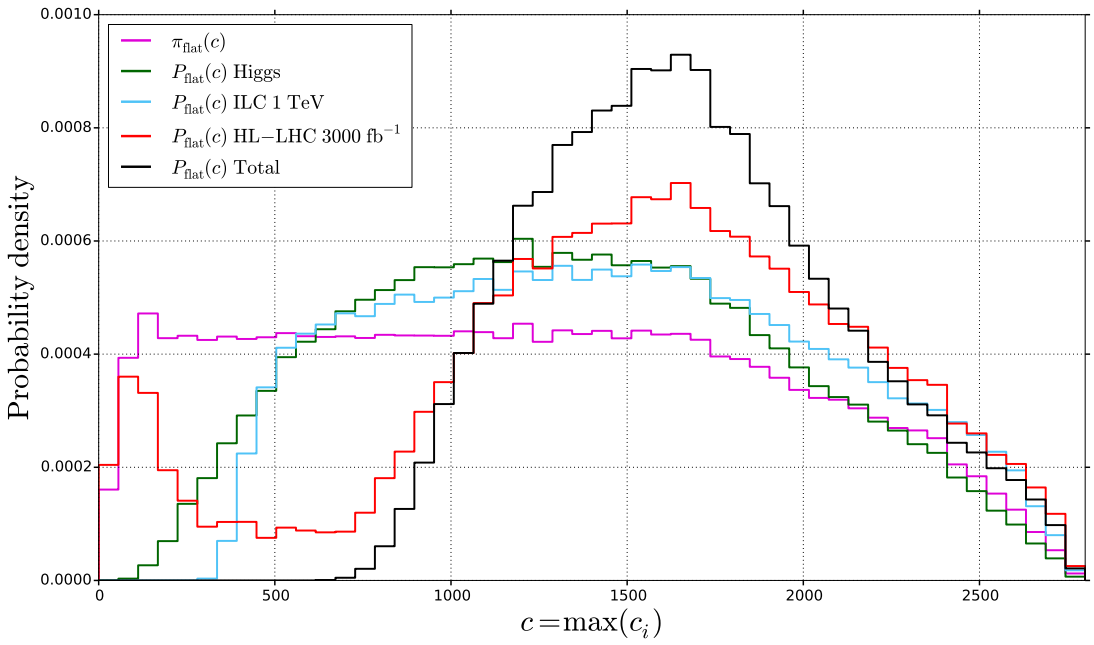

Figure 6.6: Naturalness prior and posterior distributions in the CMSSM30 scenario for flat priors in m_0 and $m_{1/2}$.

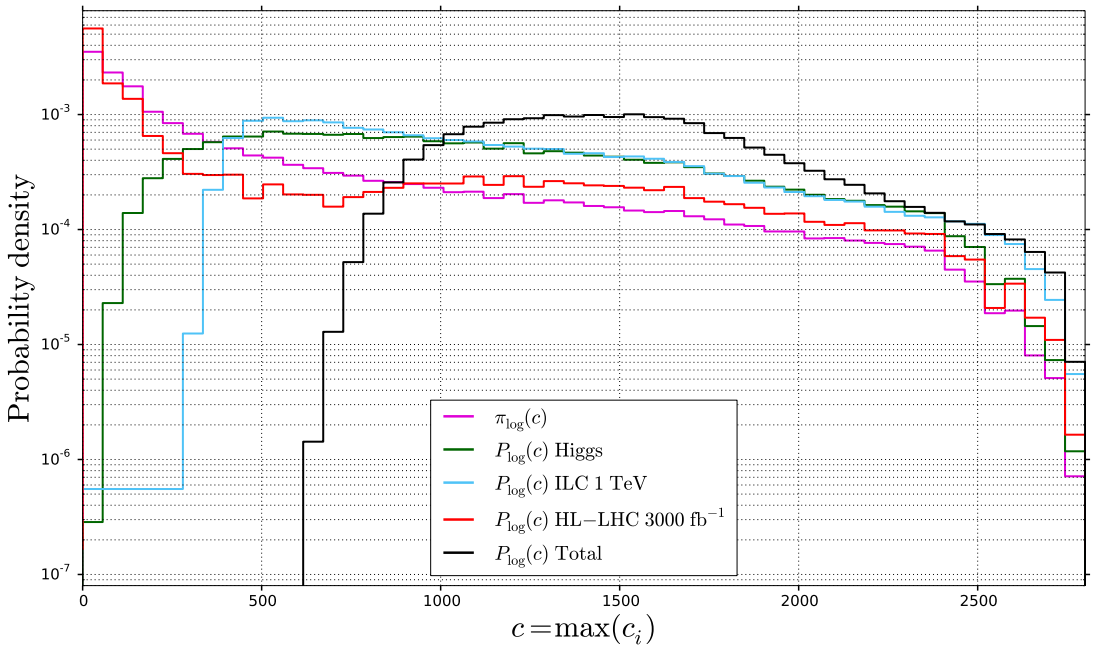

Figure 6.7: Naturalness prior and posterior distributions in the CMSSM30 scenario for log priors in m_0 and $m_{1/2}$.

Table 6.2: D_{KL} values in the CMSSM30 scenario, correponding to the priors and posteriors given in Figs. 6.6 and 6.7, for flat and log priors in m_0 and $m_{1/2}$, respectively. The ILC 0.5 TeV and HL-LHC 300 fb^{-1} likelihoods have been included in the total.

Posterior	Flat priors	Log priors
ILC 1 TeV	0.165	0.903
HL-LHC 3000 fb^{-1}	0.174	0.092
Higgs	0.101	0.672
Total	0.469	1.517

that this posterior is very similar to the naturalness prior in Fig. 6.7. Further, for flat priors, the D_{KL} values for the HL-LHC and ILC posteriors are approximately equal. The searches at the two colliders thus contribute with the same amount of information in this case. For log priors, on the other hand, we learn about ten times as much about naturalness from the ILC than from the HL-LHC, again reflecting the inefficiency of the HL-LHC searches discussed above.

6.3 The NUHM2 scenario

As discussed in Sec. 3.3, the part of the NUHM2 parameter space that we are studying in this thesis is motivated by that it both has low fine-tuning and includes the correct Higgs mass. These two things can not be obtained simultaneously in the CMSSM.

This particular NUHM2 region is investigated in Ref. [30], where it is referred to as Radiatively-driven Natural SUSY (RNS). Below, we will compare our results to Fig. 16 of that paper, included here as Fig. 6.8 for ease of reference. The only differences between the scenario we are studying and the scenario depicted in that figure is that we have fixed m_0 at 4 TeV instead of 5 TeV, in order to predict a Higgs mass as close to the measured value as possible with a different choice of RGE codes.[12] In addition, the naturalness measure used in Fig. 6.8 is so-called electroweak naturalness, not the Barbieri–Giudice measure. The difference between the two measures was briefly discussed in Sec. 3.3.

[12]We use `SOFTSUSY` versus `ISAJET` in Ref. [30], and we improve the Higgs mass calculation with `FeynHiggs`, see Sec. 5.2.

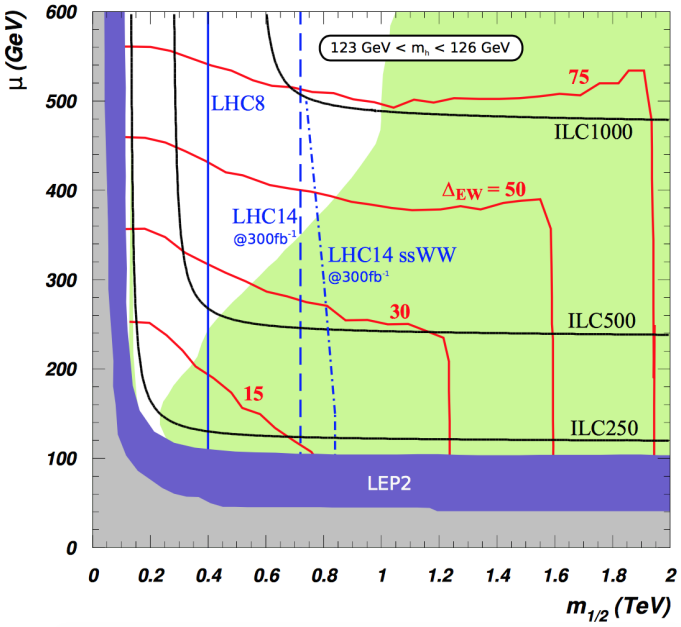

Figure 6.8: Expected naturalness reach of the LHC in the $m_{1/2}$–μ mass plane of the NUHM2 model, for $\tan\beta = 15$, $m_0 = 5$ TeV, $A_0 = -1.6m_0$ and $m_A = 1$ TeV, from Ref. [30]. Included for ease of reference. In black are shown approximate ILC reach in terms of chargino mass isocurves (ILC1000 indicates $m_{\tilde{\chi}_1^\pm} = 500$ GeV, etc.). Note that the naturalness measure in this plot, indicated by the red contours, is so-called electroweak (EW) naturalness, not the Barbieri–Giudice measure.

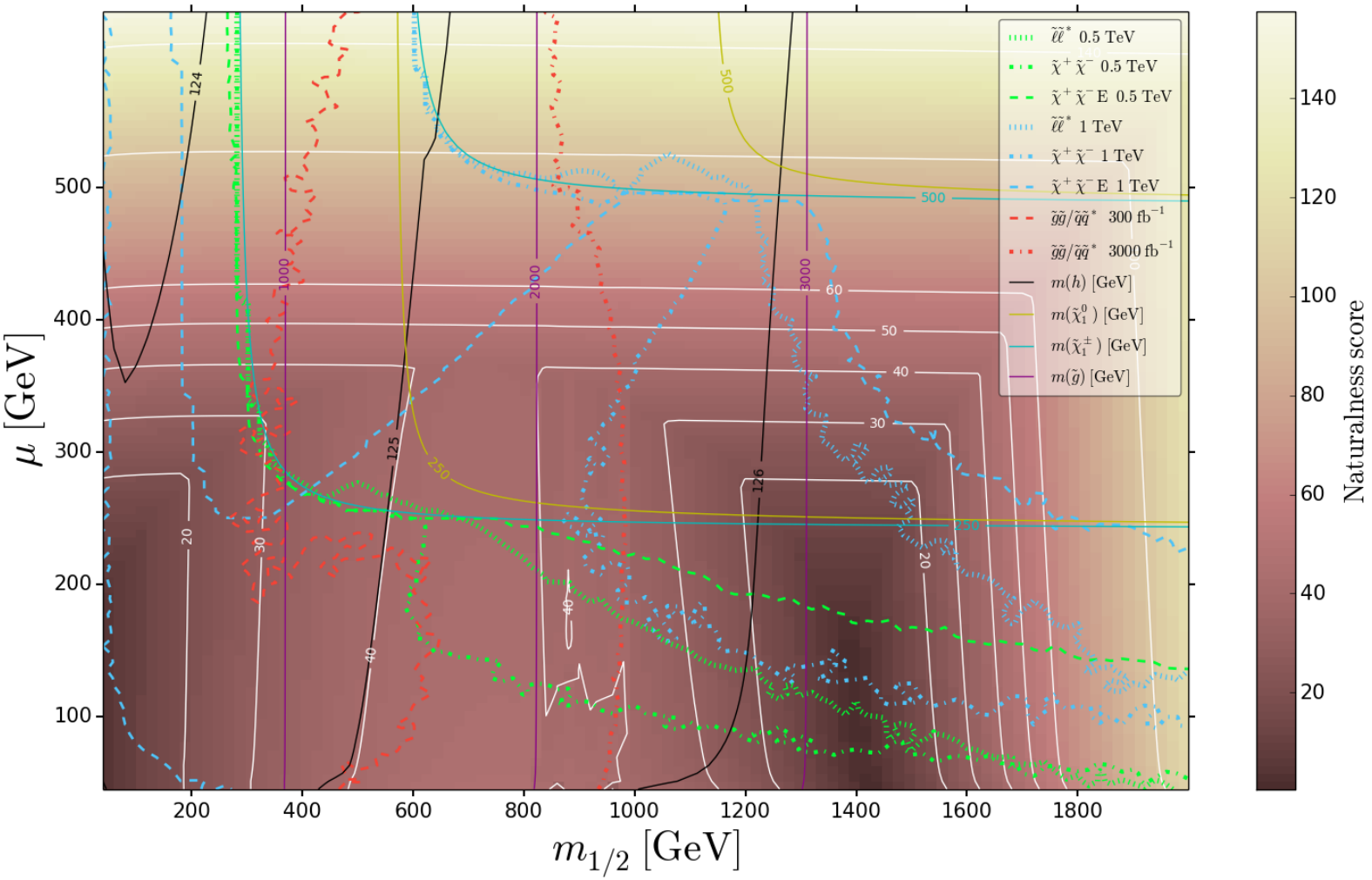

Figure 6.9: 95% CL exclusion limits for the NUHM2 scenario, with $\tan\beta = 15$, $m_0 = 5$ TeV, $A_0 = -1.6m_0$ and $m_A = 1$ TeV. The white lines are contour lines for the naturalness score. Also shown are mass contours for gluinos (purple), Higgs (black), neutralinos (yellow) and charginos (turquoise).

6.3.1 95% CL exclusion limits

Figure 6.9 shows the 95% CL exclusion limits obtained in this work for the NUHM2 scenario. In this plot, there are no unphysical areas.

As in Figs. 6.2 and 6.5, the 0.5 and 1 TeV ILC exclusion limits more or less follow the 250 and 500 GeV chargino mass contours, respectively. However, in this scenario, there are three exceptions. First, when the charginos and neutralinos become mass degenerate for large values of $m_{1/2}$, the exclusion limits fall off compared to the mass contours, as we also saw in the CMSSM10 scenario. As discussed in Sec. 6.1.1, this is because the energy release in the chargino decays becomes so small that the final state particles do not pass the selection cuts for the different analyses. Although this effect is evident for all three analyses, the chargino extended lines are strongest, as expected.

Second, both the 0.5 and 1 TeV slepton lines have some excursions above the respective chargino mass contours, indicating that something else than charginos has been produced.[13] As in the first two scenarios, it appears that the slepton analysis picks up production of $\tilde{\chi}_2^0\tilde{\chi}_1^0$, where $m_{\tilde{\chi}_2^0} \approx m_{\tilde{\chi}_1^0} \approx \mu$.

Third, the 1 TeV chargino extended line is once again completely off for small values of $m_{1/2}$, due to the cut on visible energy. However, as stated above, it has the best reach in the mass degenerate area, which it was designed for.

In this scenario we only include the $\tilde{g}\tilde{g}/\tilde{q}\tilde{q}^*$ results for the HL-LHC, since the chargino–neutralino analysis suffers from massive statistical fluctuations. The $\tilde{g}\tilde{g}/\tilde{q}\tilde{q}^*$ analysis only picks up gluino production, since the squarks are too heavy to be produced ($m_0 = 4$ TeV). As for the two CMSSM scenarios, we see that gluino masses below ~ 2000 GeV are completely excluded. This reflects that gluinos of approximately 2000 GeV is the kinematical limit for gluino production at a proton–proton collider with centre-of-mass energy $\sqrt{s} = 14$ TeV. In contrast, the ILC appears to exclude parameter points with gluino masses well above this in this particular scenario.

The results in Fig. 6.9 can be compared to Fig. 16 of Ref. [30], here given in Fig. 6.8. We see that the 3000 fb^{-1} HL-LHC exclusion limit obtained in this work is located at a higher $m_{1/2}$ value than in that figure. This is no surprise, since the luminosity used here is ten times as high as the luminosity used in Ref. [30]. Further, the ILC results obtained here are more realistic than the ILC lines (chargino mass isocurves) shown in Fig. 6.8.

6.3.2 Naturalness reach

From Fig. 6.9, we see that the naturalness score is drastically lower in this scenario than in the two CMSSM scenarios, as expected. Note that some of the naturalness contours have a peculiar shape. There is a plateu with $c \sim 40$ in the lower

[13] The sleptons are too heavy to be produced in this scenario, since m_0 is fixed at 4 TeV.

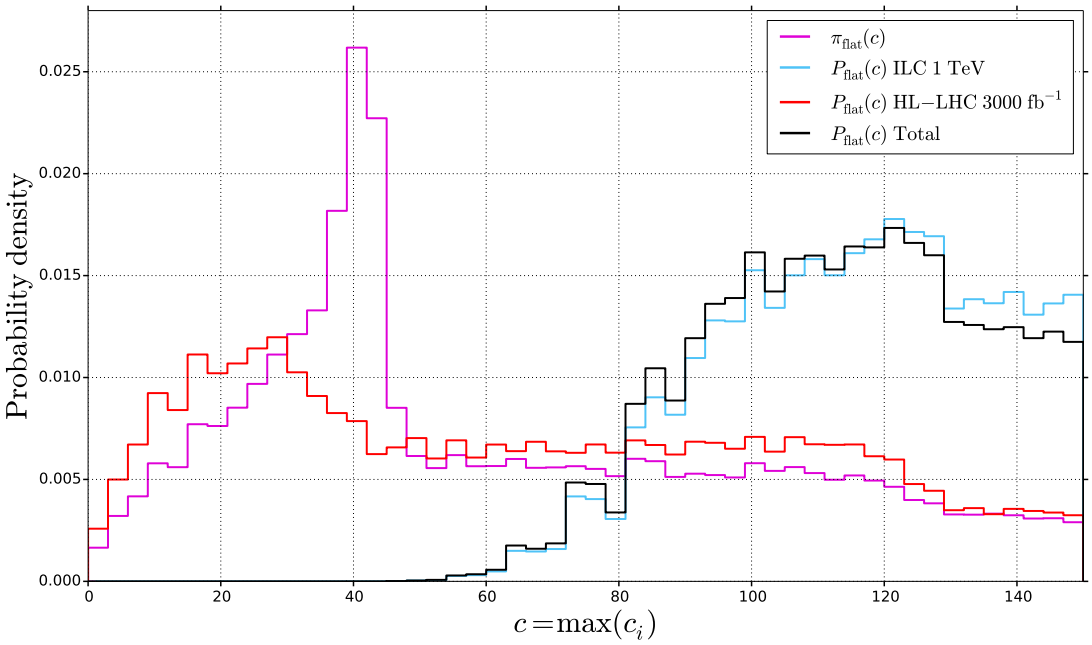

Figure 6.10: Naturalness prior and posterior distributions in the NUHM2 scenario for flat priors in m_0 and $m_{1/2}$.

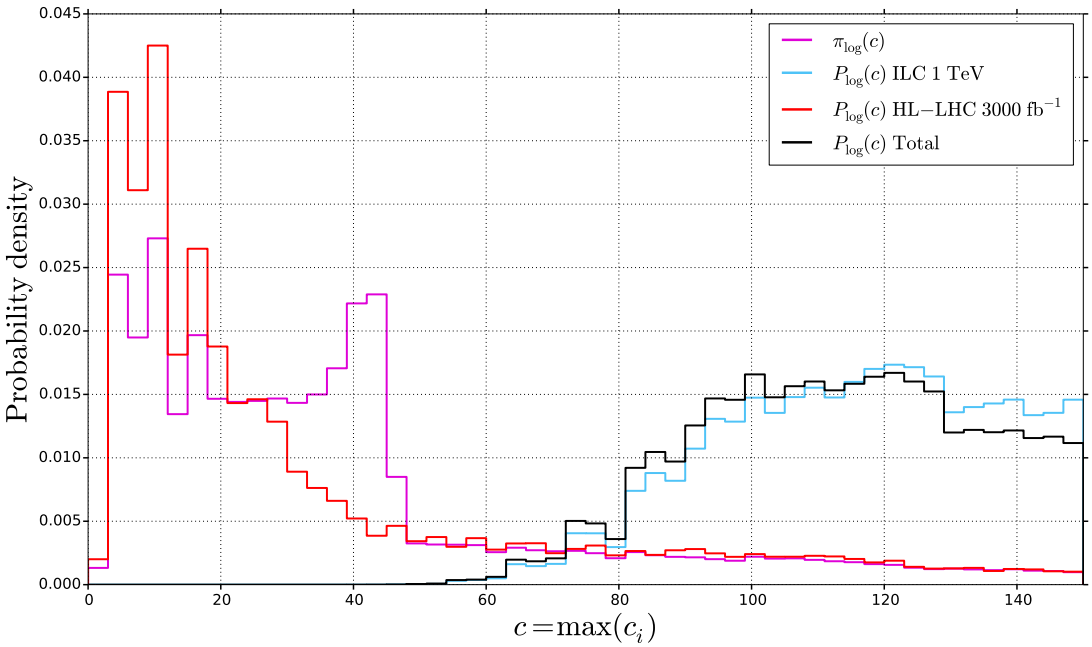

Figure 6.11: Naturalness prior and posterior distributions in the NUHM2 scenario for log priors in m_0 and $m_{1/2}$.

middle part of the plot. The naturalness score is calculated from $m_{1/2}$ and μ in this scenario, in contrast to m_0 and $m_{1/2}$, which is the case for the two CMSSM scenarios.

In Fig. 6.9, it is the combined 1 TeV chargino and chargino extended lines that enclose the largest naturalness score contour. Taking the same approach as Ref. [36], the naturalness reach of the ILC is quantified to be $c \sim 30$ in this scenario. The correponding reach in Fig. 6.8 is $c \sim 70$. By comparing the naturalness contours in these two figures, we see that they are quite similar, even though they are based on two different measures of naturalness. However, since the 1 TeV ILC line in Fig. 6.8 only depicts the kinematical limit, it does not take into account the search inefficiency due to the chargino and neutralino mass degeneration, and a higher naturalness reach is thus obtained.

Figure 6.10 shows the naturalness prior and posteriors for the different analyses in the case of flat priors in $m_{1/2}$ and μ. The Higgs posterior is not included in this case, since the complete standard deviation of 2 GeV is present in Fig. 6.9, meaning that the Higgs posterior does not contribute with very much information in this scenario. However, the Higgs likelihood has been included in the total, in addition to the ILC 0.5 TeV and HL-LHC 300 fb^{-1} likelihoods.

Due to the naturalness plateau noted above, a quite pronounced peak is seen at $c \sim 40$ for the naturalness prior. Since the 3000 fb^{-1} HL-LHC line excludes most of this plateau in Fig. 6.9, this peak is not visible in the HL-LHC posterior. Due to the peculiar distribution of the lowest naturalness scores in Fig. 6.9, the HL-LHC posterior is distributed quite evenly over all of the possible scores, although almost half of the parameter space shown in the figure is excluded. This means that the HL-LHC contributes with very little knowledge on naturalness in this scenario. In contrast, we see that the ILC posterior limits the naturalness distribution much more, and its likelihood totally dominates the total posterior.

Figure 6.11 shows the corresponding results, but for log priors in $m_{1/2}$ and μ. The features discussed above can be seen also in this figure. However, as log priors favour the lower left corner of Fig. 6.9, as well as the areas close to both axes, both the prior and the HL-LHC posterior peak at very low c values, in addition to the peak at $c \sim 40$ for the prior.

By comparing the posterior distributions for the two different prior choices, we see that the total posterior in both cases is completely dominated by the ILC likelihood. The total posteriors in Figs. 6.10 and 6.11 are virtually identical. This correponds to that the ILC searches exclude most of the parameter space shown in Fig. 6.9, so the prior choice is not very significant in this scenario. The ILC data is so strong that the total posterior is independent of the prior. The total posterior peaks at $c \sim 120$. This is thus the most probable naturalness score in the NUHM2 scenario for the given prior ranges.

The D_{KL} values corresponding to the naturalness priors and posteriors shown in Figs. 6.10 and 6.11 are given in Table 6.3. Again, we see that the information

Table 6.3: D_{KL} values in the NUHM2 scenario, correponding to the priors and posteriors given in Figs. 6.10 and 6.11, for flat and log priors in $m_{1/2}$ and μ, respectively. The ILC 0.5 TeV, HL-LHC 300 fb^{-1} and Higgs likelihoods have been included in the total.

Posterior	Flat priors	Log priors
ILC 1 TeV	1.063	2.075
HL-LHC 3000 fb^{-1}	0.088	0.132
Total	1.031	2.018

gain in general is largest when starting from log priors. In this scenario, the information gain from the ILC is $\sim$ 16 times as large as the information gain from the HL-LHC. For flat priors, the ILC information gain is $\sim$ 12 times as large. This confirms quantitatively all of the properties discussed above for the distributions.

The most important thing to note from the above discussion on naturalness in the NUHM2 scenario is that the HL-LHC searches do not exclude low naturalness scores, independent of the prior choice. The lowest naturalness scores are not excluded in the CMSSM scenarios either, however, this is due to low cut efficiency that can be ignored since the corresponding areas are excluded by earlier LHC searches, which is not the case in this scenario. In contrast, the ILC searches exclude naturalness scores up to $\sim$ 50. A linear collider with centre-of-mass energy $\sqrt{s} = 1$ TeV can tell us much more about naturalness in the NUHM2 scenario than the HL-LHC. This motivates building such a collider.

Conclusions

We set out to quantify the naturalness reach of the International Linear Collider (ILC) and the High-Luminosity Large Hadron Collider (HL-LHC) in three different supersymmetry scenarios, both in terms of the range of naturalness covered, quantified by the Barbieri–Giudice measure, and in terms of the amount of information gained about naturalness, quantified by the Kullback–Leibler divergence. The ILC results have been the focus of this thesis, while the HL-LHC results are discussed in detail in Ref. [1].

By following the prescription by Allanach et al. in Ref. [36], the naturalness reach of the ILC (HL-LHC) was quantified to be $c \sim 250(400)$, $c \sim 300(800)$ and $c \sim 30(-)$ in the CMSSM10, CMSSM30 and NUHM2 scenarios, respectively. The fact that the HL-LHC excludes higher naturalness scores than the ILC in the two CMSSM scenarios correponds to that the HL-LHC searches exclude larger areas in the mass planes of Figs. 6.2 and 6.5. Further, the hierarchy of the naturalness reach in these three scenarios was as expected.

Since the definition of naturalness reach given in Ref. [36] is rather limited, we also used Bayesian parameter estimation to investigate naturalness. This allowed us to identify the posterior distribution of the naturalness score after introducing the different searches explored in this work (assuming negative results). Further, the Kullback–Leibler divergence allowed us to compare how much we can learn about naturalness from the different collider searches.

The Kullback–Leibler (KL) divergence is a well-known measure in information and probability theory, quantifying the information gain between prior and posterior. From the literature, it appears that it has never previously been used in relation to particle physics. Although it is difficult to say anything useful about the absolute value of the KL-measure in this context, as it is prior dependent, it is a potentially powerful tool for comparing the advantages of different colliders. Here, it has been used in relation to naturalness. However, there are no limitations on what posterior it can be applied to.

After introducing all of the searches, the most probable naturalness score was roughly the same in the two CMSSM scenarios, $c \sim 1500$–1600, more or less independent of the prior choice for m_0 and $m_{1/2}$. In the CMSSM10 scenario, the Higgs likelihood completely dominated the total posterior. In the CMSSM30 scenario, however, the total posterior was dominated by the HL-LHC likelihood

for flat priors in m_0 and $m_{1/2}$, and the ILC and Higgs likelihoods for log priors. Since the HL-LHC searches used were inefficient for the lowest sparticle masses, the corresponding KL-values were somewhat ambigious.

In the NUHM2 scenario, the most probable naturalness score was $c \sim 120$ after introducing all of the searches. For both prior choices, the total posterior was completely dominated by the ILC likelihood from the 1 TeV search. The information gain from the ILC searches was over ten times as large as the information gain from the HL-LHC searches in this scenario. Surprisingly, post HL-LHC naturalness scores below $c \sim 20$, or a tuning to no worse than 5%, were allowed. Thus, if the particular variant of the NUHM2 model studied here, so-called Radiatively-driven Natural SUSY (RNS), actually describes the Universe, a linear collider with centre-of-mass energy 1 TeV would tell us much more about naturalness than the HL-LHC, which in that case would not exclude any significant naturalness scores at all. This motivates building the ILC.

Our implementation of the ILC searches detailed in Ref. [56] showed that they are effective in all three scenarios considered, with two small surprises. The upper cut on visible energy in the chargino extended search was found to have bad side effects at 1 TeV and should be increased. We also observed that the slepton analysis had surprising reach in discovering $\tilde{\chi}_2^0\tilde{\chi}_1^0$ production. A separate search optimized for $\tilde{\chi}_2^0\tilde{\chi}_1^0$ should be considered.

The present study has been limited to scanning parameter space grids instead of the full parameter spaces of the CMSSM and NUHM2 models. Due to time constraints, we have also been limited in our treatment of signal and background uncertainties. We hope that future progress in scanning tools and computer power will allow a full evaluation of the naturalness reach in these models. Such works should also study in more detail the dependence of the results on the prior ranges used.

Appendix A

Notation and conventions

Natural units, in which $\hbar = c = 1$, are used throughout this thesis. So is the relativistic four-vector notation, although the Lorentz indices are often suppressed when there is no risk of ambiguity. The most important contravariant four-vectors are the spacetime four-vector x^μ and the energy-momentum four-vector p^μ, defined as

$$x^\mu \equiv (x^0, x^1, x^2, x^3) = (t, \mathbf{x}) \tag{A.1}$$

and

$$p^\mu \equiv (p^0, p^1, p^2, p^3) = (E, p^1, p^2, p^3) = (E, \mathbf{p}). \tag{A.2}$$

Greek indices run from 0 to 3 unless otherwise noted, and repeated indices are implicitly summed over. Covariant four-vectors are defined from the contravariant ones using the metric tensor $g_{\mu\nu}$:

$$x_\mu \equiv g_{\mu\nu} x^\nu = (x^0, -x^1, -x^2, -x^3) = (t, -\mathbf{x}), \tag{A.3}$$

where the flat space metric tensor is defined by the relations

$$g_{00} = -g_{11} = -g_{22} = -g_{33} = 1, \tag{A.4}$$

$$g_{\mu\nu} = 0 \quad \text{for} \quad \mu \neq \nu. \tag{A.5}$$

Further, the following notation is used for the spacetime derivative:

$$\partial_\mu = \frac{\partial}{\partial x^\mu}. \tag{A.6}$$

The 4×4 Dirac gamma matrices are defined by the relations

$$\gamma^{\mu\dagger} = \gamma^0 \gamma^\mu \gamma^0, \tag{A.7}$$

$$\{\gamma^\mu, \gamma^\nu\} = 2g^{\mu\nu}, \tag{A.8}$$

where the curly brackets denote the anticommutator:

$$\{A, B\} \equiv AB + BA. \tag{A.9}$$

Further, the product of the gamma matrices is defined as

$$\gamma^5 \equiv i\gamma^0\gamma^1\gamma^2\gamma^3. \tag{A.10}$$

The three Pauli matrices are

$$\sigma_1 = \begin{pmatrix} 0 & 1 \\ 1 & 0 \end{pmatrix}, \quad \sigma_2 = \begin{pmatrix} 0 & -i \\ i & 0 \end{pmatrix}, \quad \sigma_3 = \begin{pmatrix} 1 & 0 \\ 0 & -1 \end{pmatrix}, \tag{A.11}$$

with commutation relations

$$[\sigma_i, \sigma_j] = 2i\epsilon_{ij}{}^k\sigma_k, \tag{A.12}$$

where the structure constants ϵ_{ijk} are given by the completely antisymmetric Levi–Civita symbol. Analogous to the Pauli matrices, the eight Gell–Mann matrices λ_i satisfy the commutation relations

$$[\lambda_i, \lambda_j] = 2if_{ij}{}^k\lambda_k, \tag{A.13}$$

where again the structure constants f_{ijk} are completely antisymmetric.

Appendix B

Modified PYCELL jet clustering routine

PYCELL is a jet clustering routine found in the Monte Carlo event generator PYTHIA 6 [53] that simulates the response of calorimeter cells to particles, and then clusters these cells to form jets using a cone algorithm. We have modified this routine in order for the jets to cluster on energy instead of transverse energy, and made some improvements in how the calorimeter is simulated in order for it to correspond better to ILC parameters. Details of these changes are described in Sec. 5.3.1. The resulting code can be found below. The changes are indicated by the green comments.

```
C*********************************************************************

      SUBROUTINE PYCELL(NJET)

C...Double precision and integer declarations.
      IMPLICIT DOUBLE PRECISION(A-H, O-Z)
      IMPLICIT INTEGER(I-N)
      INTEGER PYK,PYCHGE,PYCOMP
      !*-*-*-*-*-*-*-*-*-*-*-*-*-*-*-*-*-*-*-*-*-*-*-*-*-*
      DOUBLE PRECISION P_E(4000)
      !*-*-*-*-*-*-*-*-*-*-*-*-*-*-*-*-*-*-*-*-*-*-*-*-*-*

C...Parameter statement to help give large particle numbers.
      PARAMETER (KSUSY1=1000000,KSUSY2=2000000,KTECHN=3000000,
     &KEXCIT=4000000,KDIMEN=5000000)

C...Commonblocks.
      COMMON/PYJETS/N,NPAD,K(4000,5),P(4000,5),V(4000,5)
      COMMON/PYDAT1/MSTU(200),PARU(200),MSTJ(200),PARJ(200)
      COMMON/PYDAT2/KCHG(500,4),PMAS(500,4),PARF(2000),VCKM(4,4)
      SAVE /PYJETS/,/PYDAT1/,/PYDAT2/

```

```
C...Loop over all particles. Find cell that was hit by given particle.
      !*-*-*-*-*-*-*-*-*-*-*-*-*-*-*-*-*-*-*-*-*-*-*-*-*-*-*-*-*-*
      DO 42 II = 1,4000
        P_E(II)=0D0
   42 CONTINUE
      !*-*-*-*-*-*-*-*-*-*-*-*-*-*-*-*-*-*-*-*-*-*-*-*-*-*-*-*-*-*
      PTLRAT=1D0/SINH(PARU(51))**2
      NP=0
      NC=N
      DO 110 I=1,N
        IF(K(I,1).LE.0.OR.K(I,1).GT.10) GOTO 110
        IF(P(I,1)**2+P(I,2)**2.LE.PTLRAT*P(I,3)**2) GOTO 110
        IF(MSTU(41).GE.2) THEN
          KC=PYCOMP(K(I,2))
          !*-*-*-*-*-*-*-*-*-*-*-*-*-*-*-*-*-*-*-*-*-*-*-*-*-*-*-*-*-*
          ! Electrons (KC=11) and muons (KC=13) have been added to the
          ! list below of particles that should not be included in
          ! jets.
          !*-*-*-*-*-*-*-*-*-*-*-*-*-*-*-*-*-*-*-*-*-*-*-*-*-*-*-*-*-*
          IF(KC.EQ.0.OR.KC.EQ.12.OR.KC.EQ.14.OR.KC.EQ.16.OR.
     &    KC.EQ.13.OR.KC.EQ.11.OR.KC.EQ.18.OR.K(I,2).EQ.
     &    KSUSY1+22.OR.K(I,2).EQ.39.OR.K(I,2).EQ.KSUSY1+39) GOTO 110
          IF(MSTU(41).GE.3.AND.KCHG(KC,2).EQ.0.AND.PYCHGE(K(I,2)).EQ.0)
     &    GOTO 110
        ENDIF
        NP=NP+1
        PT=SQRT(P(I,1)**2+P(I,2)**2)
        !*-*-*-*-*-*-*-*-*-*-*-*-*-*-*-*-*-*-*-*-*-*-*-*-*-*-*-*-*-*
        P_XYZ=SQRT(P(I,1)**2+P(I,2)**2+P(I,3)**2)
        !*-*-*-*-*-*-*-*-*-*-*-*-*-*-*-*-*-*-*-*-*-*-*-*-*-*-*-*-*-*
        ETA=SIGN(LOG((SQRT(PT**2+P(I,3)**2)+ABS(P(I,3)))/PT),P(I,3))
        IETA=MAX(1,MIN(MSTU(51),1+INT(MSTU(51)*0.5D0*
     &  (ETA/PARU(51)+1D0))))
        PHI=PYANGL(P(I,1),P(I,2))
        IPHI=MAX(1,MIN(MSTU(52),1+INT(MSTU(52)*0.5D0*
     &  (PHI/PARU(1)+1D0))))
        IETPH=MSTU(52)*IETA+IPHI

C...Add to cell already hit, or book new cell.
        DO 100 IC=N+1,NC
          IF(IETPH.EQ.K(IC,3)) THEN
            K(IC,4)=K(IC,4)+1
            P(IC,5)=P(IC,5)+PT
            !*-*-*-*-*-*-*-*-*-*-*-*-*-*-*-*-*-*-*-*-*-*-*-*-*-*-*-*-*-*
            P_E(IC) = P_E(IC) + P_XYZ
            !*-*-*-*-*-*-*-*-*-*-*-*-*-*-*-*-*-*-*-*-*-*-*-*-*-*-*-*-*-*
            GOTO 110
          ENDIF
  100   CONTINUE
        IF(NC.GE.MSTU(4)-MSTU(32)-5) THEN
          CALL PYERRM(11,'(PYCELL:) no more memory left in PYJETS')
```

```
74            NJET=-2
75            RETURN
76          ENDIF
77          NC=NC+1
78          K(NC,3)=IETPH
79          K(NC,4)=1
80          K(NC,5)=2
81          P(NC,1)=(PARU(51)/MSTU(51))*(2*IETA-1-MSTU(51))
82          P(NC,2)=(PARU(1)/MSTU(52))*(2*IPHI-1-MSTU(52))
83          P(NC,5)=PT
84          !*-*-*-*-*-*-*-*-*-*-*-*-*-*-*-*-*-*-*-*-*-*-*-*
85          P_E(NC)=P_XYZ
86          !*-*-*-*-*-*-*-*-*-*-*-*-*-*-*-*-*-*-*-*-*-*-*-*
87      110 CONTINUE
88
89    C...Smear true bin content by calorimeter resolution.
90          IF(MSTU(53).GE.1) THEN
91            DO 130 IC=N+1,NC
92              PEI=P(IC,5)
93              IF(MSTU(53).EQ.2) PEI=P(IC,5)*COSH(P(IC,1))
94              !*-*-*-*-*-*-*-*-*-*-*-*-*-*-*-*-*-*-*-*-*-*-*-*
95              ! A constant term of 0.02 has been added to the standard
96              ! deviation sigma in the energy smearing below, given by
97              ! E = E + sigma*N(0,1)
98              !*-*-*-*-*-*-*-*-*-*-*-*-*-*-*-*-*-*-*-*-*-*-*-*
99      120     PEF=PEI+PARU(55)*SQRT(PEI+(0.0004/PARU(55)**2)*PEI**2
100         &        *(-2D0*LOG(MAX(1D-10,PYR(0))))*COS(PARU(2)*PYR(0))
101             IF(PEF.LT.0D0.OR.PEF.GT.PARU(56)*PEI) GOTO 120
102             P(IC,5)=PEF
103             IF(MSTU(53).EQ.2) P(IC,5)=PEF/COSH(P(IC,1))
104     130   CONTINUE
105         ENDIF
106
107   C...Remove cells below threshold.
108         IF(PARU(58).GT.0D0) THEN
109           NCC=NC
110           NC=N
111           DO 140 IC=N+1,NCC
112             !*-*-*-*-*-*-*-*-*-*-*-*-*-*-*-*-*-*-*-*-*-*-*-*
113             IF(P_E(IC).GT.PARU(58)) THEN
114             !*-*-*-*-*-*-*-*-*-*-*-*-*-*-*-*-*-*-*-*-*-*-*-*
115               NC=NC+1
116               K(NC,3)=K(IC,3)
117               K(NC,4)=K(IC,4)
118               K(NC,5)=K(IC,5)
119               P(NC,1)=P(IC,1)
120               P(NC,2)=P(IC,2)
121               P(NC,5)=P(IC,5)
122               !*-*-*-*-*-*-*-*-*-*-*-*-*-*-*-*-*-*-*-*-*-*-*-*
123               P_E(NC)=P_E(IC)
124               !*-*-*-*-*-*-*-*-*-*-*-*-*-*-*-*-*-*-*-*-*-*-*-*
```

```
125           ENDIF
126   140   CONTINUE
127         ENDIF
128
129   C...Find initiator cell: the one with highest p (originally pT) of not
          yet used ones.
130         NJ=NC
131   150   EMAX=0D0
132         DO 160 IC=N+1,NC
133           IF(K(IC,5).NE.2) GOTO 160
134           !*-*-*-*-*-*-*-*-*-*-*-*-*-*-*-*-*-*-*-*-*-*-*-*-*-*-*-*-*
135           IF(P_E(IC).LE.EMAX) GOTO 160
136           !*-*-*-*-*-*-*-*-*-*-*-*-*-*-*-*-*-*-*-*-*-*-*-*-*-*-*-*-*
137           ICMAX=IC
138           ETA=P(IC,1)
139           PHI=P(IC,2)
140           !*-*-*-*-*-*-*-*-*-*-*-*-*-*-*-*-*-*-*-*-*-*-*-*-*-*-*-*-*
141           EMAX=P_E(IC)
142           !*-*-*-*-*-*-*-*-*-*-*-*-*-*-*-*-*-*-*-*-*-*-*-*-*-*-*-*-*
143   160   CONTINUE
144         !*-*-*-*-*-*-*-*-*-*-*-*-*-*-*-*-*-*-*-*-*-*-*-*-*-*-*-*-*
145         IF(EMAX.LT.PARU(52)) GOTO 220
146         !*-*-*-*-*-*-*-*-*-*-*-*-*-*-*-*-*-*-*-*-*-*-*-*-*-*-*-*-*
147         IF(NJ.GE.MSTU(4)-MSTU(32)-5) THEN
148           CALL PYERRM(11,'(PYCELL:) no more memory left in PYJETS')
149           NJET=-2
150           RETURN
151         ENDIF
152         K(ICMAX,5)=1
153         NJ=NJ+1
154         K(NJ,4)=0
155         K(NJ,5)=1
156         P(NJ,1)=ETA
157         P(NJ,2)=PHI
158         P(NJ,3)=0D0
159         P(NJ,4)=0D0
160         P(NJ,5)=0D0
161         !*-*-*-*-*-*-*-*-*-*-*-*-*-*-*-*-*-*-*-*-*-*-*-*-*-*-*-*-*
162         P_E(NJ)=0D0
163         !*-*-*-*-*-*-*-*-*-*-*-*-*-*-*-*-*-*-*-*-*-*-*-*-*-*-*-*-*
164
165   C...Sum up unused cells within required distance of initiator.
166         DO 170 IC=N+1,NC
167           IF(K(IC,5).EQ.0) GOTO 170
168           IF(ABS(P(IC,1)-ETA).GT.PARU(54)) GOTO 170
169           DPHIA=ABS(P(IC,2)-PHI)
170           IF(DPHIA.GT.PARU(54).AND.DPHIA.LT.PARU(2)-PARU(54)) GOTO 170
171           PHIC=P(IC,2)
172           IF(DPHIA.GT.PARU(1)) PHIC=PHIC+SIGN(PARU(2),PHI)
173           IF((P(IC,1)-ETA)**2+(PHIC-PHI)**2.GT.PARU(54)**2) GOTO 170
174           K(IC,5)=-K(IC,5)
```

```
175           K(NJ,4)=K(NJ,4)+K(IC,4)
176           P(NJ,3)=P(NJ,3)+P(IC,5)*P(IC,1)
177           P(NJ,4)=P(NJ,4)+P(IC,5)*PHIC
178           P(NJ,5)=P(NJ,5)+P(IC,5)
179           !*-*-*-*-*-*-*-*-*-*-*-*-*-*-*-*-*-*-*-*-*-*-*-*-*-*-*-*-*
180           P_E(NJ)=P_E(NJ)+P_E(IC)
181           !*-*-*-*-*-*-*-*-*-*-*-*-*-*-*-*-*-*-*-*-*-*-*-*-*-*-*-*-*
182     170 CONTINUE
183
184   C...Reject cluster below minimum E (originally ET), else accept.
185         !*-*-*-*-*-*-*-*-*-*-*-*-*-*-*-*-*-*-*-*-*-*-*-*-*-*-*-*-*
186         IF(P_E(NJ).LT.PARU(53)) THEN
187         !*-*-*-*-*-*-*-*-*-*-*-*-*-*-*-*-*-*-*-*-*-*-*-*-*-*-*-*-*
188           NJ=NJ-1
189           DO 180 IC=N+1,NC
190             IF(K(IC,5).LT.0) K(IC,5)=-K(IC,5)
191     180   CONTINUE
192         ELSEIF(MSTU(54).LE.2) THEN
193           P(NJ,3)=P(NJ,3)/P(NJ,5)
194           P(NJ,4)=P(NJ,4)/P(NJ,5)
195           IF(ABS(P(NJ,4)).GT.PARU(1)) P(NJ,4)=P(NJ,4)-SIGN(PARU(2),
196        &  P(NJ,4))
197           DO 190 IC=N+1,NC
198             IF(K(IC,5).LT.0) K(IC,5)=0
199     190   CONTINUE
200         ELSE
201           DO 200 J=1,4
202             P(NJ,J)=0D0
203     200   CONTINUE
204           DO 210 IC=N+1,NC
205             IF(K(IC,5).GE.0) GOTO 210
206             P(NJ,1)=P(NJ,1)+P(IC,5)*COS(P(IC,2))
207             P(NJ,2)=P(NJ,2)+P(IC,5)*SIN(P(IC,2))
208             P(NJ,3)=P(NJ,3)+P(IC,5)*SINH(P(IC,1))
209             P(NJ,4)=P(NJ,4)+P(IC,5)*COSH(P(IC,1))
210             K(IC,5)=0
211     210   CONTINUE
212         ENDIF
213         GOTO 150
214
215   C...Arrange clusters in falling E (originally ET) sequence.
216     220 DO 250 I=1,NJ-NC
217           !*-*-*-*-*-*-*-*-*-*-*-*-*-*-*-*-*-*-*-*-*-*-*-*-*-*-*-*-*
218           EMAX=0D0
219           !*-*-*-*-*-*-*-*-*-*-*-*-*-*-*-*-*-*-*-*-*-*-*-*-*-*-*-*-*
220           DO 230 IJ=NC+1,NJ
221             IF(K(IJ,5).EQ.0) GOTO 230
222             !*-*-*-*-*-*-*-*-*-*-*-*-*-*-*-*-*-*-*-*-*-*-*-*-*-*-*-*-*
223             IF(P_E(IJ).LT.EMAX) GOTO 230
224             !*-*-*-*-*-*-*-*-*-*-*-*-*-*-*-*-*-*-*-*-*-*-*-*-*-*-*-*-*
225
```

```
226           IJMAX=IJ
227           !*-*-*-*-*-*-*-*-*-*-*-*-*-*-*-*-*-*-*-*-*-*-*-*-*-*-*-*
228           EMAX=P_E(IJ)
229           !*-*-*-*-*-*-*-*-*-*-*-*-*-*-*-*-*-*-*-*-*-*-*-*-*-*-*-*
230     230   CONTINUE
231           K(IJMAX,5)=0
232           K(N+I,1)=31
233           K(N+I,2)=98
234           K(N+I,3)=I
235           K(N+I,4)=K(IJMAX,4)
236           K(N+I,5)=0
237           !*-*-*-*-*-*-*-*-*-*-*-*-*-*-*-*-*-*-*-*-*-*-*-*-*-*-*-*
238           P_E(N+I)=P_E(IJMAX)
239           !*-*-*-*-*-*-*-*-*-*-*-*-*-*-*-*-*-*-*-*-*-*-*-*-*-*-*-*
240           DO 240 J=1,5
241             P(N+I,J)=P(IJMAX,J)
242             V(N+I,J)=0D0
243     240   CONTINUE
244     250 CONTINUE
245         NJET=NJ-NC
246
247   C...Convert to massless or massive four-vectors.
248         IF(MSTU(54).EQ.2) THEN
249           DO 260 I=N+1,N+NJET
250             ETA=P(I,3)
251             P(I,1)=P(I,5)*COS(P(I,4))
252             P(I,2)=P(I,5)*SIN(P(I,4))
253             P(I,3)=P(I,5)*SINH(ETA)
254             P(I,4)=P(I,5)*COSH(ETA)
255             P(I,5)=0D0
256     260   CONTINUE
257         ELSEIF(MSTU(54).GE.3) THEN
258           DO 270 I=N+1,N+NJET
259             P(I,5)=SQRT(MAX(0D0,P(I,4)**2-P(I,1)**2-P(I,2)**2-P(I,3)**2))
260     270   CONTINUE
261         ENDIF
262
263   C...Information about storage.
264         MSTU(61)=N+1
265         MSTU(62)=NP
266         MSTU(63)=NC-N
267         IF(MSTU(43).LE.1) MSTU(3)=MAX(0,NJET)
268         IF(MSTU(43).GE.2) N=N+MAX(0,NJET)
269
270         RETURN
271         END
272
273   C*********************************************************************
```

Bibliography

[1] M. Røysheim, "Exploring Naturalness in Supersymmetry at the High-Luminosity Large Hadron Collider," Master's thesis, Faculty of Mathematics and Natural Sciences, University of Oslo, Norway, 2016.

[2] **ATLAS** Collaboration, G. Aad *et al.*, "Observation of a new particle in the search for the Standard Model Higgs boson with the ATLAS detector at the LHC," *Phys. Lett.* **B716** (2012) 1–29, arXiv:1207.7214 [hep-ex].

[3] **CMS** Collaboration, S. Chatrchyan *et al.*, "Observation of a new boson at a mass of 125 GeV with the CMS experiment at the LHC," *Phys. Lett.* **B716** (2012) 30–61, arXiv:1207.7235 [hep-ex].

[4] Wikipedia, "Standard Model of Elementary Particles." https://en.wikipedia.org/wiki/Standard_Model. [Online, accessed September 11, 2016].

[5] N. Cabibbo, "Unitary Symmetry and Leptonic Decays," *Phys. Rev. Lett.* **10** (1963) 531–533.

[6] M. Kobayashi and T. Maskawa, "CP Violation in the Renormalizable Theory of Weak Interaction," *Prog. Theor. Phys.* **49** (1973) 652–657.

[7] B. Pontecorvo, "Inverse beta processes and nonconservation of lepton charge," *Zhurnal Eksperimental noi i Teoreticheskoi Fiziki* **34** (1957) 247.

[8] Z. Maki, M. Nakagawa, and S. Sakata, "Remarks on the Unified Model of Elementary Particles," *Progress of Theoretical Physics* **28** (1962) 870–880.

[9] E. Noether, "Invariante Variationsprobleme," *Nachrichten von der Gesellschaft der Wissenschaften zu Göttingen, Mathematisch-Physikalische Klasse* **1918** (1918) 235–257.

[10] E. Noether and M. Tavel, "Invariant Variation Problems," arXiv:physics/0503066v2. M. A. Tavel's English translation of Noether's Theorems (1918).

[11] P. W. Anderson, "Plasmons, Gauge Invariance, and Mass," *Phys. Rev.* **130** (Apr, 1963) 439–442.

[12] G. S. Guralnik, C. R. Hagen, and T. W. B. Kibble, "Global Conservation Laws and Massless Particles," *Phys. Rev. Lett.* **13** (Nov, 1964) 585–587.

[13] F. Englert and R. Brout, "Broken Symmetry and the Mass of Gauge Vector Mesons," *Phys. Rev. Lett.* **13** (Aug, 1964) 321–323.

[14] P. W. Higgs, "Broken Symmetries and the Masses of Gauge Bosons," *Phys. Rev. Lett.* **13** (Oct, 1964) 508–509.

[15] L. Alvarez-Gaume and J. Ellis, "Eyes on a prize particle," *Nature Phys.* **7** no. 1, (2011) 2–3. Editorial Material.

[16] R. P. Feynman, "Space-Time Approach to Quantum Electrodynamics," *Phys. Rev.* **76** (Sep, 1949) 769–789.

[17] M. Thomson, *Modern Particle Physics*. Cambridge University Press, 2013.

[18] V. C. Rubin, W. K. J. Ford, and N. Thonnard, "Rotational properties of 21 SC galaxies with a large range of luminosities and radii, from NGC 4605 (R = 4kpc) to UGC 2885 (R = 122 kpc)," *Astrophys. J.* **238** (June, 1980) 471–487.

[19] S. Coleman and J. Mandula, "All Possible Symmetries of the S Matrix," *Phys. Rev.* **159** (Jul, 1967) 1251–1256.

[20] R. Haag, J. T. Lopuszanski, and M. Sohnius, "All Possible Generators of Supersymmetries of the s Matrix," *Nucl. Phys.* **B88** (1975) 257.

[21] **Particle Data Group** Collaboration, K. A. Olive *et al.*, "Review of Particle Physics," *Chin. Phys.* **C38** no. 9, (2014) 090001.

[22] S. P. Martin, "A Supersymmetry primer," arXiv:hep-ph/9709356 [hep-ph]. [Adv. Ser. Direct. High Energy Phys. 18, 1 (1998)].

[23] A. Raklev, "Supersymmetry lecture notes." http://www.uio.no/studier/emner/matnat/fys/FYS5190/h15/resurser/notes.pdf. [Online, accessed September 14, 2016].

[24] **ATLAS, CMS** Collaboration, G. Aad *et al.*, "Combined Measurement of the Higgs Boson Mass in pp Collisions at $\sqrt{s} = 7$ and 8 TeV with the ATLAS and CMS Experiments," *Phys. Rev. Lett.* **114** (2015) 191803, arXiv:1503.07589 [hep-ex].

[25] J. E. Anderson, "A Conceptual Framework for Evaluating and Quantifying Naturalness," *Conservation Biology* **5** no. 3, (1991) 347–352.

[26] G. t' Hooft, *Recent developments in gauge theories*. NATO ASI series: Physics. Plenum Press, 1980. https://books.google.no/books?id=6SOaAAAAIAAJ.

[27] L. Susskind, "Dynamics of spontaneous symmetry breaking in the Weinberg-Salam theory," *Phys. Rev. D* **20** (Nov, 1979) 2619–2625.

[28] R. Barbieri and G. F. Giudice, "Upper Bounds on Supersymmetric Particle Masses," *Nucl. Phys.* **B306** (1988) 63–76.

[29] M. Papucci, J. T. Ruderman, and A. Weiler, "Natural SUSY Endures," *JHEP* **09** (2012) 035, arXiv:1110.6926 [hep-ph].

[30] H. Baer *et al.*, "Radiatively-driven natural supersymmetry at the LHC," *JHEP* **12** (2013) 013, arXiv:1310.4858 [hep-ph]. [Erratum: JHEP06, 053 (2015)].

[31] D. Sivia and J. Skilling, *Data Analysis: A Bayesian Tutorial*. Oxford science publications. Oxford University Press, 2006.

[32] E. Jaynes and G. Bretthorst, *Probability Theory: The Logic of Science*. Cambridge University Press, 2003.

[33] T. Bayes, "An essay towards solving a problem in the doctrine of chances," *Phil. Trans. of the Royal Soc. of London* **53** (1763) 370–418.

[34] S. Kullback and R. A. Leibler, "On Information and Sufficiency," *Ann. Math. Statist.* **22** no. 1, (03, 1951) 79–86.

[35] **Muon g-2** Collaboration, G. W. Bennett *et al.*, "Final Report of the Muon E821 Anomalous Magnetic Moment Measurement at BNL," *Phys. Rev.* **D73** (2006) 072003, arXiv:hep-ex/0602035 [hep-ex].

[36] B. C. Allanach, J. P. J. Hetherington, M. A. Parker, and B. R. Webber, "Naturalness reach of the large hadron collider in minimal supergravity," *JHEP* **08** (2000) 017, arXiv:0005186 [hep-ph].

[37] A. Kvellestad. Private communication.

[38] B. Allanach, "SOFTSUSY: a program for calculating supersymmetric spectra," *Comput. Phys. Commun.* **143** (2002) 305–331, arXiv:0104145 [hep-ph].

[39] A. Djouadi, M. M. Muhlleitner, and M. Spira, "Decays of supersymmetric particles: The Program SUSY-HIT (SUspect-SdecaY-Hdecay-InTerface)," *Acta Phys. Polon.* **B38** (2007) 635–644, arXiv:hep-ph/0609292 [hep-ph].

[40] H. Bahl and W. Hollik, "Precise prediction for the light MSSM Higgs boson mass combining effective field theory and fixed-order calculations," *Eur. Phys. J.* **C76** no. 9, (2016) 499, arXiv:1608.01880 [hep-ph].

[41] T. Hahn, S. Heinemeyer, W. Hollik, H. Rzehak, and G. Weiglein, "High-Precision Predictions for the Light CP -Even Higgs Boson Mass of the Minimal Supersymmetric Standard Model," *Phys. Rev. Lett.* **112** no. 14, (2014) 141801, arXiv:1312.4937 [hep-ph].

[42] M. Frank, T. Hahn, S. Heinemeyer, W. Hollik, H. Rzehak, and G. Weiglein, "The Higgs Boson Masses and Mixings of the Complex MSSM in the Feynman-Diagrammatic Approach," *JHEP* **02** (2007) 047, arXiv:hep-ph/0611326 [hep-ph].

[43] G. Degrassi, S. Heinemeyer, W. Hollik, P. Slavich, and G. Weiglein, "Towards high precision predictions for the MSSM Higgs sector," *Eur. Phys. J.* **C28** (2003) 133–143, arXiv:hep-ph/0212020 [hep-ph].

[44] S. Heinemeyer, W. Hollik, and G. Weiglein, "The Masses of the neutral CP - even Higgs bosons in the MSSM: Accurate analysis at the two loop level," *Eur. Phys. J.* **C9** (1999) 343–366, arXiv:hep-ph/9812472 [hep-ph].

[45] S. Heinemeyer, W. Hollik, and G. Weiglein, "FeynHiggs: A Program for the calculation of the masses of the neutral CP even Higgs bosons in the MSSM," *Comput. Phys. Commun.* **124** (2000) 76–89, arXiv:hep-ph/9812320 [hep-ph].

[46] P. Z. Skands, B. Allanach, H. Baer, C. Balazs, G. Belanger, *et al.*, "SUSY Les Houches accord: Interfacing SUSY spectrum calculators, decay packages, and event generators," *JHEP* **0407** (2004) 036, arXiv:0311123 [hep-ph].

[47] A. Buckley, "PySLHA: a Pythonic interface to SUSY Les Houches Accord data," *Eur. Phys. J.* **C75** no. 10, (2015) 467, arXiv:1305.4194 [hep-ph].

[48] A. Kulesza and L. Motyka, "Threshold resummation for squark-antisquark and gluino-pair production at the LHC," *Phys. Rev. Lett.* **102** (2009) 111802, arXiv:0807.2405 [hep-ph].

[49] A. Kulesza and L. Motyka, "Soft gluon resummation for the production of gluino-gluino and squark-antisquark pairs at the LHC," *Phys. Rev.* **D80** (2009) 095004, arXiv:0905.4749 [hep-ph].

[50] W. Beenakker, S. Brensing, M. Kramer, A. Kulesza, E. Laenen, and I. Niessen, "Soft-gluon resummation for squark and gluino hadroproduction," *JHEP* **12** (2009) 041, arXiv:0909.4418 [hep-ph].

[51] W. Beenakker, S. Brensing, M. n. Kramer, A. Kulesza, E. Laenen, L. Motyka, and I. Niessen, "Squark and Gluino Hadroproduction," *Int. J. Mod. Phys.* **A26** (2011) 2637–2664, arXiv:1105.1110 [hep-ph].

[52] T. Sjöstrand, S. Ask, J. R. Christiansen, R. Corke, N. Desai, *et al.*, "An Introduction to PYTHIA 8.2," *Comput.Phys.Commun.* **191** (2015) 159–177, arXiv:1410.3012 [hep-ph].

[53] T. Sjostrand, S. Mrenna, and P. Z. Skands, "PYTHIA 6.4 Physics and Manual," *JHEP* **05** (2006) 026, arXiv:hep-ph/0603175 [hep-ph].

[54] M. Cacciari, G. P. Salam, and G. Soyez, "FastJet User Manual," *Eur. Phys. J.* **C72** (2012) 1896, arXiv:1111.6097 [hep-ph].

[55] M. Cacciari, G. P. Salam, and G. Soyez, "The Anti-k(t) jet clustering algorithm," *JHEP* **0804** (2008) 063, arXiv:0802.1189 [hep-ph].

[56] H. Baer, A. Belyaev, T. Krupovnickas, and X. Tata, "Linear collider capabilities for supersymmetry in dark matter allowed regions of the mSUGRA model," *JHEP* **02** (2004) 007, arXiv:hep-ph/0311351 [hep-ph].

[57] F. E. Paige, S. D. Protopopescu, H. Baer, and X. Tata, "ISAJET 7.69: A Monte Carlo event generator for pp, anti-p p, and e+e- reactions," arXiv:hep-ph/0312045 [hep-ph].

[58] **ATLAS** Collaboration, G. Aad *et al.*, "Search for Supersymmetry at the high luminosity LHC with the ATLAS experiment," Tech. Rep. ATL-PHYS-PUB-2014-010, CERN, Geneva, July, 2014. http://cds.cern.ch/record/1735031.

[59] W. Beenakker, R. Hopker, M. Spira, and P. M. Zerwas, "Squark and gluino production at hadron colliders," *Nucl. Phys.* **B492** (1997) 51–103, arXiv:hep-ph/9610490 [hep-ph].

[60] J. M. Bernardo and A. F. M. Smith, *Bayesian Theory*. John Wiley & Sons, 2008.